

**OPTIMIZATION OF GRAPHENE OXIDE WITH METHYL- $\beta$ -CYCLODEXTRIN AND  
CARBON NANOTUBES WITH POLYPYRROLE FOR REMOVAL OF LEAD (II) AND  
COPPER (II) IONS FROM WATER**

**BY**

**NYAIRO WILFRIDA NYANDUKO**

**A THESIS SUBMITTED IN FULFILLMENT OF THE REQUIREMENTS FOR THE  
DEGREE OF DOCTOR OF PHILOSOPHY IN CHEMISTRY**

**DEPARTMENT OF CHEMISTRY**

**MASENO UNIVERSITY**

**©2018**

## DECLARATIONS

### BY THE CANDIDATE

This thesis is my original work and has not been previously presented for a degree in Maseno University or in any other university. All sources of information herein have been supported by relevant references.

Signature..... Date.....

Nyairo, Wilfrida Nyanduko

PHD/SC/00058/2014

### BY THE SUPERVISORS

This thesis has been submitted for examination with our approval as the university supervisors

#### Supervisors

- |  |   |
|--|---|
| 1. Prof. Chrispin Kowenje<br>Maseno University<br>Department of Chemistry<br>Kenya<br>Signature.....Date.....  | 2. Dr. David Ongeru<br>Maseno University<br>Department of Chemistry<br>Kenya<br>Signature.....Date..... |
| 3. Dr. Eker Yasin<br>Necmettin Erbakan University<br>Department of Engineering<br>Turkey<br>Signature  Date...29/11/2018. |   |

## **ACKNOWLEDGEMENT**

Great appreciation goes to Prof. Chrispin Kowenje and Dr. David Ongeri of Maseno University and Dr. Eker Yasin, Dr Erhan Zhor, Dr. Ilker Akin, Prof. Haluk Bingol and Prof. Ali Tor of Necmettin Erbakan University (Konya-Turkey), for providing the much needed advice, support and laboratory space. I also appreciate the support and encouragement provided by my research group members; particularly my classmate-Victor Shikuku and Wesley Omwoyo Nyaioti. I also recognize the assistance provided by the technical staff of Necmettin Erbakan University - Mohammed Esat.

Special thanks go to the German Academic Exchange Service (DAAD) through the International Network in Sustainable Water Management in Developing Countries/Excellence Centre for Development Cooperation (SWINDON/EXCEED) for financial support for travel and stay in Konya-Turkey and the National Council for Science, Technology and Innovation (NACOSTI) for the financial support for laboratory supplies. My most sincere appreciation also goes to Prof. Samuel Pare the then regional coordinator SWINDON/EXCEED for facilitating the travel and stay in Turkey.

Last but not least, I appreciate and acknowledge the love and support I have continuously received from my family: Hellen, Carol, Edna, Edwin, Sarah, Charlie, Bob and Chrispin Nyairo.

## **DEDICATION**

To my family: Patrick, Jordan and Andrew Owoche.

## ABSTRACT

Heavy metals pose risks to the humans and the environment. Lead (II) and copper (II) are of particular concern because they can cause irreversible damage to vital body organs. Their sources include leaded paints, old water piping systems, pesticides, fertilizers and metal recycling plants. Various methods such as adsorption have been used to remove these metals from wastewater. The total surface area and surface functionalities of an adsorbent affect the adsorption of the adsorbate. Conventional adsorbents such as clay which are considered to be inexpensive have been found to have moderate surface areas hence do not adsorb heavy metals to appreciable levels. This challenge could be met by exploring advanced adsorbents whose surfaces can be manipulated to introduce functional groups that have an adsorption affinity for heavy metal cations onto their surfaces. Currently, research is focused on designing carbon-based nanomaterials such as graphene oxide (GO) and carbon nanotubes (CNT) for the removal of heavy metals from water. Optimization and derivatization of these adsorbents by other groups such as  $\beta$ -cyclodextrin, enhance their adsorption efficiencies. The objectives of this study were to synthesize, characterize and optimize the adsorption characteristics of GO conjugated with methyl- $\beta$ -cyclodextrin (GO-m $\beta$ CD) and oxygenated CNT coated with polypyrrole (oMWCNT/Ppy). GO-m $\beta$ CD and oMWCNT/Ppy were synthesized, characterized and applied as adsorbents to determine the adsorption behavior of Pb(II) and Cu(II) from aqueous solutions. Pristine and oxidized carbon nanotubes (pMWCNT and oMWCNT) were used as reference adsorbents for oMWCNT/Ppy and graphene oxide (GO) a reference for GO-m $\beta$ CD. The GO-m $\beta$ CD was synthesized through *in situ* aggregation of GO and m $\beta$ CD while oMWCNT/Ppy was synthesized using *in situ* oxidative polymerization method. Scanning electron microscopy (SEM), Fourier transform infrared (FTIR) spectroscopy, Raman spectroscopy and thermogravimetric analysis (TGA) and X-ray Diffraction (XRD) showed that oMWCNT/Ppy and GO-m $\beta$ CD were used to characterize the synthesized adsorbents. The experimental data of means of triplicates were determined at a confidence level of 95%. The adsorption processes fitted better to the Langmuir isotherm than Freundlich isotherm indicating that the adsorption was monolayer. The adsorption data fitted better onto the pseudo-second order kinetic model than pseudo-first order kinetic model implying that the adsorption process involved both the adsorbate and the adsorbent. The adsorption capacities indicated that derivatization of oMWCNT with Ppy significantly ( $p \leq 0.05$ ) enhanced its adsorption capacity for both Pb(II) and Cu(II) by 50.1% and 43.9%, respectively. Equally, the derivatization of GO with m $\beta$ CD makes it a better adsorbent for Pb(II) than pure GO by 43.8% although this was not applicable for Cu(II). The uptake of the metal ions in a single metal system was significantly higher ( $p \leq 0.05$ ) than that of binary metal ion system when oMWCNT/Ppy was applied. In addition, the desorption studies indicate that the composite adsorbents, GO-m $\beta$ CD and oMWCNT/Ppy can be used repeatedly up to five times with minimal loss of their initial adsorption capacity. More heavy metal species and these derivatives need to be investigated to come up with a wider conclusions on the adsorption capacity of these derivatives.

## TABLE OF CONTENTS

DECLARATIONS .....	ii
ACKNOWLEDGEMENT .....	iii
DEDICATION .....	iv
ABSTRACT .....	v
TABLE OF CONTENTS .....	vi
ABBREVIATIONS.....	x
LIST OF TABLES .....	xi
LIST OF FIGURES.....	xii
<b>CHAPTER 1: INTRODUCTION .....</b>	<b>1</b>
1.1 Background of study .....	1
1.2 Statement of the problem .....	5
1.3 Objective of the Study.....	6
1.4 Specific objectives.....	6
1.5 Research Questions .....	6
1.6 Null hypothesis ( $H_0$ ).....	7
1.7 Justification .....	7
1.8 Significance of the Study .....	8
<b>CHAPTER 2: LITERATURE REVIEW .....</b>	<b>9</b>
2.1 Heavy metal ions in water: sources of contamination and effects .....	9
2.1.1 Lead .....	10
2.1.2 Copper .....	10
2.2 Conventional techniques for the removal of heavy metals .....	11
2.3 Carbon based nanoadsorbents .....	13
2.3.1 Graphene adsorbents and its derivatives .....	14

2.3.2 Carbon nanotubes (CNT) adsorbents .....	17
2.4 Synthesis of the adsorbents .....	21
2.4.1 Synthesis graphene oxide composites .....	21
2.5 Characterization of graphene oxide and carbon nanotubes .....	22
2.5.1 Characterization of graphene oxide and composite.....	23
2.5.2 Characterization of multi-walled carbon nanotubes and composite.....	25
2.6 Factors affecting the adsorption of heavy metal ions on an adsorbent. ....	26
2.6.1 Initial pH of the solution.....	26
2.6.2 Contact time and initial concentration.....	27
2.7 Adsorption of metal ions onto GO and CNT composites .....	27
2.7.1 Adsorption mechanism of GO and its composites .....	29
2.7.2 Adsorption mechanism of CNT and its composites .....	31
2.8 Competitive adsorption .....	32
2.9 Regeneration of adsorbents .....	32
<b>CHAPTER 3: MATERIALS AND METHODS.....</b>	<b>35</b>
3.1 Chemicals and reagents .....	35
3.2 Equipment .....	35
3.3 Synthesis.....	36
3.3.1 Synthesis of GO and GOm $\beta$ CD .....	36
3.3.2 Synthesis of the oMWCNT and oMWCNT/Ppy .....	37
3.4 Characterization of GO, GO-m $\beta$ CD, pMWCNT, oMWCNT and oMWCNT/Ppy .....	38
3.4.1 Functional group changes.....	38
3.4.2 Specific surface area.....	38

3.4.3 Analysis of Morphology.....	39
3.4.4 The concentration of metal ion solution after adsorption and desorption .....	39
3.4.5 Analysis of order and disorder in hexagonal carbon .....	39
3.4.6 Crystallinity of GO and GO-m $\beta$ CD .....	39
3.4.7 Thermal stability.....	40
3.5 Adsorption Experiments.....	40
3.5.1 Preparation of the Cu <sup>2+</sup> and Pb <sup>2+</sup> Solutions .....	40
3.5.2 Effect of initial pH.....	40
3.5.3 Effect of contact time .....	40
3.5.4 Competitive sorption studies .....	41
3.6 Regeneration of the adsorbents .....	41
3.7 Statistical Analysis .....	41
<b>CHAPTER 4: RESULTS AND DISCUSSION.....</b>	<b>43</b>
4.1 GO-m $\beta$ CD nanocomposite.....	43
4.1.1 Synthesis and Characterization of GO and GO-m $\beta$ CD .....	43
4.1.2 Sorption of Cu(II) and Pb(II) onto GO-m $\beta$ CD.....	46
4.1.3 Competitive sorption studies .....	55
4.1.4 Regeneration of adsorbent studies.....	56
4.2 The oMWCNT-polypyrrole nanocomposite .....	57
4.2.1 Synthesis and Characterization.....	57
4.2.2 Adsorption studies .....	62
4.2.3 Competitive sorption studies .....	72

4.2.4 Studies on the regeneration of the adsorbents .....	73
<b>CHAPTER 5: SUMMARY, CONCLUSIONS AND RECOMMENDATIONS.....</b>	<b>74</b>
5.1 Summary .....	74
5.2 Conclusions .....	74
5.3 Recommendations .....	75
5.4 Suggestions for future studies .....	75
<b>REFERENCES .....</b>	<b>76</b>
<b>APPENDICES .....</b>	<b>93</b>

## ABBREVIATIONS

AAS	Atomic Absorption Spectrometer
$\beta$ CD	Beta cyclodextrin
BET	Brunauer, Emmett and Teller
CDs	Cyclodextrins
CNT	Carbon nanotubes
CVD	Chemical vapor deposition
DFT	Density Functional Theory
FTIR	Fourier transform infrared spectroscopy
GO	Graphene oxide
GO-m $\beta$ CD	Methyl- $\beta$ -cyclodextrin modified graphene oxide
m $\beta$ CD	Methyl- $\beta$ -cyclodextrin
MWCNT	Multi-walled carbon nanotubes
pMWCNT	Pristine multi-walled carbon nanotubes
O-CNT	Oxidized carbon nanotubes
oMWCNT	Oxidized multi-walled carbon nanotubes
oMWCNT/Ppy	Polypyrrole coated oxidized multi-walled carbon nanotubes
Ppy	Polypyrrole
rGO	Reduced graphene oxide
SEM	Scanning electron microscopy
SSA	Specific surface area
SWCNT	Single-walled carbon nanotubes
TGA	Thermogravimetric analysis
%T	Percentage transmittance
XRD	X-ray Diffraction

## LIST OF TABLES

Table 1: A summary of the merits and demerits of some heavy metal ions removal techniques.	12
Table 2: Various adsorbents and their respective specific surface area.....	13
Table 3: Sorption capacities of graphene and its derivatives for some heavy metal ions from aqueous solutions at various conditions.....	17
Table 4: The sorption capacities of raw and oxidized CNT for some divalent cations in aqueous solutions at various conditions.....	19
Table 5: Kinetic parameters of pseudo-first-order and pseudo-second-order equation for Pb(II) and Cu(II) sorption on GO and GO- m $\beta$ CD at initial concentration of 10 mg/L. ....	51
Table 6: The means of metal ions adsorbed at varying initial metal ion concentration. ....	52
Table 7: Langmuir and Freundlich isotherm constants for Pb(II) sorption on GO and GO-m $\beta$ CD .....	53
Table 8: Comparison of the sorption capacities of the adsorbents in this study with those in literature. ....	54
Table 9: Means of metal ions in a single and binary metal ion system. ....	55
Table 10: The physical properties of the pMWCNT, oMWCNT and oMWCNT/Ppy .....	60
Table 11: The means of Pb(II) and Cu(II) ions uptake by pMWCNT, oMWCNT and oMWCNT/Ppy at varying initial metal ion concentration.....	65
Table 12: Langmuir and Freundlich isothermic constants for Pb(II) and Cu(II) sorption on pMWCNT, oMWCNT and oMWCNT/Ppy .....	67
Table 13: Kinetic parameters of pseudo-first order and pseudo-second order equation for Pb(II) and Cu(II) sorption on pMWCNT, oMWCNT and oMWCNT/Ppy at concentration = 10 mg/L.....	68
Table 14: Comparison of the sorption capacities of the adsorbents in this study with those in literature .....	71

## LIST OF FIGURES

Fig. 1: Schematic of the structure of graphene sheet .....	14
Fig. 2: The structure of a single sheet of graphene oxide .....	15
Fig. 3 The structure of $\beta$ -cyclodextrin molecule .....	16
Fig. 4: Structure representation of SWCNT and MWCNT .....	18
Fig. 5: Schematic of oxidation of CNT .....	20
Fig. 6: Representation of the structure of polypyrrole.....	20
Fig. 7: Desorption rate of Cu(II) from GO at different pH values of HCl solution .....	33
Fig. 8: Desorption rate of Pb(II) from CNT at different pH values of HCl and HNO <sub>3</sub> solution .	34
Fig. 9: Picture of yellow dispersed GO.....	37
Fig. 10: The schematic diagram showing the synthesis of GO-m $\beta$ CD composite.....	37
Fig. 11: The schematic flow diagram of coating oMWCNT with Ppy.....	38
Fig. 12: FTIR spectra of (a) GO (b) m $\beta$ CD and (c) GO-m $\beta$ CD.....	44
Fig. 13: SEM images of (a) GO and (b) GO-m $\beta$ CD.....	44
Fig. 14: Raman spectra GO and GO-m $\beta$ CD.....	45
Fig. 15: XRD patterns of GO and GO-m $\beta$ CD .....	46
Fig. 16: Effect of pH on sorption of (a) Pb(II) and (b) Cu(II) by GO and GO-m $\beta$ CD (1 mg/mL dosage, contact time: 2 h, concentration: 10 mg/L).....	47
Fig. 17: Effect of contact time on sorption of (a) Pb(II) and (c) Cu(II) on GO and GO-m $\beta$ CD and pseudo-second-order kinetics of (b) Pb(II) and (d) Cu(II) sorption on GO and GO-m $\beta$ CD (1mg adsorbent/mL solution, pH: 6, contact time: 120 min, concentration, 10 mg/L). ...	49

Fig. 18: The plots of intra-particle diffusion (a) and liquid film diffusion (b) for the sorption of Pb(II) on GO and GO-m $\beta$ CD.....	50
Fig. 19: Sorption isotherm for (a) Pb(II) and (b) Cu(II) by GO and GO-m $\beta$ CD (pH: 6, 1 mg adsorbent/mL solution, concentration: 10-200 mg/L) .....	52
Fig. 20: Sorption of Pb(II) ions onto GO-m $\beta$ CD in the presence of Cu(II) ions .....	55
Fig. 21: Desorption of Pb(II) from GO-m $\beta$ CD at different pH values .....	56
Fig. 22: The reusability of GO-m $\beta$ CD in five consecutive cycles.....	57
Fig 23: The FT-IR spectra of pMWCNT, oMWCNT and oMWCNT/Ppy .....	58
Fig. 24: The SEM micrographs of pMWCNT (a), oMWCNT (b) and the oMWCNT/Ppy (c) ....	59
Fig. 25: The particle distribution the pMWCNT, oMWCNT and oMWCNT/Ppy .....	60
Fig. 26: Raman spectra of pMWCNT, oMWCNT and oMWCNT/Ppy .....	61
Fig. 27: TGA spectra of pMWCNT, oMWCNT and oMWCNT/Ppy .....	62
Fig. 28: Effect of pH on sorption of (a) Pb(II) and (b) Cu(II) by pMWCNT, oMWCNT and oMWCNT/Ppy (1 mg/mL dosage, contact time = 1 h, concentration = 10 mg/L).....	63
Fig. 29: Sorption isotherm of (a) Pb(II) pH = 6 and (b) Cu(II) pH = 5 on pMWCNT, oMWCNT and oMWCNT/Ppy (pH = 5, m/V = 1 mg/mL, concentration = 10-100 mg/L) .....	66
Fig. 30: Effect of contact time on sorption of (a) Pb(II) pH = 6 and (b) Cu(II) pH = 5 on pMWCNT, oMWCNT and oMWCNT/Ppy (m/V = 1 mg/mL, concentration = 10 mg/L) .....	69
Fig. 31: Plots of intra-particle diffusion for the sorption of (a) Pb(II) and (b) Cu(II) on pMWCNT, oMWCNT and oMWCNT/Ppy (m/V = 1mg/mL, concentration = 10 mg/L)	70
Fig. 32: Sorption of (a) Pb(II) ions and (b) Cu(II) ions onto oMWCNT/Ppy in a single and binary metal ion system .....	72
Fig 33: The reusability of oMWCNT/Ppy in five cycles.....	73

# CHAPTER 1

## INTRODUCTION

### 1.1 Background of study

Water quality has emerged as a global issue and will become increasingly important in the future because pure clean drinking water is an important factor in determining the quality of life. However, industrial effluents from acid mines, agrochemical plants, textile plants, tanneries, electroplating facilities, and agricultural runoffs containing residues of pesticides and fertilizers among other anthropogenic activities are presenting challenges in providing clean water (Reza & Singh, 2010). These activities have caused redistribution of heavy metals in the aquatic systems such that these polluting metal ions have reached levels that present harm to both humans and aquatic life (Marques, Rosa, & Pinheiro, 2000). The challenge of removing these heavy metals from the wastewater before discharging it to the environment is still unmet.

The heavy metal ions are non biodegradable and hence they tend to bioconcentrate in living things and at certain levels they become toxic. These metals include: lead, copper, mercury, arsenic, chromium, cadmium among others. Lead has been found in paints, while copper is found in pesticides. Both of these metals have been found in old water piping systems, metal recycling plants, dumpsites and some traces are found in fertilizers (Ochieng, Lalah & Wandiga, 2007; Ndeda & Manohar, 2014). Locally, lead poisoning has been reported in Uhuru-Owino slums in Mombasa which was as a result of discharge from a lead-acid accumulator recycling plant (Okeyo & Wangila, 2012). Recently, the Kenya Bureau of Standards (Kebs) reported that the sugar meant for household use contained high levels of copper and lead (Kebs, 2018). Lead and copper metals are of particular interest because exposure to high levels of lead attacks the brain and the nervous system (Joachim & Felistas, 2000) and accumulation of copper in the body can damage to vital body organs such as the kidney, liver and brain (Bertinato & L'Abbe, 2004; Nordberg, Flower, Nordberg, & Friberg 2007). The removal of these metals from the environment is paramount in order to prevent or reduce the damage caused by these metals in humans

Numerous water treatment methods have been used and reported to remove heavy metals from wastewater, these include; membrane filtration, chemical precipitation, electrochemical techniques, solvent extraction, coagulation-flocculation, ion-exchange, evaporation,

concentration and adsorption among other methods (Droste & Gehr, 1997; Li *et al.*, 2003a; Sekar, Sakthi, & Rengaraj, 2004; Kurniawan, Chan, Lo, & Babel, 2006a; Liu, Bai & Ly, 2008). The disadvantages associated with most of these methods are the consumption of large amounts of reagents and energy, and as a consequence they produce large amounts of toxic sludge that need further treatment. Another limitation is the high equipment capital cost, requirement of specialized personnel and time consumption (Kurniawan, Chan, Lo, & Babel, 2006b). However, the adsorption method has received a lot of attention recently due to its versatility, robustness, simplicity and cost effectiveness for the removal of pollutants from water (Babel & Kurniawan, 2003).

The surface properties of an adsorbent such as pore size distribution and surface functionalities have an influence on its adsorption capacity. Larger surface area results to increased exposure of the adsorbates to the active sites of the adsorbent during sorption (Mohanty, Das, & Biswas 2008). Several natural adsorbents such as activated carbon made from wool, egg and coconut shell (Sekar *et al.*, 2004), and banana peel (Annadurai, Juang, & Lee, 2003) have been studied for adsorption. Other common adsorbents like; resins (Diniz, Doyle, & Ciminelli, 2002), clay (Amer, Khalili, & Awwad, 2010; Alsewailem & Aljlil, 2013) and zeolites (Biskup & Subotic, 2004) have also been studied. Despite the fact that these materials are readily available and relatively inexpensive, they have relatively low adsorption efficiencies due to their relatively moderate surface area to volume ratio, long diffusion paths and irregular adsorption sites (Wan Ngah & Hanafiah, 2008; Barakat, 2011). The listed drawbacks have led to the continued research for more innovative adsorbents with higher adsorption efficiencies.

The advancement in nanotechnology has led to the development of nanoadsorbents that have large surface area, accessible active sites and short diffusion paths. These nanoadsorbents include the carbon based adsorbents; graphene, carbon nanotubes and their composites which have been reported to possess a great potential of removing heavy metal ions from water (Zhao, Ren, & Chen, 2012). Graphene; an atom-thick single layer of carbon atoms in a closely packed honeycomb hexagonal two-dimensional lattice, is the basic building block for graphitic materials such as graphene oxide, fullerene, carbon nanotubes (CNT) and other carbon materials (Geim & Novoselov, 2007).

Graphene and its related nanocomposites have been studied for various applications including; energy related materials, sensors, biomedical materials because of their excellent mechanical, electrical, thermal properties and large surface area (Novoselov *et al.*, 2004; Park & Rouff, 2009). Due to its high specific surface area (theoretical value,  $2630 \text{ m}^2 \text{ g}^{-1}$ ), graphene based adsorbents have been synthesized and applied in the removal of heavy metal ions from aqueous solutions (Huang *et al.*, 2011; Hao *et al.*, 2012; Sui, Meng, Zhang, Ma, & Cao, 2012). The introduction of different functional groups is a possible route to enhance the adsorptive performance of graphene and related materials. As a result, large quantities of lead and copper adsorbed by graphene oxide (GO), an oxidized derivative of graphene, has been attributed to a larger surface area and the oxygen functionalities of the graphene oxide (Wu *et al.*, 2013; Opeyemi, Adebola, Gururaj, & Aderemi, 2014).

The presence of effective functional groups for sorption enhances the sorption capabilities of a sorbent by forming specific bonds with metal ions and improving its dispersion properties in aqueous solutions. Cyclodextrins (CDs) are composed of glucose units that have a truncated conical shape characterized by hydrophobic inner cavity and hydrophilic exterior containing hydroxyl groups. Studies have shown that cyclodextrins can selectively bind organic and inorganic molecules through their hydrophobic cavities by forming guest-host complexes (Li *et al.*, 2013; Wang *et al.*, 2014, Shanshan, Yang, Xiaobin, Fengbao, & Guoliang, 2014). In addition, the exterior hydroxyl groups on the CDs have been reported to form complexes with metal ions (Badruddoza, Tay, Hidayat, & Uddin, 2011; Huang, Liu, Zhang, Xu, & Hu, 2012). The hydrophilic exterior of CDs makes them dispersive reagents due to their excellent film-forming ability, as a result CDs have been used to disperse or functionalize graphene (Guo *et al.*, 2010). The methyl- and hydroxy- substituted  $\beta$ CDs are more water soluble derivatives of  $\beta$ CDs (Zhang *et al.*, 2014). Though GO has shown great potential in the sorption of heavy metal ions, attaching of  $\beta$ CDs onto it has been seen to enhance its dispersibility property (Konkena & Vasudevan, 2012; Zhang *et al.*, 2014) hence attaching methyl-beta-cyclodextrin (m $\beta$ CD) onto GO may result to a composite that is more dispersible in water and thus enhancing its adsorption capacity. The combined properties of the m $\beta$ CD and GO may result to a composite with superior adsorption capacity compared to the m $\beta$ CD or GO adsorbent used individually. Thus, there is need to understand the nature and interaction of such an adsorbent for the removal of lead (II) and copper (II) ions from water.

Carbon nanotubes (CNT) are also being widely studied for various applications including electrical materials and water remediation due to their unique properties such as high conductivity, chemical stability and large surface area (An *et al.*, 2001; Kim, Nam, Ma, & Kim, 2006; Rao, Lu, & Su, 2007). CNT and functionalized CNT have been found to have good adsorbent capacities for heavy metal ions in aqueous solutions due their unique morphologies (Li *et al.*, 2002; Lu & Chiu, 2006; Rao *et al.*, 2007).

On the other hand, polypyrrole (Ppy) is a polymer matrix that carries charges via  $\pi$ -electrons on nitrogen atoms that provides a good prospect for its applications in adsorption of heavy metal ions (Seid, Chouder, Maouche, Bakas, & Barka, 2014; Mahmud, Hosseini, & Yahya, 2014). Several composites of Ppy have been studied for the removal of heavy metal ions from water including; bantomite-Ppy composite (Alawa, Srivastava, Srivastava, & Palsania, 2015) and rice husk ash-Ppy (Sobhy & Reyad, 2015). Oxidised CNT are better adsorbents than pristine CNT because the negative charges of oxygen functional groups on the surface of the CNT donate electron pairs to metal ions facilitating cation exchange (Shim, Park, & Ryu, 2001; Dai, He, & Li, 2003), and also these groups make CNT hydrophilic enhancing their adsorption capacity. Therefore, a composite of CNT and Ppy would utilize both the electron pairs of the functional groups on the CNT surface and the  $\pi$ -electrons from the amine groups on Ppy- with possible prospects of improved heavy metal removal from water through synergy between these two nanoadsorbents. Sahmetlioglu, Wilma, Acts, & Skylark (2014) performed a column study on the adsorption of Pb(II) from aqueous solution using such a composite. However, there is limited understanding, if any, on the adsorption capacity of OCNT/Ppy composite through batch adsorption process. A study, therefore, is necessary to synthesize OCNT/Ppy composite and study its application in the batch adsorption of heavy metals like copper (II) and lead (II) ions from water for better understanding of the chemistry involved.

The adsorption capacities of adsorbents to remove metal ions from water have been reported to be a function of the initial pH of the solution, contact time, initial metal ion concentration and adsorbent dosage (Kosa, Al-Zhrani, & Salam, 2012; Wu *et al.*, 2013). The equilibrium adsorption conditions of the proposed adsorbents are also not yet reported; therefore, the optimum adsorption conditions of pH, contact time, initial metal ion concentration should be established.

Sorption of ions is a competitive process between ions present in a solution; hence, the study of removal of single metal ions in solution has imperfect practical applications (Li *et al.*, 2003a). Instead competitive adsorption is what takes place when two or more metals adsorb to the same adsorption sites in wastewater (Stafiej & Pyrznska, 2007; Ryan, Tartakovsky, & Amon, 2011). The relative efficiencies of the nanocomposites have been reported in competitive adsorption studies to be relatively higher for individual metal ion in solution than in binary metal aqueous solutions (Li *et al.*, 2003a; Sitko *et al.*, 2013). Hence, there is need to establish the competitive adsorption capacities of these proposed adsorbents in removing heavy metals in the presence of other metal ions.

The cost effectiveness of any adsorbent is its reusability. The repeated use of an adsorbent through adsorption-desorption cycles reduces the overall cost of the adsorbent. Desorption of the metal ions from the surface of the adsorbent strongly depends on the pH of the regeneration solution. Studies on the regeneration of both CNT and GO have shown that desorption of metal ions is higher at lower pH than at higher pH (Li *et al.*, 2005; Wu *et al.*, 2013). The adsorbents of CNTs and GO have shown the potential of being reused in a number of treatment times. Hu *et al.* (2010) and Vukovic *et al.* (2011) reported that iron oxide/MWCNT/CDs and eMWCNT could be utilized up to five cycles, respectively. According to Wu *et al.* (2013) the adsorption capacity of GO was maintained above 95% of its initial capability after five cycles and above 90% after ten cycles. There is no documentation showing the viability of the proposed adsorbents in order to establish the how many times they can be reused.

## **1.2 Statement of the problem**

Heavy metals in water are a risk to human health. Several methods of water treatment that have been used to remove the heavy metals have unmet challenges such as need for high operational pressures, aggregation and high consumption of reactants. The use of adsorbents is, at present, the most popular method used to treat wastewater. However, the problems associated with the conventional adsorbents include relatively moderate surface area and irregular adsorption sites hence they have relatively lower absorption capacities. Graphene and carbon nanotubes have relatively large surface area than conventional adsorbents; however, there is need to enhance their adsorption efficiencies by grafting onto them other functionalized nano-adsorbents to increase their performance through synergy. The adsorption of any adsorbent is dependent on the

conditions of target adsorbates such as pH and concentration, hence, the need for optimization of these conditions. At the same time, the presence of other adsorbates related to target adsorbates in the same solution have an effect on the adsorption efficiency of any adsorbent, therefore, their influence should be determined.

There is need, therefore, to develop adsorbents with more efficient adsorption capacities for heavy metal ions like Cu(II) and Pb(II) ions from water. This challenge could be tackled by studying the synthesis of GO grafted with materials like methyl- $\beta$ -cyclodextrin and polypyrrole conjugated oxidized multi-walled CNT nanocomposites and apply these nanocomposites in the removal of Cu(II) and Pb(II) ions from water. This development challenge invites the need for understanding the nature of the interacting materials by characterizing them.

### **1.3 Objective of the Study**

#### **General objective**

To synthesize and characterize graphene oxide modified with methyl- $\beta$ -cyclodextrin and oxidized multi-walled carbon nanotubes incorporated with polypyrrole adsorbents, and optimize the removal of copper (II) ions and lead (II) ions from aqueous solution using these adsorbents.

#### **1.4 Specific objectives**

In order to achieve the above broad objective, this work intended to:

- i. Synthesize and characterize graphene oxide modified with methyl- $\beta$ -cyclodextrin
- ii. Synthesize and characterize oxidized multi-walled carbon nanotubes incorporated with polypyrrole (oMWCNT/Ppy).
- iii. Determine the effects of pH, contact time and concentration of the Cu(II) ions and Pb(II) ions using the derived adsorbents.
- iv. Determine the competitive sorption on the adsorbents of metal ions in binary aqueous systems.
- v. Determine the reusability of adsorbents.

#### **1.5 Research Questions**

- i. Can graphene oxide be functionalized with methyl- $\beta$ -cyclodextrin?

- ii. Can oxidized multi-walled carbon nanotubes be functionalized with polypyrrole?

### **1.6 Null hypothesis (H<sub>0</sub>)**

- iii. The efficiency of the synthesized GO-m $\beta$ CD and oMWCNT/Ppy nanocomposite is not affected by changes in pH, contact time and concentration of the Cu(II) ions and Pb(II) ions in their removal.
- iv. There is no sorption competition by an individual metal ion on adsorption with the other metal ion in the same solution.
- v. The synthesized nanocomposites cannot be reused

### **1.7 Justification**

Bioaccumulation of heavy metal ions in the human body is a health concern because the presence of an unacceptable levels of Pb(II) and Cu(II) ions in the body cause irreversible damage to vital body organs. The removal of these metal ions from the environment is paramount. The development of an adsorbent that has higher adsorption efficiency than the conventional adsorbents for these heavy metal ions offers a solution to the reduction of these metal ions from water. This would contribute in minimizing the risks these metals pose to humans. Thus the focus has shifted to nanomaterials due to their remarkable properties such as high surface to volume ratio, ability to self-assemble and high specific reactivity. The economy of adsorbents dictates that an adsorbent should be relatively cheap and effectively recyclable for daily and extensive use. These nanoadsorbents are expected to have high adsorption capacities and to be effectively regenerated. In addition, the present extensive application of graphene and carbon nanotubes in many fields implies that there would be large scale production resulting to low costs. These properties, their cost effectiveness and ease of production would make them suitable alternative materials for the removal of heavy metal ions from water. Further still, functionalizing these carbon materials with other nanoadsorbents would result to nanocomposites that are expected to work faster and have relatively higher binding capacity for the target heavy metal ions. The adsorption efficiency of any adsorbent is uniquely dependent on specific application conditions of the adsorbates which include the pH, contact time and concentration of adsorbates. Thus, maximum

utilization of the adsorbents demands that adsorption is performed at the optimum adsorption conditions of target adsorbates. Furthermore, an understanding of the competition for sorption sites on the adsorbents for adsorbates occurring together with target adsorbates should also be established.

### **1.8 Significance of the Study**

The derivatization of graphene oxide and CNT with other nanoadsorbents would result to the formation of nanocomposites with relatively higher adsorption efficiencies than the conventional adsorbents thus reducing the cost of removing heavy metals from water. The knowledge on the optimum adsorption conditions of pH, contact time and metal ion concentration by these adsorbents will help the user -at industrial or domestic levels- on the effective way to apply these adsorbents economically.

Knowledge of the adsorption efficiency of these adsorbents for one metal ion in the presence of another metal in a solution will lead to optimum use of then adsorbent. On the other hand, the knowledge on the reusability of these adsorbents would lead to their maximum utilization, hence reduce their overall cost.

## CHAPTER 2

### LITERATURE REVIEW

In this section the following will be discussed: the sources of heavy metal ions in water and the effects of heavy metal ions on humans, the conventional techniques for removal of heavy metal ions in water, the carbon based nanoadsorbents in particular graphene and carbon nanotubes, the synthesis and characterization of graphene and carbon nanotube composites, factors influencing the sorption of heavy metal ions on an adsorbent, the sorption mechanisms, competitive sorption of metal ions and regeneration of adsorbents.

#### **2.1 Heavy metal ions in water: sources of contamination and effects**

Toxic heavy metals which include: lead, copper, zinc, mercury, cadmium, arsenic, chromium and nickel are of particular concern in wastewater treatment. They originate from anthropogenic sources such as domestic wastewater, untreated industrial effluents, municipal wastewater and fertilizers (Reza and Singh, 2010). These trace elements in water interfere with the survival and growth of aquatic life (Odiete, 1999), and also present a long-term source of contamination to higher trophic organisms through the food chain (Odiete, 1999; Loska & Wiechula, 2003). Some heavy metals such as manganese iron, chromium, copper and zinc are essential micronutrients but their presence in large quantities may be extremely dangerous (Rao Ramesh, Rao & Sessaiah, 2006; Nordberg, Flower, Nordberg, & Friberg, 2007).

Lead sources include leaded paints and some water piping systems while copper emanates from pesticides, fertilizers and old water piping systems. Locally, Okeyo & Wangila (2012) reported lead poisoning in the Owino Uhuru slums in Mombasa which was emanating from smelting of recycled lead-acid accumulators. The report indicated that population within this environment and those working within plant had been exposed to high levels of lead from the plant. In a study on the blood lead levels in selected areas in Kenya, Kimani (2007) found out that there was a significant environmental and occupational human exposure to lead in Nairobi. Lead and copper exposure results to the irreversible damage on vital body organs. Lead poisoning can lead to damages on the brain and the central nervous system while copper can cause damage to the kidney, brain and liver. This study therefore focused on the heavy metals lead and copper metal ions and their removal from water.

### **2.1.1 Lead**

Lead is non-biodegradable toxic heavy metal that easily accumulates in the human body. Some of the sources of lead include lead paints, some water pipes and emissions from metal recycling plants (Okeyo & Wangila, 2012). Trace levels are also found in fertilizers (Mortvedt, 1995; Lawrence & Brian, 2002). When discharged into the environment before proper treatment, industrial and municipal wastewater, results to accumulation of lead in the ecosystem which is eventually transported into water bodies (Stokinger, 1981).

Lead bioconcentrates and bioaccumulates in food chains resulting to a myriad of problems in living things (Needleman, 2004). Such problems include disruption of biosynthesis of haemoglobin, a rise in blood pressure, kidney damage, miscarriages and abortions, disruption of the nervous system, brain damage and decline in fertility in men through sperm damage (Joachim & Felistas, 2000). Lead entering into the aquatic system exerts a specific toxic effect on fish blood and tissues (Mousa & Khattab, 2003; Vosyliene & Kazlauskiene, 2004). It also causes neurological problems which occur during foetal development (Goyer & Clarkson, 2001).

According to United States Environmental protection agency the permissible limit of lead for surface water is 0.005 parts per million (ppm) (US EPA, 2016). However, studies have shown the levels of lead in surface water to be above these permissible limits. For instance, in Rift Valley lakes in Kenya the levels of Pb(II) in surface water were reported to be in the range of 0.0025-0.563 ppm (Ochieng *et al.*, 2007) and in Nairobi Dam, Kenya in a range of 11.67-16.78 ppm (Ndeda & Manohar, 2014). It is, therefore, necessary to remove lead ions from wastewater.

### **2.1.2 Copper**

Copper is introduced to water systems through industrial plants such as in the manufacture of fungicides, wood and phosphate fertilizers and also from some metal piping systems and municipal wastewater (Dameron & Howe, 1998). It has been used to control algal growth in water bodies and when poorly used it becomes toxic to living things (Horne & Dunson, 1995)

Copper is an essential micronutrient at low concentrations for animal metabolism. It aids in the electron transfer processes such as iron in haemoglobin, photosynthesis in plants and the terminal step of mitochondrial respiration and hence copper influences life and supports functions like production of red blood cells and carbohydrate synthesis (US EPA, 1980). However, in humans,

excess copper intake causes Menke's disease and Wilson's disease, generic disorders associated with accumulation of copper and damage to the vital body organs such as the kidney, liver and brain (Prasad & Oberleas, 1976; Bertinato & L'Abbe, 2004; Nordberg *et al.*, 2007).

The analysis of heavy metals in surface water in Rift valley lakes in Kenya by Ochieng *et al.* (2007) shows that the levels of copper ions were in the range of 0.0047-0.1 ppm and according to Ndeda & Manohar (2014) the copper levels in Nairobi Dam, Kenya were found to be in the range of 2.99-4.90 ppm. These levels of copper in these selected areas exceeded the US EPA tolerance limit for copper in surface water, which is 0.005 ppm. This gives an indication of the status of the surface water in this region. Continued research on methods of effectively removing copper ions from wastewater is, therefore, paramount.

## **2.2 Conventional techniques for the removal of heavy metals**

The removal of these heavy metal ions from water has been achieved using various techniques which include; membrane filtration, ion exchange, chemical precipitation, electrochemical deposition, solvent extraction, photocatalysis, coagulation-flocculation, evaporation, concentration, flotation and adsorption (Droste & Gehr, 1997; Li *et al.*, 2003a; Sekar *et al.*, 2004; Kurniawan *et al.*, 2006b; Liu, Bai & Ly, 2008). These methods have a given number of capabilities as well as limitations. For instance, membrane filtration process has high separation selectivity but it has high operational costs related to membrane fouling. Chemical precipitation is easy to operate and has low capital cost but it presents the problem of discharge of large quantities of hazardous waste. Coagulation-flocculation also produces large volumes of sludge while ion exchange which has high efficiency in the removal of heavy metals but presents the problem pollution through regeneration of resins (Marques *et al.*, 2000; Kurniawan *et al.*, 2006a; Al-Rashid, Somerfield, & Hilal, 2011; Abbas *et al.*, 2016). The merits and demerits of some of these techniques are summarized in Table 1.

Table 1: A summary of the merits and demerits of some heavy metal ions removal techniques

<b>Technique</b>	<b>Merits</b>	<b>Demerits</b>	<b>Ref.</b>
<b>Chemical precipitation</b>	Simple to operate and low capital cost	Large sludge generation, sludge disposal and ineffective for removal of low concentration of metal ions	Kurniawan <i>et al.</i> , 2006
<b>Ion exchange</b>	High removal efficiency	Resins are expensive and regeneration causes further pollution	Diniz <i>et al.</i> , 2002
<b>Coagulation and flocculation</b>	Good sludge settling and also removes turbidity	Large sludge generation and must be followed with other treatment techniques	Chang & Wang, (2007)
<b>Membrane filtration</b>	High separation selectivity and low pressure requirement	Membrane fouling hence costly and complex to operate	Kurniawan <i>et al.</i> , 2006
<b>Adsorption</b>	Easy operating conditions and high removal efficiency	Low selectivity	Barakat, 2011

Adsorption has of late received a lot of attention due to its simplicity and cost effectiveness for the removal of pollutants from water. At the same time, the adsorbents used can be regenerated using appropriate desorption processes (Kosa *et al.*, 2012). Clay (Alsewailem & Aljlil, 2013), activated carbon (Sekar *et al.*, 2004) and zeolites (Biskup & Subotic, 2004) are some of the adsorbents that have been reported for adsorption of heavy metal ions from water.

Natural clay is a low cost adsorbent but it has a relatively low specific surface area, thus relatively low adsorption capacity. For instance, the Brunauer, Emmett and Teller (BET) specific surface area (SSA) of kaolinite clay and that of illite clay has been reported to be 20 m<sup>2</sup> g<sup>-1</sup> (Suraj, Iyer, & Lilathambika, 1998) and 41 m<sup>2</sup> g<sup>-1</sup> (Macht *et al.*, 2011), respectively. However, modification of clay has been reported to enhance its adsorption capacity (Unuabonah, Olu-Owolabi, Adebowale, & Ofomaja, 2007; Amer *et al.*, 2010).

Other adsorbents that have been employed for the adsorption of metal ions include activated carbon (Hasar, 2003, Sekar *et al.*, 2004; Rao *et al.*, 2006), and those adsorbents obtained from readily available organic waste such as bagasse (Rao, Parwate & Bhole, 2002; Karnitz *et al.*, 2006), rice husks (Wong, Lee, Low, & Haron, 2003), crab shell (An, Park, & Kim, 2001), orange and banana peels (Annadurai, Juang, & Lee, 2003), peat (Ho & McKay, 2000), sludge (Pan, Lin,

& Hwa, 2003), reed black liquor (Sun, Zhang, Yang, & Li, 2007) among others. Some of the reported BET SSA values of activated carbon include; that obtained from sewage sludge with value of  $179 \text{ m}^2 \text{ g}^{-1}$  (de Andres, Orjales, Narros, de la Fuente, & Encarnacion, 2013) and from cassava peel with value of  $1183 \text{ m}^2 \text{ g}^{-1}$  (Sudaryanto, Hartono, Irawaty, Hindarso, & Ismadji, 2006).

Activated carbon adsorbent has widely been used in domestic and industrial water treatment; however, it is associated with the challenges of column fouling and high cost of regeneration. These materials may be readily available but they have irregular adsorption sites and some have relatively low adsorption capacity for the heavy metal ions. This has led to the continued research for more innovative adsorbents whose surfaces can be manipulated in order to attach other materials on them that have affinity for metal ions, to enhance their adsorption efficiencies.

Recent focus has thus been put on nanoadsorbents such as graphene and carbon nanotubes. Table 2 shows a list of various known adsorbents and the reported specific surface areas and as indicated, graphene has the highest specific surface area (SSA) of  $2630 \text{ m}^2 \text{ g}^{-1}$  and that of clay is  $41 \text{ m}^2 \text{ g}^{-1}$ . Thus this work focuses on these nanocarbon adsorbents.

Table 2: Various adsorbents and their respective specific surface area

<b>Adsorbent</b>	<b>SSA (<math>\text{m}^2\text{g}^{-1}</math>)</b>	<b>Method</b>	<b>References</b>
<b>Clay(Illite)</b>	41	$\text{N}_2$ gas adsorption	Macht <i>et al.</i> , 2011
<b>Activated carbon</b>	179	$\text{N}_2$ gas adsorption	Andres <i>et al.</i> , 2013
	1183	$\text{N}_2$ gas adsorption	Sudaryanto <i>et al.</i> , 2006
<b>Zeolites</b>	756	$\text{N}_2$ gas adsorption	Vyas & Kumar, 2004
<b>Graphene</b>	2630	Theoretical	Stoller <i>et al.</i> , 2008
<b>Graphene</b>	818	$\text{N}_2$ gas adsorption	Zhou <i>et al.</i> , 2014
<b>GO</b>	736.6	Methylene blue	Montes-Navajas <i>et al.</i> , 2013
<b>SWCNT</b>	1315	Theoretical	Peigney <i>et al.</i> , 2001
<b>MWCNT</b>	200	Theoretical	Peigney <i>et al.</i> , 2001
<b>MWCNT</b>	22.38	$\text{N}_2$ gas adsorption	Zhu <i>et al.</i> , 2003
	1670	$\text{N}_2$ gas adsorption	Raymundo-Pinero <i>et al.</i> , 2005

### 2.3 Carbon based nanoadsorbents

The search for carbon based adsorbents with higher SSA has led to the exploration on the adsorption abilities of carbon nanoadsorbents. These materials and their derivatives have been reported to have appreciably better adsorption capabilities than the conventional adsorbents such

as clay. Notable carbon based adsorbents that have been applied in the removal of heavy metal ions from water are graphene and CNT.

### 2.3.1 Graphene adsorbents and its derivatives

Graphene is a one atom thick  $\pi$ -conjugated hexagonal layer of carbon atoms as depicted by Roberts *et al.* (2010) in Fig.1 Recent research has found a great potential in graphene, its oxidized form - graphene oxide and its composites - in the adsorption of heavy metal ions from water. Since it was first isolated by Geim and Novoselov in 2007, graphene has been applied in many other areas due to its unique properties such as large specific surface area (Stoller, Park, & Zhu, 2008; Wang *et al.*, 2013), high thermal and electrical conductivity (Balandin *et al.*, 2008; Buglione, Bonanni, Ambrosi, & Pumera, 2012; He *et al.*, 2012) and high mechanical strength (Lee, Wei, & Kysar, 2008; Singh Chauhan & Mishra, 2011) among others. These properties, especially, the high specific surface area and strong adsorption capacity, have made graphene to find many areas of application including desalination of water (Cohen-Tanugi and Grossman, 2012), efficient adsorbents for other water pollutants (Huang *et al.*, 2011; Ren *et al.*, 2011; Leng, Guo, & Su, 2012; Zhang, Shi, & Zhang, 2013) and photocatalysis (An *et al.*, 2012; Khan, Chetia, & Vardhaman, 2012). However, aggregations through  $\pi$ - $\pi$  interactions of graphene sheets decrease the available surface area and reduce its adsorption capacity. This problem is tackled by introducing hydrophilic functionalities onto the surface of graphene sheets. The functionalities include oxygen containing groups or cyclodextrins.

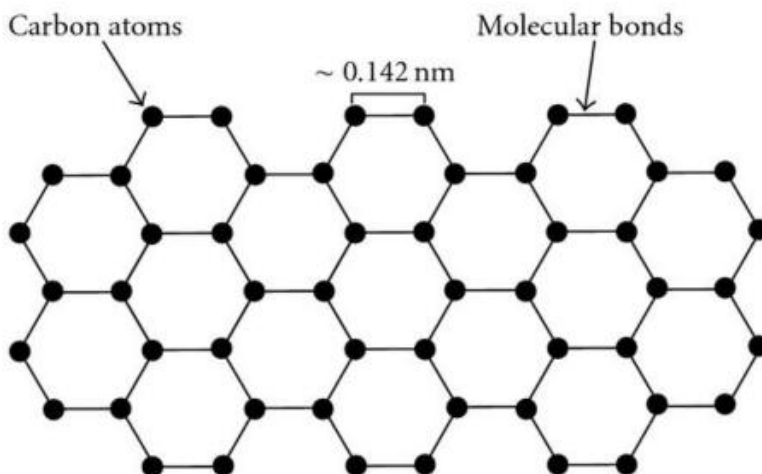


Fig. 1: Schematic of the structure of graphene sheet (Roberts *et al.*, 2010)

Oxidation and subsequent functionalization of graphene with molecules, which are hydrophilic and have affinity for target analytes improves the selectivity of graphene as an adsorbent and prevents aggregation (Sitko *et al.*, 2013). Based on this, various derivatives of graphene have been reported and applied in environmental remediation, and there is still need to further develop derivatives with improved selectivity and with low or possibly no aggregation. GO and reduced graphene oxides (rGO) are derivatives of graphene containing many functional groups such as -O-, -OH and -COOH, which form complexes with metal ions. The functional groups within and on the edges of GO sheets (Zadeh, Yu, Dehghan, Sbarski, & Harding, 2014), as seen in Fig 2, allows for modification and incorporation of different nanomaterials and polymers onto GO sheets to suit different applications (Yang *et al.*, 2010; Liu, Chen, Hu, Wu, & Wang 2011; Liu *et al.*, 2011; Madarang *et al.*, 2012). In most cases, these nanomaterials are either dispersal agents or they have additional functional groups to remove pollutants from water or both. The presence of dispersing agents such as cyclodextrins in graphene and its derivatives is desirable to enhance their adsorptive performance.

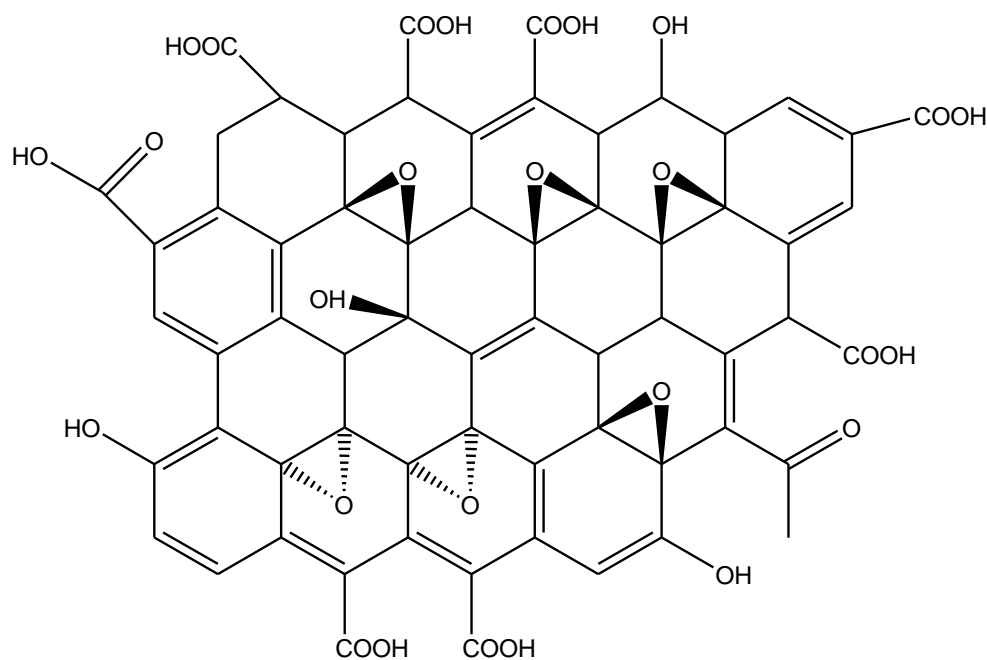


Fig. 2: The structure of a single sheet of graphene oxide (Zadeh *et al.*, 2014)

Cyclodextrins (CDs) are composed of six ( $\alpha$ -CD), seven ( $\beta$ -CD), or eight ( $\gamma$ -CD) glucose units with a truncated cone shape as shown in Fig. 3. They are characterized by a hydrophobic inner cavity and a hydrophilic exterior that enables them to form host-guest complexes with other molecules.

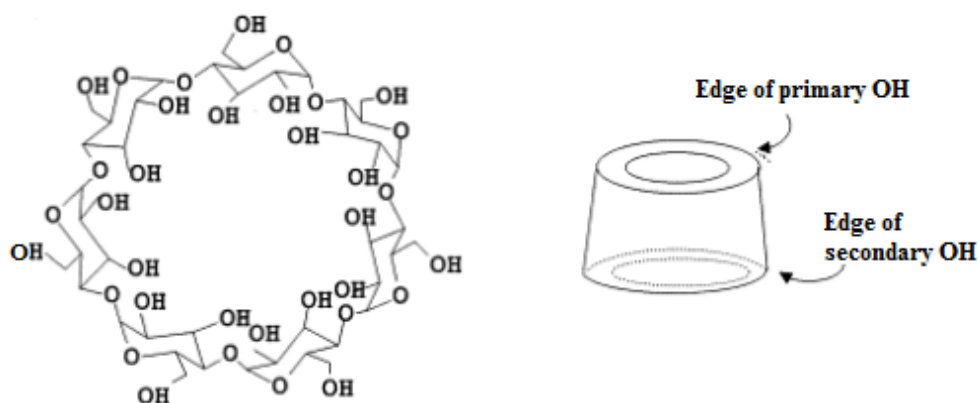


Fig. 3 The structure of  $\beta$ -cyclodextrin molecule (Rizzarelli & Vecchio, 1999)

CDs have been used to disperse and functionalize graphene (An *et al.*, 2010; Konkana & Vasudevan, 2012) due to their excellent film-forming ability and inclusion function. These unique properties allow selective entrapment of organic (Xu, Wang, Wan, Lin, & Wang, 2011) and heavy metal ions (Badruddoza, *et al.*, 2011; Abdolmaleki, Mallakpour, & Borandeh, 2015). The  $\beta$ CD incorporated on GO has been reported in the removal of  $\text{Cr}^{6+}$  (Li *et al.*, 2013; Wang *et al.*, 2014), methylene blue dyes (Fan *et al.*, 2012; Shanshan *et al.*, 2014) and sensing of phenolic organic pollutants (Xu *et al.*, 2011) in water. The hydroxyl groups on the exterior of  $\beta$ CD can form complexes with metals; hence it can remove metal ions from water (Badruddoza *et al.*, 2011; Huang *et al.*, 2012). Badruddoza *et al.* (2011) reported the removal of copper ions from water using carboxylatedmethyl  $\beta$ CD. GO $\beta$ CD has been reported for the removal of  $\text{Cr}^{6+}$  and cationic dyes (Fan *et al.*, 2012; Shanshan *et al.*, 2014), however, there is limited documentation on the removal of cationic metal ions using GO-m $\beta$ CD. Table 3 shows some of the reported studies on the application of graphene and its derivatives in the removal of heavy metal ions

from aqueous solutions as well as their sorption capacities in various conditions. It shows that graphene oxide is a better adsorbent than pristine graphene because it has the oxygen containing functional groups.

Table 3: Sorption capacities of graphene and its derivatives for some heavy metal ions from aqueous solutions at various conditions

Adsorbent/Ref.	Metal	q <sub>m</sub> (mg/g)	Application conditions			
			pH	I <sub>0</sub> (mg/L)	Temp(K)	C <sub>t</sub> (h)
Graphene <sup>a</sup>	Pb	22.4	4.0	40	303	15
Graphene <sup>a</sup>	Pb	35.2	4.0	40	303	15
GO <sup>b</sup>	Pb	-	-	100	-	1/3
GO <sup>f</sup>	Pb	1119	5.0		Room	
EDTA-GO <sup>c</sup>	Pb	367	6.8	5-300	Room	24
TiO <sub>2</sub> -GO <sup>d</sup>	Pb	35.6	5.6	-		-
GO <sup>e</sup>	Cu	117.5	5.3	-	-	2.5
GO <sup>f</sup>	Cu	294	5.0	-	Room	2

**a**-Huang *et al.* (2011), **b**-Opeyemi *et al.* (2014), **c**-Madadrang *et al.* (2012), **d**- Lee *et al.* (2012), **e**-Wu *et al.* (2013), **f**- Sitko *et al.* (2013), q<sub>m</sub>- maximum metal removal, I<sub>0</sub>- Initial metal ion concentration, C<sub>t</sub>- contact time

The βCD is water soluble and its derivative mβCD is considered to be even more soluble hence a better dispersive reagent (Zhang *et al.*, 2014). The GO-mβCD composite to be prepared in this study, will be expected to display better dispersibility, minimal aggregation and thus increased adsorption capacity through the aspect of synergic effect between the GO and mβCD. There is need, therefore, to synthesize GO-mβCD composite for the removal of lead (II) ions and copper (II) ions from water.

### 2.3.2 Carbon nanotubes (CNT) adsorbents

A CNT is sheet of graphene warped into a tube. Single individual tubes are known as single-walled carbon nanotubes (SWCNT), while concentric tubes are referred to as multi-walled carbon nanotubes (MWCNT) as shown in Fig 4. Common methods employed in their synthesis are arc discharge, laser ablation and chemical vapour deposition. The reactive sites of CNT are found on their fullerene ends which are usually functionalized to generate -COOH, -OH or -C=O (Dai *et al.*, 2003). Since CNT were first discovered by Iijima (1991) they have received attention due to their excellent properties such as high chemical and thermal stability and high

specific surface area of which they have found many areas of applications. They have been used in fuel cells (Che, Lakshmi, Fisher, & Martin, 1998), secondary batteries (Gao *et al.*, 1999) and for environmental remediation through adsorption of heavy metal ions and anions in solutions (Li *et al.*, 2002; Li *et al.*, 2003a) and other pollutants such as dioxin (Long & Yang, 2001), chlorobenzene (Peng *et al.*, 2003) and herbicides (Biesaga & Pyrzynska, 2006).

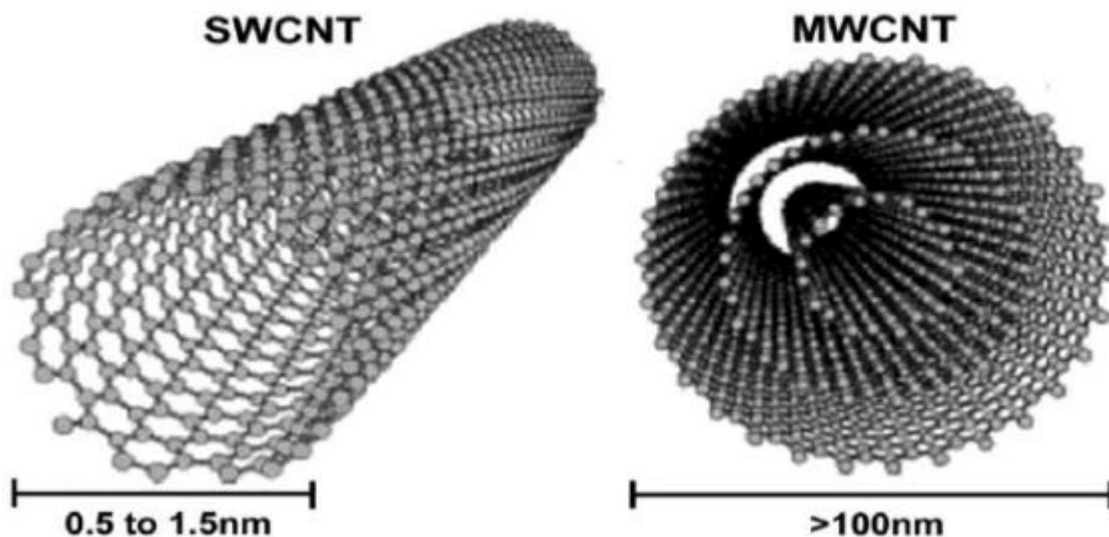


Fig. 4: Structure representation of SWCNT and MWCNT (Malhotra, Srivastava & Augustine, 2015)

Several studies have been done and reported on pristine and surface oxidized CNT sorption for divalent cations ( $\text{Cu}^{2+}$ ,  $\text{Cd}^{2+}$ ,  $\text{Ni}^{2+}$ ,  $\text{Pb}^{2+}$  and  $\text{Zn}^{2+}$ ) in aqueous solutions as well as their sorption capacities at various conditions. The Table 4 shows that the sorption capacities of metals ions by raw CNT are very low but they significantly increase after oxidation by  $\text{HNO}_3$ ,  $\text{NaOCl}$  and  $\text{KMnO}_4$  solutions (Rao *et al.*, 2007). The oxidation generates functional groups on the surface of the CNT that cause a rise in the negative charge which donates electron pairs to metal ions facilitating cation exchange (Shim *et al.*, 2001; Li *et al.*, 2002; Dai *et al.*, 2003; Shen *et al.*, 2010). Fig. 5 shows the schematic oxidation of CNT using various oxidizing agents and the adsorption of divalent metal ions. These functional groups on the surfaces of the tubes facilitate the attachment of other nanomaterials such as polypyrrole, thiophene among others onto CNT for various applications.

Table 4: The sorption capacities of raw and oxidized CNT for some divalent cations in aqueous solutions at various conditions

Adsorbents/Ref.	$q_m$					Conditions			
	Cd <sup>2+</sup>	Cu <sup>2+</sup>	Ni <sup>2+</sup>	Pb <sup>2+</sup>	Zn <sup>2+</sup>	pH	Temp	Mass	C <sub>0</sub>
CNT <sup>a</sup>				1.00		7.0	room	0.05	2-14
CNT(HNO <sub>3</sub> ) <sup>a</sup>				49.95		7.0	Room	0.05	2-14
SWCNT <sup>b</sup>			9.22			7.0	25	0.05	
SWCNT(NaOCl) <sup>b</sup>			47.9			7.0	25	0.05	
MWCNT <sup>b</sup>			7.53			7.0	25	0.05	
MWCTs(NaOCl) <sup>b</sup>			38.5			7.0	25	0.05	
CNT <sup>c</sup>	1.1					5.5	25	0.05	9.5
CNT(KMnO <sub>4</sub> ) <sup>c</sup>	11.0					5.5	25	0.05	9.5
CNT(HNO <sub>3</sub> ) <sup>c</sup>	5.1					5.5	25	0.05	9.5
SWCNT <sup>d</sup>					11.23	7.0	25	0.05	10-80
SWCNT(NaOCl) <sup>d</sup>					43.66	7.0	25	0.05	10-80
MWCNT <sup>d</sup>					10.21	7.0	25	0.05	10-80
CNT(HNO <sub>3</sub> ) <sup>e</sup>				35.6		5.0	25	0.05	10-80
CNT(HNO <sub>3</sub> ) with Xylene-Fe <sup>f</sup>				14.8		5.0	Room	0.02	10-60
CNT(HNO <sub>3</sub> ) with benzene-Fe <sup>f</sup>				11.2					
CNT(HNO <sub>3</sub> ) with Propylene <sup>f</sup>				59.8					
CNT(HNO <sub>3</sub> ) with Methane-Ni <sup>f</sup>				82.6					
MWCNT(HNO <sub>3</sub> ) <sup>g</sup>	10.9	24.5	97.1			5.0	Room	0.05	
MWCNT <sup>h</sup>				2.0		5.5	Room	0.15	10-50
MWCNT(HNO <sub>3</sub> ) <sup>h</sup>				23.0		5.5	Room	0.15	10-50
MWCNT(cyclodextrin) <sup>h</sup>				12.3		5.5	Room	0.2	10-50

a-Li *et al.* (2002), b-Lu & Liu (2006), c-Li *et al.* (2003b), d-Lu & Chiu (2006), e- Li *et al.*(2005), f- Li *et al.* (2006), g-Li *et al.* (2003a), h- Hu *et al.* (2010).  $q_m$  = maximum sorption capacity (mg/g), Temp = temperature (°C), mass of adsorbent g/100mL solution, C<sub>0</sub> = initial metal ion concentration (mg/L).

Polypyrrole (Ppy) is a conducting polymer useful in composite materials (Pruneanu, Resel, Leising, Brie, & Grauper, 1997; Ding & Ram, 2005). Its unique properties such as electrical conductivity, environmental stability, nontoxicity, low cost and ease of preparation (Pruneanu *et al.*, 1997; Wu & Lin, 2006) makes it useful in combining it with nanoparticles to enhance the sensing of biomolecules (Spain, Keyes, & Forster, 2013) and removing of heavy metal ions (Hosseini, Mahmud, Yahya, Ibrahim, & Djordjevic, 2015).

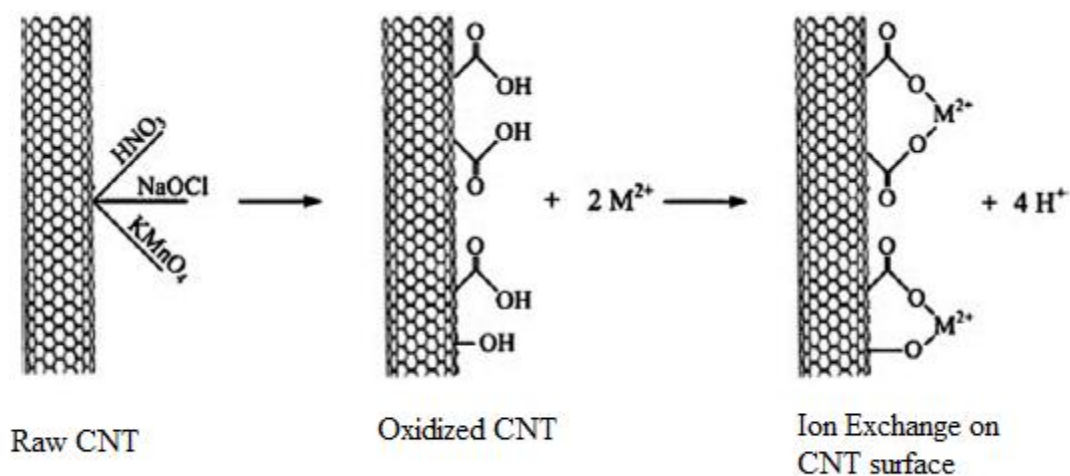


Fig. 5: Schematic of oxidation of CNT (Rao *et al.*, 2007)

Ppy carries charges via  $\pi$ -electrons on nitrogen atoms in the polymer matrix (as shown in Fig. 6) which provides a good prospect for its applications in adsorption of heavy metals. To maintain charge neutrality, some of the counter ions are incorporated into the growing polymer chain. The sorption of Cr (VI) onto Ppy/ $\text{Fe}_3\text{O}_4$  has been previously reported and it was seen to be time dependent (Bhaumik, Setshedi, Maity, & Onyango, 2013).

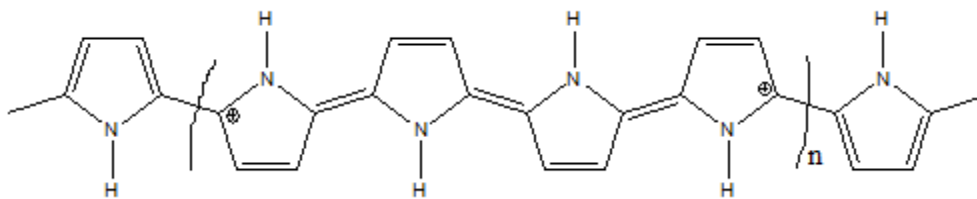


Fig. 6: Representation of the structure of polypyrrole

In this study, Ppy will be utilized as the covalent modifier to fabricate functionalized MWCNT which is relatively soluble in water. It is, therefore, necessary to synthesize a composite of oxidized CNT coated with Ppy denoted as OMWCNT/Ppy and establish its interaction with lead (II) and copper (II) ions.

## 2.4 Synthesis of the adsorbents

Combining other nanoadsorbents onto GO or OMWCNT could generate composites which may have positive interactive or synergetic properties that could be better than individual GO and OMWCNT adsorbents. The following are the reported processes that have been used to attach other nanoadsorbents to GO and OMWCNT.

### 2.4.1 Synthesis graphene oxide composites

Graphene oxide is obtained by the oxidation of the abundantly available natural graphite flakes. Oxidation of graphite was first reported by Brodie (1859) in which graphite flakes were oxidized with sulphuric acid and fuming nitric acid. Since then, the oxidation process has undergone several modifications to improve the level of oxidation; such as the Hummers method in which oxidation of graphite begins with the use sodium nitrate and sulphuric acid mixture followed by further oxidation with potassium permanganate. A modification of Hummers' method (Marcano *et al.*, 2010) is the highly used and common technique. It involves preoxidation of graphite using potassium pentoxide and potassium persulphate followed by a further oxidation using potassium permanganate. Hydrogen peroxide is added to reduce the excess potassium permanganate. The attachment of  $\beta$ CD onto GO has been reported to be either covalent (Feng, Max, & Lin, 2012; Konkena & Vasudevan, 2012; Zhang *et al.*, 2014) or non covalent (Guo *et al.*, 2010; Kuila *et al.*, 2012). Covalent attachment exploits the reactive carboxylic groups at the edges of GO sheets which are linked to the  $\beta$ CD cavities via an amide bond by using appropriate linkers. For instance, Konkena and Vasudevan (2012) reacted the carboxylic groups on GO with  $\beta$ -aminocyclodextrin using 1-ethyl-3-(3-dimethylaminopropyl)-carbodiimide hydrochloride (EDC) and N-hydroxy succinimide (NHS) as linkers. While non covalent attachment involves physically mixing GO with  $\beta$ CD that results aggregation. Covalent linkage involves the use of many chemicals that are used as linkers which makes the method more costly and environmentally unfriendly. Therefore, the synthesis of GO-m $\beta$ CD composite in this study was done by attachment of m $\beta$ CD onto GO through *in situ* aggregation. There is need to determine the nature and chemistry for this GO-m $\beta$ CD composite for application in sorption.

### **2.4.2 Synthesis of multi-walled carbon nanotube composite**

The CNT undergo oxidation to alter their surface properties such as surface area, surface charge, hydrophilicity and dispersion thus enhancing their adsorption capacity. The most common technique used is acid treatment, in which different oxidizing agents (such as HNO<sub>3</sub>, HF, HNO<sub>3</sub> and H<sub>2</sub>SO<sub>4</sub> combined, KMnO<sub>4</sub> are used), at different concentrations have been reported (Li *et al.*, 2002; Li *et al.*, 2003b; Lu & Liu 2006). Different oxidation procedures (sonication, soaking, refluxing), varying oxidation temperature and duration have also been employed (Xing, Chusuei, & Hull, 2005; Wepasnick *et al.*, 2011; Andrade *et al.*, 2013). The acid treatment mainly introduces carboxylic groups on the CNT surfaces. Another technique used to introduce oxygen containing groups on CNT surfaces is microwave-excited surface wave plasma treatment (Hu *et al.*, 2010; Ren *et al.*, 2011). The surface of OMWCNT can be modified further by use of polymers to improve their adsorption capacity for metal ions.

Polymer attachment onto CNT is covalent (Massoumi, Jaymand, Samadi, & Entezami, 2014) or non covalent (Chang, Wu, & Lin, 2014). Covalent linkage involves the activation of the carboxylic groups on the CNT surfaces which are linked to the polymers through grafting (Ma, Siddiqui, Marom, & Kim, 2010). On the other hand, non covalent linkage of polymers to CNT involves mixing of a monomer and CNT followed by the usual chemical oxidative polymerization using an appropriate oxidant such as ferric chloride, ferric sulfate among others (Omarova, Trchova, Kovarova, & Stejskal, 2003). The attachment is achieved through van der Waals forces and  $\pi$ - $\pi$  stacking between the CNT and the polymer chains containing aromatic rings. The non covalent method is easy to use, environmentally friendly and inexpensive. Hence, this study will apply the non covalent approach in the synthesis of the composite of CNT and Ppy. The chemistry and nature of this composite for batch adsorption process need to be determined.

### **2.5 Characterization of graphene oxide and carbon nanotubes**

Characterization provides information such as the morphology, composition, crystalline structure of a given material, which may give insight on the mechanism action of the material concerned. At the same time, characterization is a vital tool for showing whether the attachment of one adsorbent to another to form the composite is successful or not. The following are the techniques commonly used for characterization of GO and CNT.

### 2.5.1 Characterization of graphene oxide and composite

Several techniques have been applied in the characterization of GO and its composites in order to understand the mechanism of GO and its composites in the removal of heavy metals from water. These techniques include; Fourier transform infrared spectroscopy (FTIR), Raman spectroscopy, X-ray diffraction (XRD), scanning electron microscopy (SEM) and thermogravimetric analysis (TGA).

FTIR spectroscopic analysis is a tool that characterizes the GO and its composites by distinctly showing the functional groups present in the materials. Normally the characteristic peak at  $3430\text{ cm}^{-1}$  would be associated with the O–H stretching and vibrations of the skeletal hydroxyl groups, while the peak around  $1630\text{ cm}^{-1}$  indicates the skeletal graphitic domains of (C=C) in GO, the peak at  $1725\text{ cm}^{-1}$  shows the C=O stretching of COOH and  $1043\text{ cm}^{-1}$  bands that are associated with C–O stretching mode in hydroxyl or epoxy groups COH/COC as noted by Zhang *et al.* (2014). The FTIR spectrum of  $\beta$ CD have been reported to show absorption bands at  $2923\text{ cm}^{-1}$  and  $1367\text{ cm}^{-1}$  corresponding to the  $-\text{CH}_2-$  stretching and  $-\text{CH}-$  bending vibrations, respectively, and the characteristic band of the coupled C–O/C–C vibrations at  $1020\text{ cm}^{-1}$  (Fan *et al.*, 2013; Zhang *et al.*, 2013). The composite GO-m $\beta$ CD spectra has the characteristic peak at  $1630\text{ cm}^{-1}$  of GO and the characteristic band C–O/C–C of CD, as well as, the characteristic peak  $3400\text{ cm}^{-1}$  of -OH is found in both GO and  $\beta$ CD spectra (Zhang *et al.*, 2013).

FTIR spectroscopy analyzes molecules with a dipole moment the Raman focuses on molecules with polarizable bonds. Hence, some IR-inactive modes are Raman active and vice versa; as a result Raman technique complements IR spectroscopy. Raman spectroscopy uses a laser to interact with molecular vibrational modes and phonons in a sample, shifting the laser energy down (Stokes) or up (anti-Stokes) through inelastic scattering (Gardiner, 1989). It is therefore useful in the characterization of graphene and related materials, especially in distinguishing the ordered and disordered carbon in a structure. The main peaks of interest resulting from the Stokes photon energy shift caused by laser excitation of graphene (Saito, Hoffman, Dresselhaus, Jorio, & Dresselhaus, 2011) are; G-band ( $< 1580\text{ cm}^{-1}$ ) a primary in plane vibrational mode associated with graphitic two dimensional hexagonal lattice corresponding to  $\text{sp}^2$  of carbon, 2D ( $2690\text{ cm}^{-1}$ ) second order overtone of a different in plane vibration and the D-band ( $< 1350\text{ cm}^{-1}$ ) which represents  $\text{sp}^3$ -hybridized carbon which is associated with disorder in the graphitic

skeleton (Wang, Zhan, Qiao, & Ling, 2011). The D peak is invisible in pristine graphene but as the amount of disorder in graphene increases Raman intensity for the disorder peaks increases. The ratio of their intensity ( $I_D/I_G$ ) is therefore used to indicate the rate of disorder present in the graphitic skeleton in graphene and carbon nanotubes. Monitoring of oxidation of multi walled carbon nanotubes by Raman spectroscopy has been reported (Osswald, Havel, & Gogosti 2006; Costa, Borrowiak-Palen, Kruszynska, Bachimatink, & Kalenczuk, 2008). Song *et al.* (2013) and Wang *et al.* (2014) reported that after attaching  $\beta$ CD onto GO there is an increase in the  $I_D/I_G$  ratio which result from an increase in defects on the GO surface resulting from the incorporation of  $\beta$ CD and an increase in the number of  $C_{sp^3}$  present in the structure of CD.

The XRD patterns have been reported to show strong diffraction peak of GO is located at  $2\theta = 10.7^\circ$  which corresponds to GO (001) crystallographic plane as observed by Hu *et al.* (2014). However, after incorporating  $\beta$ CD broad peaks appear in place of the sharp peak on GO due to disordered stacking resulting from the introduction of  $\beta$ CD onto GO and a broad peak at  $2\theta = 18^\circ$  which is associated with  $\beta$ CD is observed (Hu *et al.*, 2014; Zhou *et al.*, 2014). The XRD peaks can therefore be used to determine the incorporation of other molecules onto GO.

SEM is an important tool for examining the morphology and topography of a material. Studies show that the morphologies of GO reveal large two dimensional layers stacked together which appear smooth albeit with few wrinkles. However, after modification with  $\beta$ CD the layer stacking becomes distorted while the surface gains some wrinkles (Song *et al.*, 2013; Zhang *et al.*, 2014). This tool can be used to determine the extent of modification of the GO with other molecules.

The TGA analysis of GO powder has been reported to show a weight loss below  $200^\circ\text{C}$  which is attributed to the loss off adsorbed water and a subsequent loss of weight at the temperature range of  $200\text{-}800^\circ\text{C}$  which is associated to the degradation of the oxygen functionalities (Konios, Stylianakis, Stratakis, & Kymakis, 2014). The  $\beta$ CD thermogram shows remarkable loss of weight below  $100^\circ\text{C}$  which is due to the hydrophilic groups in its exterior and a subsequent drastic weight loss around  $300^\circ\text{C}$ , which could be due to decomposition of the  $\beta$ CD (Hu *et al.*, 2014). The thermograms of GO composites have been reported to exhibit a weight loss in the range  $200\text{-}800^\circ\text{C}$  which has been attributed to the degradation of the oxygen functionalities (Song *et al.*, 2013; Hu *et al.*, 2014).

The functional groups, morphology, crystallographic structure of the GO-m $\beta$ CD are not known. The need to characterize the composite will also show the extent to which the m $\beta$ CD has been attached to the GO.

### 2.5.2 Characterization of multi-walled carbon nanotubes and composite

Various techniques have been employed to study the characteristics of CNT and their composites, some of these techniques are; FTIR, Raman spectroscopy, SEM, BET and TGA.

The FTIR analysis is useful in giving information on the functional groups in a material. The spectrum of pristine CNT has been reported to show 3436 cm<sup>-1</sup>, 2926 cm<sup>-1</sup> and 1637 cm<sup>-1</sup> corresponding to -OH, C-H and C=C stretchings, and after acid treatment the CNT show additional bands at 1725 cm<sup>-1</sup> associated with the C=O stretching in the COOH group as well as the 1360 cm<sup>-1</sup> and 1050 cm<sup>-1</sup> weak broad bands, attributed to C-O stretching in lactones (Vukovic *et al.*, 2011; Zhang & Xu, 2015). While the Ppy spectrum has the 1547 cm<sup>-1</sup> and 1462 cm<sup>-1</sup> band for C=C and C-C stretching vibration of pyrrole ring, respectively and the characteristic peaks at 780 cm<sup>-1</sup> and 1176 cm<sup>-1</sup> assigned to pyrrole ring vibrations (Sun, Xu, Wang, & Mao, 2002). The Raman spectroscopy is a vital tool at showing the changes in the graphitic skeleton of CNT which is similar to that in GO as indicated in section 2.5.1.

The SEM micrographs provide useful information on the morphology and topology of a material. Pristine CNT tend to agglomerate as a result their SEM pictures have been reported to show bundling and entangled nanotubes this phenomenon is attributed to their nano size and  $\pi$ - $\pi$  interaction. However, after acid treatment there is less entangling which is attributed to the introduction of oxygen functionalization on CNT surfaces (Rurille *et al.*, 2007). While the SEM micrographs of Ppy appear as flower-like particles. This is a useful tool in determining the incorporation of other molecules onto the CNT it therefore would complement the other characterization models.

The specific surface area and pore size distribution for CNT and its composites can be determined through BET adsorption data. BET analysis of CNT shows that they are microporous and that the micropores volume is decreased after the acidic treatment of pristine CNT which is due to the removal of amorphous carbons ( $C_{sp^3}$ ) (Li *et al.*, 2006).

The thermogravimetric experiments performed under N<sub>2</sub> have shown a slight weight loss at a temperature below 100°C which is associated with the evaporation of physi-sorbed water as has

been reported by Datsyuk *et al.* (2008). This is followed by further weight loss at temperature range 150-500°C corresponding to degradation of the carboxyl and hydroxyl groups on the oMWCNT walls and at above 800°C another weight loss attributed to the degradation of amorphous carbon was observed by Datsyuk *et al.* (2008). There is need to characterize the composite formed so as to establish the composition, graphitic structure and morphology in order to understand its adsorption mechanism.

## **2.6 Factors affecting the adsorption of heavy metal ions on an adsorbent.**

The main factors affecting the adsorption of heavy metal ions on the surfaces of CNT and GO and their derivatives include, among others, the initial pH of the solution, initial metal ion concentration of the solution, contact time, adsorbent dosage, and counter ions in the solution and temperature of the solution.

### **2.6.1 Initial pH of the solution**

Solution pH has been identified as the most important factor influencing sorption of metal ions because it affects surface properties of adsorbents such as CNT and GO. In addition, the pH of a solution has an influence on the hydrolysis, complexation and speciation of metal ions (Rao *et al.*, 2007; Kosa *et al.*, 2012). The sorption of cations is lower at low pH due to competition of sorption sites between hydrogen ions and the metal cations but at higher pH value the sorption of cations is higher due to electrostatic interactions between the cations and the CNT and GO negative surface. Maximum removal of Cu<sup>2+</sup> by CNT and their composites have been reported at pH 5 (Li *et al.*, 2003a, Li *et al.*, 2003c; Li *et al.*, 2010), pH 6 (Wu, 2007) and pH 7 (Tofighy & Mohammad, 2011). The maximum removal of Pb<sup>2+</sup> by CNT has been observed at pH 5 (Kabbashi *et al.*, 2009; Li *et al.*, 2002), pH 6 (Ren *et al.*, 2011), pH 6.2 (Vukovic *et al.*, 2011) and pH 7 (Tofighy and Mohammad, 2011). The maximum adsorption capacities of Cu<sup>2+</sup> by GO have been reported at pH 5 (Sitko *et al.*, 2013) and pH 5.3 (Lee & Yang, 2012). The maximum removal of Pb<sup>2+</sup> by GO has been observed at pH 5 (Sitko *et al.*, 2013), pH 5.6 (Lee & Yang, 2012), pH 6.8 (Madadrang *et al.*, 2012) and pH 7 (Musico *et al.*, 2013).

The influence of pH on the adsorption capacity of Cu<sup>2+</sup> and Pb<sup>2+</sup> by GOMβCD and OMWCNT/Ppy is not known. This work, therefore, determined the optimum pH of adsorption by these adsorbents for the copper and lead ions mentioned for an efficient adsorption process.

### 2.6.2 Contact time and initial concentration

The contact time has a considerable effect on the adsorption of metal ions onto adsorbents. The adsorption of the ions usually increases with increase in contact time until equilibrium is attained (Fu & Wang, 2011). The equilibrium is dependent on the initial concentration of the metal ion solution. For instance, the reported equilibrium time for the sorption of  $Pb^{2+}$  by CNT from a solution of metal ion concentration of 10 and 30 mg/L was 20 min and 60 min, respectively (Li *et al.*, 2005). The sorption of  $Ni^{2+}$  by CNT took 2 h to reach equilibrium at initial metal concentration of 60 mg/L but at initial concentration of 30 mg/L the equilibrium was established in 1 h (Rao *et al.*, 2007; Ren *et al.*, 2011 Gupta *et al.*, 2015). However, Wu *et al.* (2013) reported the equilibrium time of 120 min for the sorption of  $Cu^{2+}$  onto GO from solutions of initial metal ion concentration 50, 100 and 150 mg/L. The effect of contact time and initial metal ion concentration on the adsorption of  $Pb^{2+}$  and  $Cu^{2+}$  by the proposed GO-m $\beta$ CD and OMWCNT/Ppy adsorbents are not known and should, therefore, be established.

### 2.7 Adsorption of metal ions onto GO and CNT composites

The adsorption capacity of graphene and CNT is influenced by their surface properties such as surface area and pore size distribution. The presence of different functional groups is another possible route to enhance their adsorption performance; hence the oxidation of graphene to graphene oxide and CNT to oxidized CNT (O-CNT) offers considerable influence on adsorption. Therefore, the large surface area and the oxygen containing adsorption sites on GO and O-CNT are largely responsible for adsorption of metal ions (Rao *et al.*, 2007; Zhao, Li, Re, Chen, & Wang, 2011). Further, their adsorption capacities can be improved by derivatization with other nanomaterials that have affinity for metal ions.

The adsorption data can be modeled using different equations including pseudo-first and second-order rate equation, Langmuir, Freundlich, Dubinin-Radushkevich (D-R) and diffusion models among others. The sorption of metal ions onto GO and CNTs are commonly correlated with Langmuir and Freundlich equations. The change in adsorption with time is usually fitted in the pseudo-first-order (Lagergren, 1898) and pseudo-second-order Ho and Mc Kay (2000) kinetic models. The linearized forms of pseudo-first-order and pseudo-second-order equations are expressed as shown in eq. 1 and eq. 2, respectively;

$$\log(q_e - q_t) = \log q_e - k_1 t \quad (\text{Eq. 1})$$

$$\frac{t}{q_t} = \frac{1}{q_e} t + \frac{1}{k_2(q_e)^2} \quad (\text{Eq. 2})$$

where,  $q_t$  and  $q_e$  are amounts adsorbed in  $\text{mg g}^{-1}$  at equilibrium and time  $t$ , respectively, while  $k_1$  and  $k_2$  represents the first-order rate and second-order rate constant of adsorption, respectively. The pseudo-first-order reaction implies that the reaction rate depends only on the concentration of one the reactants while the pseudo-second-order rate is determined by the concentration of two reactants simultaneously. Thus, the pseudo-second-order rate indicates that both the concentrations of the adsorbent and adsorbates (the metal ions) are involved in the adsorption process.

In most cases, the adsorption of metal ions by the GO and CNT adsorbents follows the pseudo-second-order (Gao *et al.*, 2008). The adsorption diffusion approach can also be applied to determine the diffusion mechanisms of the adsorbents. Adsorption diffusion approach is known to follow four consecutive steps, namely; bulk diffusion -transfer of the ions from the solution to the boundary film surrounding the adsorbent, film diffusion - diffusion from the film to the external surface of the adsorbent, intra-particle diffusion - diffusion in the internal structure of the adsorbent and diffusion on the external surface of the adsorbent (Qui *et al.*, 2009). The first and last steps are very fast hence the adsorption diffusion process is controlled by the film diffusion and intra-particle diffusion. The intra-particle model (Eq.3) and the liquid film model (Eq.4) are expressed as;

$$q_t = k_p t^{1/2} + C \quad (\text{Eq. 3})$$

where,  $q_t$  is the adsorption capacity at a given time  $t$ ,  $k_p$  is the intra-particle rate constant in  $\text{mg g}^{-1} \text{min}^{-1/2}$  while  $C$ , is a constant related to the thickness of the boundary layer.

$$\ln(1 - F) = -k_{fd} t \quad (\text{Eq. 4})$$

where,  $F$  is the fractional attainment of equilibrium ( $F = q/q_e$ ), and  $k_{fd}$  ( $\text{min}^{-1}$ ) is the film diffusion rate coefficient.

The frequently utilized models for describing the equilibrium studies for adsorption of metal ions on solid surfaces are Langmuir and Freundlich models. The linearized forms of Langmuir and Freundlich isotherm models are expressed in (Eq.5) and (Eq. 6), respectively.

$$\frac{1}{q_e} = \frac{1}{bq_{max}} \cdot \frac{1}{C_e} + \frac{1}{q_{max}} \quad (\text{Eq. 5})$$

$$\log q_e = \frac{1}{n} \log C_e + \log k_f \quad (\text{Eq. 6})$$

where  $q_e$  (mg g<sup>-1</sup>) is the amount of metal ions adsorbed per unit mass of the adsorbent at equilibrium;  $C_e$  (mg L<sup>-1</sup>) is the equilibrium concentration of metal ions remaining in solution; while  $q_{max}$  and  $b$  are the constants related to the Langmuir adsorption capacity of adsorbents and adsorption affinity of the binding sites, respectively. The  $k_f$  value relates to the relative adsorption capacity while  $n$  represents the extent to which the adsorption depends on the equilibrium concentrations. The Langmuir equation was primarily designed to describe gas-solid phase adsorption and is used to quantify the adsorption capacity of an adsorbent. The model works on the assumptions that at maximum adsorption only a monolayer is formed and that the molecules of the adsorbate do not deposit on each other (Elmorsi, 2011). The model is therefore applicable in adsorption processes involving homogeneous surfaces. The Freundlich equation fits with sorption on the heterogenous surface. Nevertheless, these models have been adopted for liquid-solid phase systems and studies show that both models represent the sorption of different metal ions on GO and CNT (Vukovic *et al.*, 2011; Wu *et al.*, 2013; Sitko *et al.*, 2013). In most cases, one model can best describe the sorption process. Lead ions adsorption onto GO can best be described by Langmuir equation (Madadrang *et al.*, 2012; Musico *et al.*, 2013; Sitko *et al.*, 2013) in other cases the sorption process correlated well with Freundlich model like in the sorption of copper ions onto GO as described by (Wu *et al.*, 2013). The adsorption of lead ions onto CNTs was best described using Langmuir (Hu *et al.*, 2010; Vukovic *et al.*, 2011), in some cases it fitted well with Freundlich (Li *et al.*, 2005)

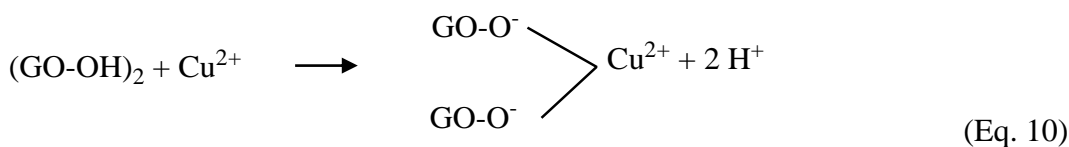
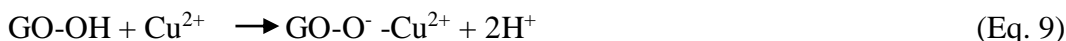
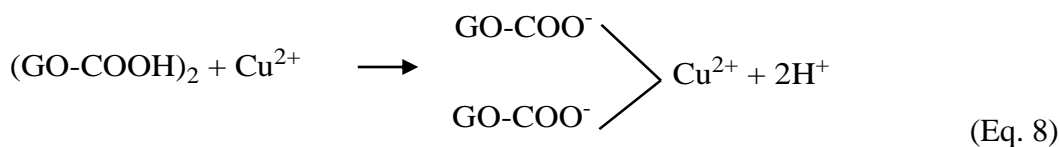
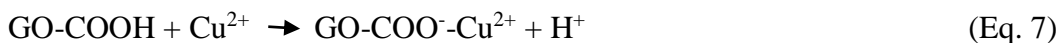
Modeling the adsorption data obtained in the application of the proposed adsorbents using these isothermic and kinetic models would be useful in determining the maximum sorption capacities and sorption mechanisms of the proposed adsorbents

### 2.7.1 Adsorption mechanism of GO and its composites

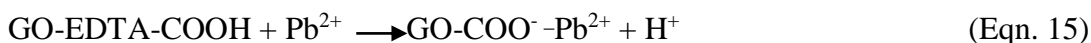
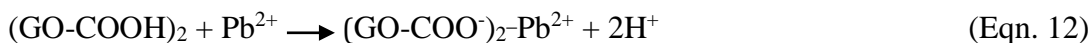
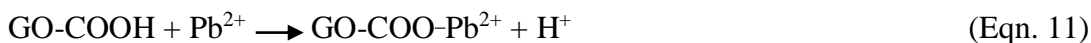
Graphene oxide contains functionalities on its surface such as –COOH, –C=O and –OH. Studies have attributed the adsorption of the metal ions by GO to these functional groups as well as the

larger surface area (Sitko *et al.*, 2013). The adsorption of Cu(II) onto GO has been reported to be through complexation, electrostatic attraction and ion exchange (Fu and Wang, 2011; Wu *et al.*, 2013).

Sitko *et al.* (2013) tested the sorption of divalent metal ions of Cu, Pb, Cd and Zn both in single and binary metal systems on GO. The optimum sorption capacities for Pb(II), Cd(II), Zn(II) and Cu(II) in single metal system were 1119, 530, 345 and 294 mg g<sup>-1</sup>, respectively. The isotherm data fitted well with the Langmuir model, implying monolayer coverage of heavy metal ions on GO, while the kinetics data was well described by the pseudo-second-order model. Therefore, the sorption kinetics of the metal ions was attributed to chemisorption resulting from the interaction of the metal ions with the functional groups on the surface of GO. Wu *et al.* (2013) also investigated the adsorption of Cu(II) using GO and reported adsorption capacity of 117 mg g<sup>-1</sup> for Cu(II) and the adsorption mechanism as shown in Eqns 7-10. The adsorption data fitted well to the Freundlich isotherm model implying that adsorption was on a heterogenous surface.



Madadrang *et al.* (2012) studied the adsorption capacity of pristine GO and GO-(*N*-trimethoxysilylpropyl) ethylenediamine triacetic acid nanocomposite. The study showed that the composite's adsorption capacity for Pb(II) was 525 mg g<sup>-1</sup> which was significantly higher than that of pristine GO (estimated at 367 mg g<sup>-1</sup>), the adsorption mechanism was as shown in Eqns 11-16. The experimental data fitted well on the Langmuir adsorption isotherm and pseudo-second-order kinetic model.



A study conducted by Musico *et al.* (2013) to investigate the adsorption of Pb(II) using a GO-poly(*N*-vinylcarbazole) nanocomposite adsorption capacity, indicated an adsorption capacity of 887.98 mg g<sup>-1</sup>. The adsorption studies showed Langmuir applicability whereas the kinetics data fitted well with pseudo-second-order kinetic model. The sorption data obtained from the proposed adsorbents should be also fitted for its conformity to the Langmuir and Freundlich adsorption models as well as the pseudo- first-order and pseudo-second-order kinetic models in order to deduce the adsorption mechanisms of the proposed adsorbents

### 2.7.2 Adsorption mechanism of CNT and its composites

The sorption mechanisms reported for metal ions by CNT include: - electrostatic attraction, physical adsorption and sorption-precipitation (Gupta *et al.*, 2015). The CNT establish  $\pi$ - $\pi$  electrostatic attractions with divalent metal ions (Lu & Liu 2006; Rao *et al.*, 2007; Xu, Tan, Chen, & Wang, 2008; Vukovic *et al.*, 2011). The other common chemical interaction is that between the CNT surface functional groups and the metal ions as represented in Fig. 5. A study conducted by Li *et al.* (2003a) established the uptake of metal ions by CNT was a combination of electrostatic attraction and sorption-precipitation.

Vukovic *et al.* (2011) compared the sorption performance of pristine, oxidized, ethylenediamine and diethylenetriamine modified multi-walled carbon nanotubes (raw-MWCNT, o-MWCNT, e-MWCNT and d-MWCNT, respectively) in removing Pb(II) from water. The Pb(II) maximum adsorption capacities of raw-MWCNT, o-MWCNT, e-MWCNT and d-MWCNT at 318K were 5.21, 40.79, 44.19 and 58.26 mg g<sup>-1</sup>, respectively. The equilibrium data was best fitted to the Langmuir isotherm model, indicating that the active binding sites on the adsorbent surface were homogenous for Pb(II) sorption. The pseudo-second-order model described the sorption process,

indicating that the chemical adsorption involved electron exchange between the adsorbent and the adsorbate ( $\text{Pb}^{2+}$ ).

In a separate study, Kosa *et al.* (2012) investigated the potential of MWCNT enhanced by a chelating agent (8-hydroxyquinoline). The experiment compared the sorption capacities of pristine MWCNT and 8-hydroxyquinoline modified carbon nanotubes (8-HQ-MWCNT) for Cu(II), Pb(II), Cd (II) and Zn (II) from water. The calculated results indicated that the maximum adsorption capacities for Cu(II), Pb(II), Cd(II) and Zn(II) by pristine MWCNT were 0.080, 0.064, 0.011 and 0.063, respectively. While the sorption capacities for Cu(II), Pb(II), Cd (II) and Zn (II) onto the 8-HQ-MWCNT adsorbent were 0.080, 0.076, 0.032 and 0.075, respectively.

The adsorption data obtained from adsorption of Pb(II) and Cu(II) by the proposed adsorbents need to be modeled onto the isothermic equations in order to establish the maximum adsorption capacity of these adsorbents

## **2.8 Competitive adsorption**

The competitive adsorption of metals for sorption sites take place when there are different metal ions in a given a solution. Competitive studies conducted by Stafiej & Pyrznska (2007) showed that the adsorption of  $\text{Cu}^{2+}$  by CNT decreased when it was in a binary metal system with other metal ions. Li *et al.* (2003a) also carried out both single and competitive sorption of  $\text{Pb}^{2+}$ ,  $\text{Cu}^{2+}$  and  $\text{Cd}^{2+}$  onto CNT and the study established that the sorption of these metal ions decreased from 97.08, 28.49 and 10.86  $\text{mg L}^{-1}$  to 27.6, 17.6 and 2.4  $\text{mg L}^{-1}$ , respectively, in a tertiary system. The competitive adsorption of binary aqueous metal cations also showed that the sorption capacity of  $\text{Pb}^{2+}$  and  $\text{Cu}^{2+}$  by GO decreased (Sitko *et al.*, 2013). There is no documentation, however, showing competitive sorption of metal ions by GO-m $\beta$ CD and OMWCNT/Ppy.

## **2.9 Regeneration of adsorbents**

The repeated viability of an adsorbent through adsorption-desorption cycles is important because it reduces the overall cost of the adsorbent. Desorption of the metal ions from the surface of the adsorbent strongly depends on the pH of the regeneration solution. Studies on the regeneration of both CNT and GO have shown that desorption of metal ions is higher at lower pH than at higher pH (Li *et al.*, 2005; Wu *et al.*, 2013). At lower pH desorption is high because of the increase in

the concentration of  $H^+$  ions resulting to an increased force for ion exchange between the cations and  $H^+$  thus the cations go into solution (Febrianto *et al.*, 2009)

Fig. 7 shows desorption of Cu(II) from GO by adjusting pH values of the solution. It is observed that, desorption is increases as the pH of the solution is decreased. Desorption decreases as the pH of the solution approaches 5, and is very low at  $pH > 5$ . Similarly, desorption of Pb(II) from CNT at varying pH solution conducted by Li *et al.* (2003) also shows that 100% desorption at  $pH < 2$  (Fig. 8).

These studies on the reusability of both GO and CNT indicate that the  $GO/\beta CD$  and  $OMWCNT/Ppy$  composites, if synthesized, may also have a potential to be reused. However, there are no studies showing that they can be regenerated.

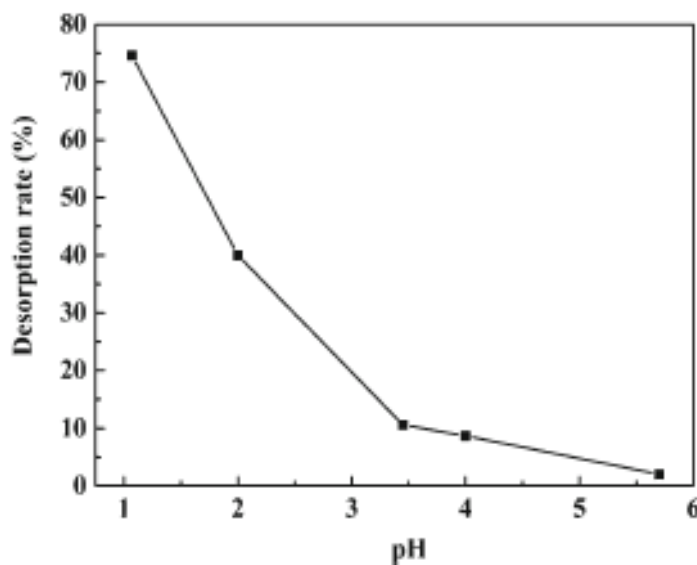


Fig. 7: Desorption rate of Cu(II) from GO at different pH values of HCl solution (Wu *et al.*, 2013)

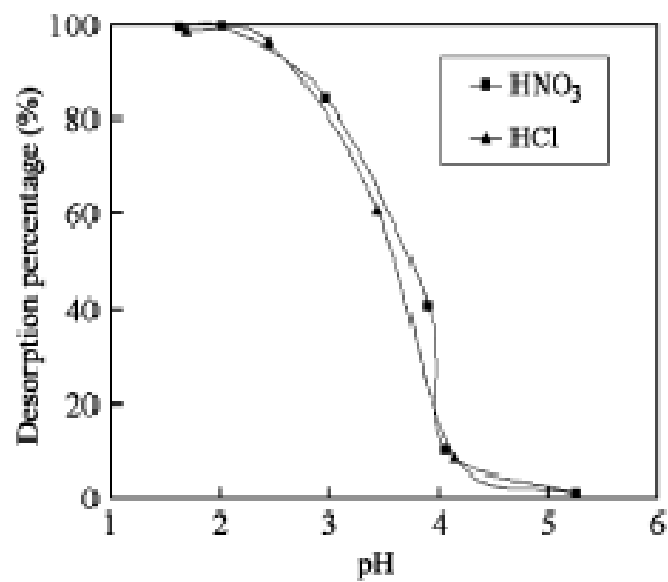


Fig. 8: Desorption rate of Pb(II) from CNT at different pH values of HCl and HNO<sub>3</sub> solution (Li *et al.*, 2005)

## CHAPTER 3

### MATERIALS AND METHODS

This section discusses the materials and methods that were used in the synthesis, characterization and optimization of the proposed adsorbents.

#### 3.1 Chemicals and reagents

The chemicals used include; natural graphite flakes (20  $\mu\text{m}$ , 99.8% pure) - Sigma Aldrich (Germany) and MWCNT (Nanografi-Turkey) with an average external diameter of 10 nm and average length of 1.5  $\mu\text{m}$ , with purity of more than 95% and an estimated surface area of  $\sim 300 \text{ m}^2 \text{ g}^{-1}$ . Copper (II) nitrate tri-hydrate  $[\text{Cu}(\text{NO}_3)_2 \cdot 3\text{H}_2\text{O}]$ , anhydrous lead (II) nitrate,  $[\text{Pb}(\text{NO}_3)_2]$ , potassium bromide (KBr), sodium hydroxide (NaOH), hydrochloric acid (HCl), sulfuric acid ( $\text{H}_2\text{SO}_4$ ), potassium persulphate ( $\text{K}_2\text{S}_2\text{O}_8$ ), phosphorous pentoxide ( $\text{P}_2\text{O}_5$ ), potassium permanganate ( $\text{KMnO}_4$ ), hydrogen peroxide ( $\text{H}_2\text{O}_2$ ), ferric chloride ( $\text{FeCl}_3$ ), nitric acid ( $\text{HNO}_3$ ) and acetone were purchased from Merck Co (Germany), methyl- $\beta$ -cyclodextrin and pyrrole, purchased from Sigma Aldrich (Germany). All the chemicals and reagents used were of analytical grade. Deionized water was used for preparation, dilution and analytical purpose.

#### 3.2 Equipment

The changes in the functional groups in the CNT adsorbents were recorded by FT-IR Spectrum 2000, Perkin-Elmer, Germany. The FT-IR spectra of the GO and GO-m $\beta$ CD were determined by attenuated reflectance FT-IR fitted with a diamond crystal (Nicolet iS-5, USA). The specific surface area (SSA) and pore distribution of the CNT and its nanocomposites were determined using a Quadrasorb Evo 4, Quantachrome, USA gas adsorption analyzer.

The morphology of the adsorbents was determined by Scanning Electron Microscopy (SEM) and the micrographs recorded on Zeiss Evo ls10 SEM-UK. The concentration of the copper ions and lead ions after sorption was determined by Atomic Adsorption Spectrometer (Analytikjena contrAA 300, AAS - Germany).

Raman microscopy was performed by Renishaw in Via Raman microscope (Renishaw plc UK) while X-ray diffractometer (GNR APD 2000 PRO - Italy) was used to determine the crystallography of GO and GO-CD. The thermal stability of the MWCNT and the composite was determined using a Thermogravimetric Analyzer (Setsys Evolution TGA Setaram- France). The

ultrasonicator used was (Bandelin Electronic UW 3100, Berlin-Germany), the sonicating bath was Bandelin Sonorex electronic RK 100H, Berlin- Germany and centrifuge was Hettich Zentrifugen Universal 320, Germany.

### 3.3 Synthesis

The synthesis of both GO and its composite GO-m $\beta$ CD and OCNT and its composite OCNT/Ppy was carried out as follows.

#### 3.3.1 Synthesis of GO and GOm $\beta$ CD

Graphene oxide (GO) was prepared from natural graphite flakes, by a modified Hummers' method (Marcano *et al.*, 2010). Graphite flakes (5 g) were put into a 250 mL round-bottomed flask, which had 98% H<sub>2</sub>SO<sub>4</sub> (60 mL), K<sub>2</sub>S<sub>2</sub>O<sub>8</sub> (5 g), P<sub>2</sub>O<sub>5</sub> (5 g) and placed on a magnetic stirrer. Then, the temperature was gradually raised to 80°C and kept at this temperature for 6 h to form pre-oxidized graphite. The pre-oxidized graphite was washed using distilled water and dried at room temperature. This pre-oxidized graphite (5 g) was further oxidized by 150 mL of 98% H<sub>2</sub>SO<sub>4</sub> in ice-water bath at -10°C with gradual addition of 22.5 g KMnO<sub>4</sub> into the mixture followed with repeated stirring and cooling. The mixture was stirred for 48 h at 35°C. Subsequently, 2.8 L of deionized water was added to the mixture accompanied by continuous stirring. Finally, 25 mL of 30% H<sub>2</sub>O<sub>2</sub> solution was slowly added to the mixture followed by stirring with a magnet stirrer until the colour of the dispersion changed from black to yellow (Fig. 9). The synthetic product, GO, was filtered and washed with HCl (5 wt%) and deionized water, respectively. The prepared GO solid was dried at 60°C in a vacuum oven for 12 h.

Graphene oxide methyl-beta cyclodextrin (GO-m $\beta$ CD) was synthesized as described by Guo *et al.* (2010). A 20 mL portion of the homogeneous dried graphene oxide dispersion (0.5 mg mL<sup>-1</sup>) was mixed with 20 mL of 80 mg mL<sup>-1</sup> methyl- $\beta$ -cyclodextrin aqueous solution and thoroughly shaken for 30 min in an ultrasonicator. The mixture was then heated to reflux at 50°C for 12 h to obtain the GO-m $\beta$ CD nanocomposite. The resulting material was centrifuged at 4000 rpm and washed three times with distilled water to remove excess m $\beta$ CD and vacuum dried at 50°C for 12 h in a vacuum dried oven.



Fig. 9: Picture of yellow dispersed GO

The schematic diagram showing the synthesis of GO-m $\beta$ CD composite is shown in Fig. 10. The prepared GO-m $\beta$ CD and GO solids were then characterized for functional group, morphology, surface area and thermal stability.

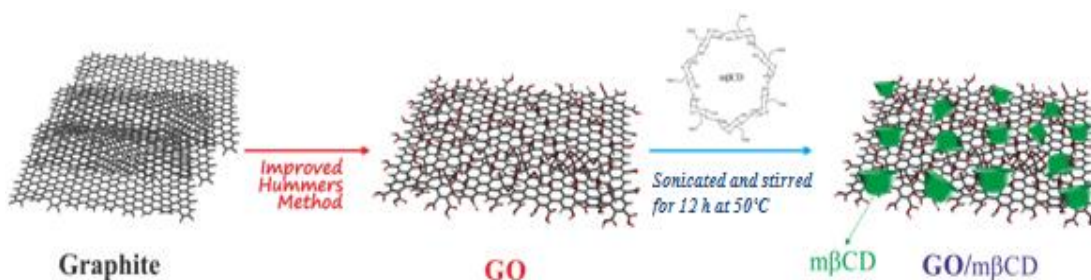


Fig. 10: The schematic diagram showing the synthesis of GO-m $\beta$ CD composite

### 3.3.2 Synthesis of the oMWCNT and oMWCNT/Ppy

Oxidized MWCNT was prepared through chemical oxidation (Stafiej & Pyrznska, 2007; Datsyuk *et al.*, 2008). MWCNT (0.3 g) were dispersed in 70 mL of 8 M concentrated nitric acid solution in a round bottomed flask and sonicated for 2 h at 40°C in a sonicating bath. The mixture, mounted with a magnetic stirrer was then refluxed in an oil bath for 24 h at 80°C. The resultant mixture was vacuum filtered and the oMWCNT formed were washed in excess deionized (DI) water to neutral pH 7 before vacuum drying the black residue at 90°C for 12 h.

To obtain the composite, 0.1 g of oMWCNT were dispersed in 20 mL DI water in an ultrasonicator for 30 minutes, 0.2 mL pyrrole was then added to the dispersion and thoroughly stirred for 5 minutes by an ultrasonicator. *In situ* polymerization of oMWCNT was then initiated by adding 2 g of anhydrous FeCl<sub>3</sub> to the mixture and stirred for 3 h (Hosseini *et al.*, 2015). The product was vacuum filtered and repeatedly rinsed with distilled water, followed by addition of acetone to remove adhering oligomers. Thereafter, the black composite was washed again with distilled water before vacuum drying for 8 h in an oven at 60°C. The schematic flow diagram of coating oMWCNT with Ppy is shown in Fig. 11.

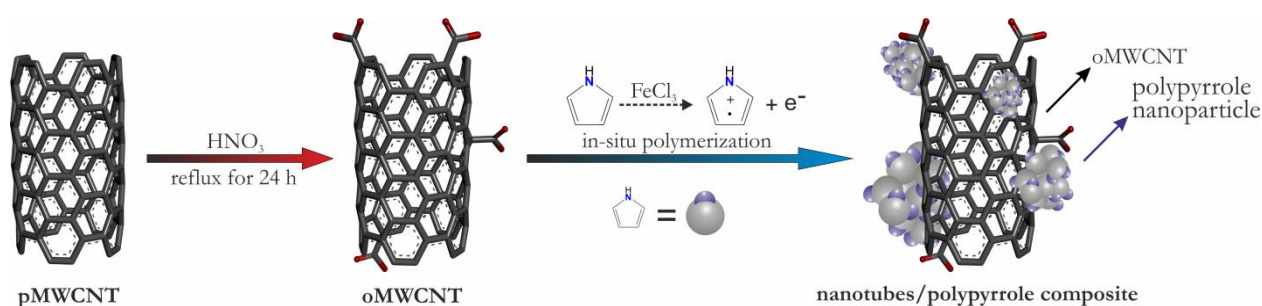


Fig. 11: The schematic flow diagram of coating oMWCNT with Ppy

### 3.4 Characterization of GO, GO-mβCD, pMWCNT, oMWCNT and oMWCNT/Ppy

#### 3.4.1 Functional group changes

The changes of the functional groups on the adsorbents were determined using FTIR microscopy using a KBr disk. A pressed pellet was prepared by grinding the sample powder with IR grade KBr in a mortar and the scan was done over a wavelength range of 4000-400 cm<sup>-1</sup>.

The FT-IR spectra of the GO and GO-mβCD were determined by attenuated reflectance FT-IR equipped with diamond crystal. First, the crystal surface was thoroughly cleaned using acetone. The acetone was allowed to completely evaporate before the sample was pressed onto the diamond crystal to obtain the spectrum over a wavelength range of 4000-400 cm<sup>-1</sup> in transmission mode.

#### 3.4.2 Specific surface area

The SSA and pore distribution of the CNT and its nanocomposites were determined using Brunauer, Emmett and Teller (BET) and Density Functional Theory (DFT) models for N<sub>2</sub> adsorption/desorption at 77K. The preweighed samples were degassed for 6 h by applying a combination of heat at a temperature of 280°C and a vacuum pressure of 1 atm. This was to

remove any previously absorbed contamination from the surface and the pores. The samples were then cooled and the adsorption gas N<sub>2</sub> passed through the samples tube in controlled increments of pressure (P/P<sub>0</sub>= 0.2) to obtain the adsorption isotherms.

### **3.4.3 Analysis of Morphology**

The morphology of the adsorbents was determined by Scanning Electron Microscopy (SEM). The sample was thinly and compactly spread on a stub that had an adhesive and mounted on a specimen holder. The analyses were then performed using an electron beam accelerated at a voltage of 20 kV and a beam current of 50 pA.

### **3.4.4 The concentration of metal ion solution after adsorption and desorption**

The concentration of the copper ions and lead ions after adsorption was determined by Atomic Adsorption Spectrometer (AAS) using acetylene flame with the beam of lead and copper wavelengths 217 nm and 324 nm, respectively. The calibration curves (see appendix) were prepared before each experiment using standard solutions of copper (II) nitrate tri-hydrate [Cu(NO<sub>3</sub>)<sub>2</sub>·3H<sub>2</sub>O] and anhydrous Pb(NO<sub>3</sub>)<sub>2</sub>.

### **3.4.5 Analysis of order and disorder in hexagonal carbon**

Analysis of order-disorder in hexagonal carbon was performed by a Raman microscope using a laser operated at a wavelength of  $\lambda = 514$  nm at an output power of 1.0 mW under an objective lens x 20 magnification with 30 seconds exposure time.

### **3.4.6 Crystallinity of GO and GO-m $\beta$ CD**

The crystalline nature of GO and GO-m $\beta$ CD was done on X-ray diffractometer equipped with Cu K $\alpha$  radiation ( $\lambda = 0.15418$  nm). The samples were first pressed into a uniform layer onto the sample holder to form a smooth surface. After loading the sample, the voltage and current was slowly adjusted to 40.0 kV and 29.82 mA, respectively before scanning. The interlayer distance can be calculated using Bragg's Eqn 17.

$$d = \frac{n\lambda}{2 \sin \theta} \quad (\text{Eqn 17})$$

where  $d$  is the interlayer distance,  $n$  is an integer,  $\theta$  is the incident angle and  $\lambda$  is the wavelength of the x-ray.

### 3.4.7 Thermal stability

The thermal stability of the MWCNT and the composite was determined using a Thermogravimetric Analyzer in a dry nitrogen atmosphere. Initial samples were weighed at  $5 \pm 0.1$  mg each and then heated at a rate of  $10^\circ\text{C}$  per min from 100 to  $1000^\circ\text{C}$ .

## 3.5 Adsorption Experiments

The adsorption procedures to determine the influence of adsorption conditions such as pH, initial metal concentration and contact time were carried out in triplicates following reported procedures (Hu *et al.*, 2010; Vukovic *et al.*, 2011).

### 3.5.1 Preparation of the $\text{Cu}^{2+}$ and $\text{Pb}^{2+}$ Solutions

The stock solutions ( $1000 \text{ mgL}^{-1} \text{ Cu}^{2+}$  and  $\text{Pb}^{2+}$ ) were prepared by dissolving 3.8250 g copper (II) nitrate tri-hydrate  $[\text{Cu}(\text{NO}_3)_2 \cdot 3\text{H}_2\text{O}]$  and 1.599 g anhydrous  $\text{Pb}(\text{NO}_3)_2$ , respectively, in 100 mL of deionized water in a 1 L volumetric flasks. The flasks were then topped to the mark using deionized water. From each of the stock solutions 0.25, 1.25, 2.5, 12.5 and 25 mL were pipetted into a 250 mL volumetric flask then diluted using deionized water to the mark to make solutions of 1, 5, 10, 50 and 100 mg/L of  $\text{Cu}^{2+}$  and  $\text{Pb}^{2+}$ .

### 3.5.2 Effect of initial pH

An adsorbent of mass 20 mg placed in a 20 mL metal ion solution of concentration 10 mg/L was used in all adsorption experiments. The pH of the stock solution was adjusted by using 0.1 M  $\text{HNO}_3$  or 0.1 M  $\text{NaOH}$ . All the adsorption experiments were performed at room temperature at a pH value of 4 - 6.

### 3.5.3 Effect of contact time

The effect of contact time on heavy metal adsorption was investigated using the predetermined optimum pH from section 3.5.2 above. A pH 6 and pH 5 were used for determining the of  $\text{Pb}(\text{II})$  and  $\text{Cu}(\text{II})$ , respectively. In each experiment an adsorbent of mass 20 mg in 20 mL of 10 mg/L metal ion solution was used and the contact time was varied from 5 to 120 min at the optimum pH. Using the initial metal ion concentration,  $C_0$  and the final metal ion concentration,  $C_t$

obtained after a given contact time was determined using AAS. The amount of each metal ions adsorbed,  $q_t$ , after a given contact time was then calculated using the equation given below,

$$q_t = \frac{V(C_o - C_t)}{m} \quad (\text{Eq. 18})$$

where;

$q_t$  = maximum amount of metal ions adsorbed after time  $t$  ( $\text{mg g}^{-1}$ )

$C_o$  = initial metal ion concentration ( $\text{mg L}^{-1}$ )

$C_t$  = final metal ion concentration after a specific contact time interval ( $\text{mg L}^{-1}$ )

$V$  = volume of metal solution used (L)

$m$  = mass of adsorbent used (g)

### 3.5.4 Competitive sorption studies

The competitive sorption experiments of Cu(II) and Pb(II) by the adsorbents were carried out in Cu(II)/Pb(II) mixture. The experiments were carried out by adding 10 mg of the adsorbent into metal ion solution of initial concentration 5 or 10 mg/L at the predetermined optimum pH. This was stirred at 200 rpm for 2 h and the final concentrations of metal ions from each adsorbent were determined by AAS.

### 3.6 Regeneration of the adsorbents

The metal ion-pretreated adsorbents were put into 25 mL  $\text{HNO}_3$  solution with pH adjusted at 1.0, 2.0, 3.0, 4.0 and 5.0, followed by agitating for 2 h after every adjustment to desorb the adsorbed metal into solution. The adsorbed metal ions were desorbed and dissolved in solution. Consecutive sorption–desorption cycles were repeated five times using the same adsorbent to determine its reusability. The solution was collected by centrifugation and the amount of metal ions desorbed measured using AAS.

### 3.7 Statistical Analysis

All the sorption experimental data are means of triplicates determined at confidence level of 95% to test the significance of the analytical results. A completely randomized single factor design and students t-test ( $p \leq 0.05$ ) was used to check the variations in the adsorbents and the sorption

in the different metal ion systems. Statistical analysis was performed using SAS statistical application linear model.

## CHAPTER 4

### RESULTS AND DISCUSSION

This section deals with the synthesis and characterization of GO and GO-m $\beta$ CD, as well as oMWCNT and oMWCNT/Ppy and the sorption characteristics of these adsorbents for Pb(II) and Cu(II) from aqueous solutions.

#### 4.1 GO-m $\beta$ CD nanocomposite

##### 4.1.1 Synthesis and Characterization of GO and GO-m $\beta$ CD

Fig. 12 indicates FTIR spectra of GO, m $\beta$ CD and GO-m $\beta$ CD which shows the characteristic peak of GO at 3400 cm<sup>-1</sup> and associated with the O–H stretching and vibrations of the skeletal hydroxyl groups (Sitko *et al.*, 2013; Zhang *et al.*, 2014), while 1725 cm<sup>-1</sup>, 1630 cm<sup>-1</sup> and 1043 cm<sup>-1</sup> bands are associated with the C=O of COOH, C=C of the non-oxidized graphitic skeleton and C–O stretching mode in hydroxyl or epoxy groups COH/COC, respectively as noted by Zhang *et al.* (2014). As shown in the m $\beta$ CD spectra the absorption bands at 2923 cm<sup>-1</sup> and 1367 cm<sup>-1</sup> correspond to the –CH<sub>2</sub>– stretching and –CH– bending vibrations, respectively and the characteristic band of the coupled C–O/C–C vibrations at 1020 cm<sup>-1</sup> (Fan *et al.*, 2012; Huang *et al.*, 2012). The GO-m $\beta$ CD spectra has the characteristic peak at 1630 cm<sup>-1</sup> of GO and the characteristic band C–O/C–C of CD. In addition, the characteristic peak 3400 cm<sup>-1</sup> of -OH is found in both GO and m $\beta$ CD spectra. This indicates that m $\beta$ CD was successfully physically attached onto the surface of GO.

The SEM micrographs of GO and GO-m $\beta$ CD in Fig. 13, show that the plane sheets of GOs appear to be smooth with very few wrinkles, but the GO-m $\beta$ CD is rough with more wrinkles due to the packing of the nanoparticles. This is similar to that observed by Song *et al.* (2013), an indication that a packing of molecules onto the GO did take place.

The Raman spectroscopy is useful in the characterization of carbonaceous materials, especially to distinguish the ordered and disordered carbon in the structure. The Raman spectra for GO and GO-m $\beta$ CD are shown in Fig. 14, the G-band at < 1580 cm<sup>-1</sup> is associated with graphitic 2 dimensional hexagonal lattice corresponding to sp<sup>2</sup> stretching modes of carbon while the D-band at < 1350 cm<sup>-1</sup> represents sp<sup>3</sup>-hybridized carbon which is associated with disorder in the graphitic skeleton.

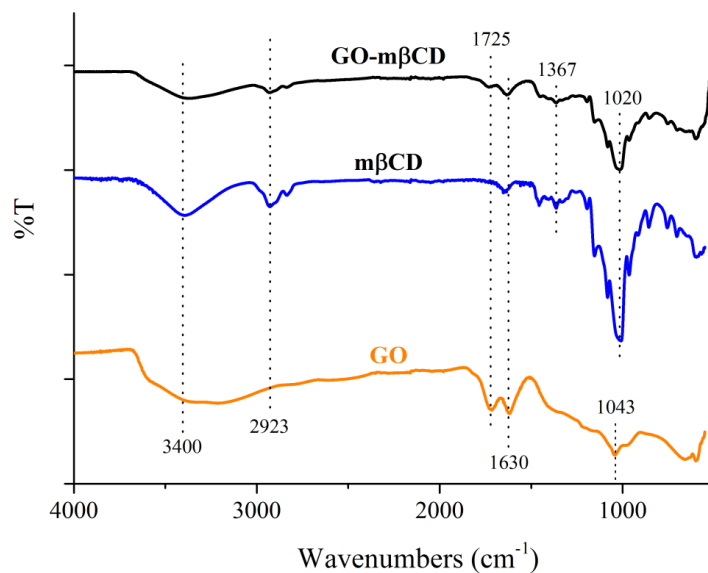


Fig. 12: FTIR spectra of (a) GO (b) mβCD and (c) GO-mβCD

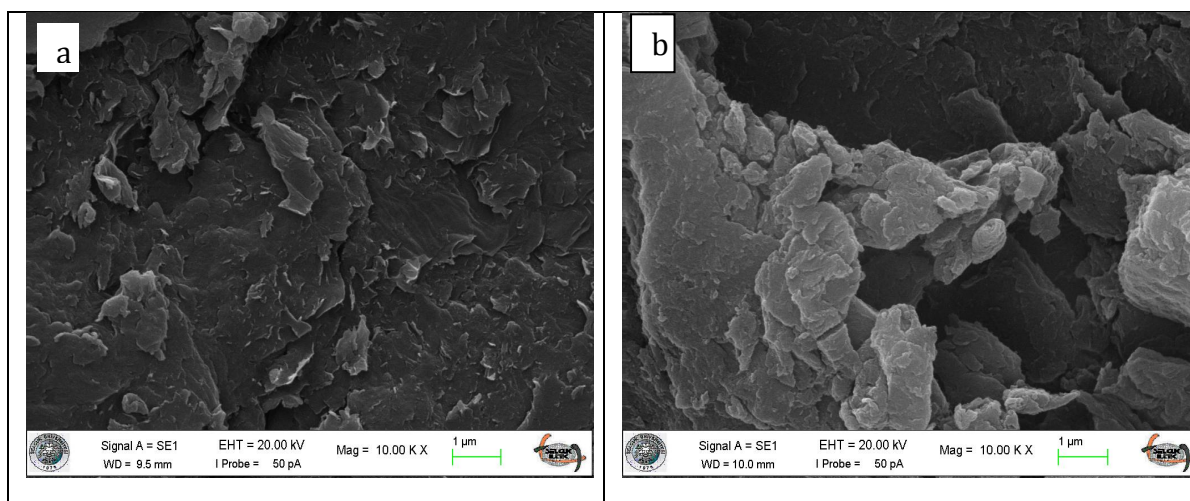


Fig. 13: SEM images of (a) GO and (b) GO-mβCD

The intensity of the D-band is denoted as  $I_D$  which indicates disorder in graphitic skeleton and that of the G-band is denoted as  $I_G$  represents the ordered graphene skeleton, thus, the ratio of  $I_D/I_G$  is used to indicate relative disorder present in the graphitic skeleton (Costa *et al.*, 2008). The  $I_D/I_G$  ratios of the GO and GO-mβCD obtained in this study were 0.88 and 0.93, respectively as shown in Fig. 14. The increase in  $I_D/I_G$  ratio in GO-mβCD suggests that there was an increase in defects on the GO which can be attributed the incorporation of mβCD onto the GO surface.

An increase in disorder associated with increase in the number of  $C_{sp^3}$  present in the structure of GOCD was also noted by Song *et al.* (2013) and Wang *et al.* (2014).

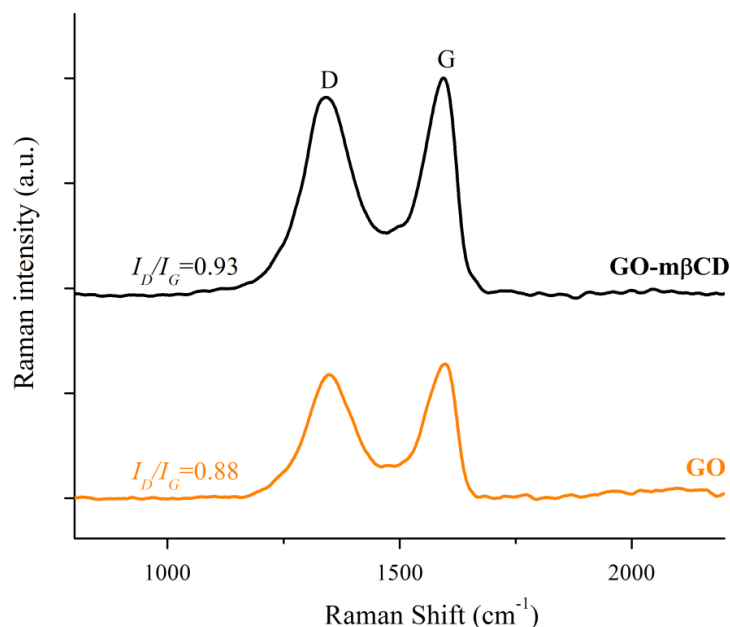


Fig. 14: Raman spectra GO and GO-m $\beta$ CD

The XRD patterns of GO, m $\beta$ CD and GO-m $\beta$ CD are shown in Fig. 15. The sharp diffraction peak of GO is located at  $2\theta = 9.0^\circ$  corresponding to GO (001) crystallographic plane. The interlayer distance of GO was calculated using Bragg's Eqn 17.

The interlayer distance obtained was 0.98 nm which shows that the interlayer spacing in GO was much wider than that of graphite which has been reported at 0.34 nm ( $2\theta = 26.5^\circ$ ) by Sitko *et al.* (2013). The wide interlayer distance of GO confirms the introduction of functional groups onto the graphite structure as observed by Hu *et al.* (2014). The XRD pattern of m $\beta$ CD on the other hand, shows prominent peaks at  $2\theta$  values of  $12.5^\circ$  and  $19^\circ$ , while the GO-m $\beta$ CD spectrum shows broad peaks at about  $2\theta = 9^\circ$  of GO and  $2\theta$  values of about  $12.5^\circ$  and  $18^\circ$  of the CD indicating that there is a mix in the stacking resulting from the settlement of m $\beta$ CD onto GO this result is similar to that as observed by Hu *et al.* (2010) and Zhou *et al.* (2014).

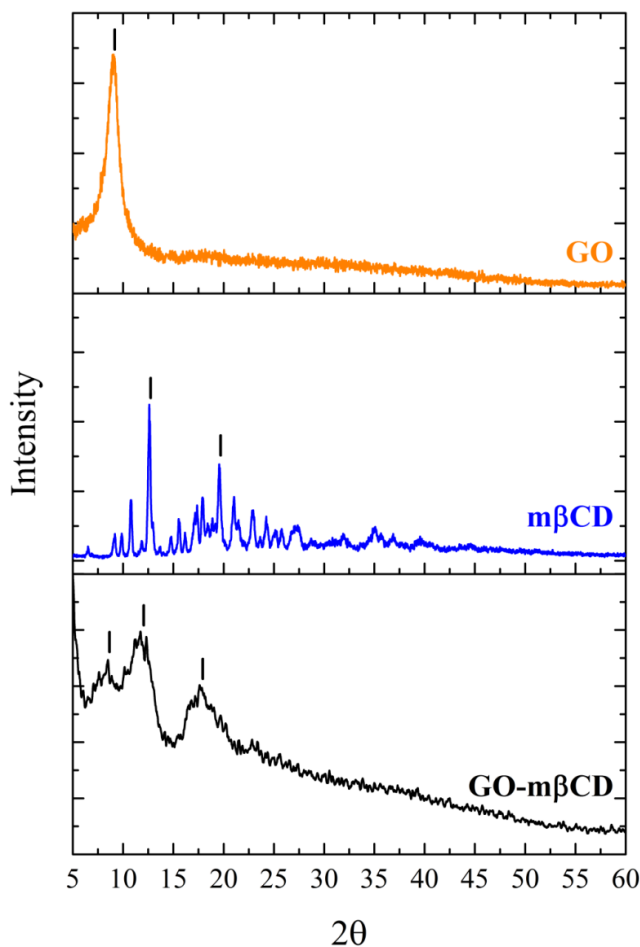


Fig. 15: XRD patterns of GO and GO-m $\beta$ CD

## 4.1.2 Sorption of Cu(II) and Pb(II) onto GO-m $\beta$ CD

### 4.1.2.1 Effect of initial pH

The pH of a solution has been identified as the most important factor influencing sorption of metal ions because it affects surface properties of adsorbents. In addition, the pH of a solution has an influence on the hydrolysis, precipitation, complexation and speciation of Pb ions and Cu ions (Xu *et al.*, 2008). The effect of initial solution pH on the removal of Pb(II) and Cu(II) by GO and GO-m $\beta$ CD was investigated (Fig. 16). The sorption of Pb(II) ions onto GO (Fig. 16a) was almost constant at pH 4.0-6.0 and for GO-m $\beta$ CD a slight rise from 4.0 to 6.0, where the removal was ca. 87% and ca. 90%, respectively, at pH 4. The point of zero charge of GO has been reported to be 3.8-3.9 (Zhao, Li, Re, Chen, & Wang, 2011), hence, at pH > 3.8 GO surface is expected to be negatively charged. At the same time, the predominant species of lead ions at pH <

6.0 is  $Pb^{2+}$ ; the uptake of this species thus takes place through its electrostatic interaction with the negatively charged GO surface.

On the other hand, a rise in sorption of  $Pb(II)$  with increase in pH in GO-m $\beta$ CD could be attributed to the hydroxyl groups of the CD which are polar as suggested by Konkena & Vasudevan (2012) thus making the GO-m $\beta$ CD surface charged. A similar observation was made by Hu *et al.* (2010), who found that the introduction of cyclodextrin onto MWCNT/iron oxide composite enhanced the sorption capacity of the composite for  $Pb(II)$  ions. This suggests that the sorption of  $Pb(II)$  by GO-m $\beta$ CD is through surface electrostatic attraction, hence the hydroxyl groups on the CD cavities enhanced the sorption capacity of GO.

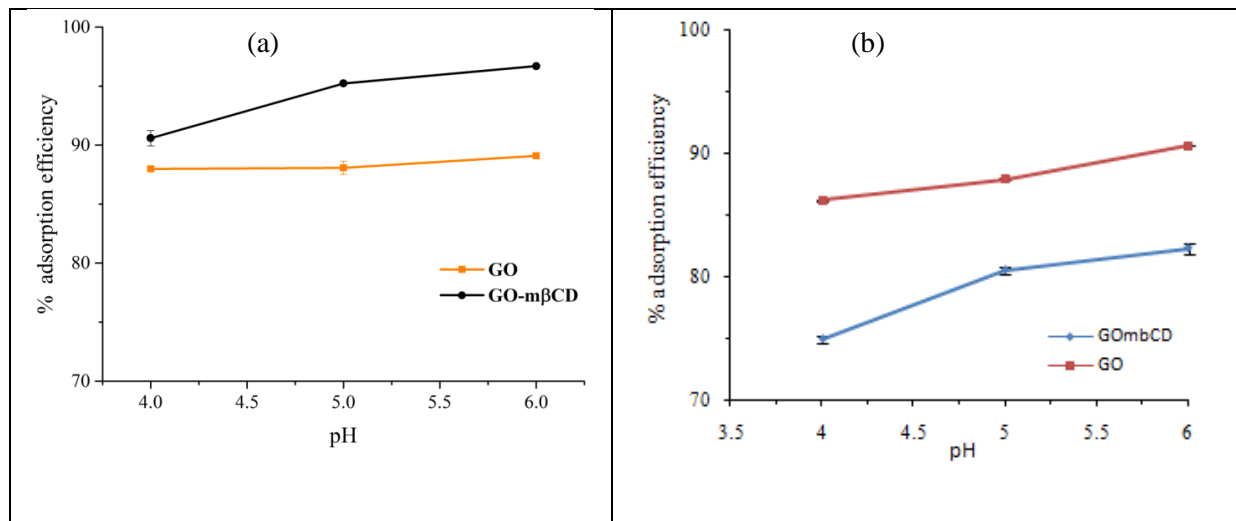


Fig. 16: Effect of pH on sorption of (a)  $Pb(II)$  and (b)  $Cu(II)$  by GO and GO-m $\beta$ CD (1 mg/mL dosage, contact time: 2 h, concentration: 10 mg/L)

Similarly, the sorption of  $Cu(II)$  ions onto both GO and GO-m $\beta$ CD (Fig.16b) was a slight rise from 4.0 to 6.0, where the removal was ca. 86% and ca. 75%, respectively, at pH 4. This is because the pH has an influence on the surface characteristics of the adsorbent. The increase in pH leads to an increase in the negative charge of the adsorbent which favors the electrostatic attraction between the  $Cu(II)$  and the  $COO^-$  or  $O^-$  on the GO surface forming metal ion complex (Wu *et al.*, 2013). The same observation is made in regards to the GO-m $\beta$ CD adsorbent, however, the uptake of  $Cu(II)$  by GO-m $\beta$ CD is lower than of GO. This could possibly be

attributed to the fact that in the attachment of m $\beta$ CD to GO through hydrogen bonding reduces the COO<sup>-</sup> on GO that could otherwise been available for the uptake of Cu(II) ions which is also not compensated by the O<sup>-</sup> groups on the m $\beta$ CD. However, the percentage sorption for both adsorbents was highest at pH=6 but at pH>6 there was precipitation. Subsequent analysis was henceforth performed at pH=6.

#### 4.1.2.2 Effect of contact time

The sorption behavior of Pb(II) and Cu(II) by GO and GO-m $\beta$ CD with respect to contact time was carried out at pH 6.0 and pH 5.0, respectively, by varying the treatment time from 0 to 120 min. As shown in (Fig. 17a), the uptake of Pb(II) by both adsorbents was very fast during the first 20 min before attaining equilibrium needed at 40 min. However, the equilibrium time for uptake of Cu(II) was lower as shown in (Fig. 17c). This is different from the observation made by Sitko *et al.* (2013), in which equilibrium time of the sorption of both Pb<sup>2+</sup> and Cu<sup>2+</sup> by GO was established at 60 min. Similarly, the observation by Wu *et al.* (2013) different metal ion concentration of 50, 100 and 150 mg L<sup>-1</sup>, equilibrium time was 120 min for sorption of Cu<sup>2+</sup> onto GO.

The changes in sorption with time were also fitted in the pseudo-first-order (Lagergren, 1898) and pseudo-second-order Ho and Mc Kay (2000) kinetic models. The linearized form of pseudo-second-order equation is expressed as eq. 1 and 2 in section 2.7 above.

The slope of  $t/q_t$  versus  $t$  (Fig. 17b and 17d) was used to calculate  $k_2$ . Table 5 shows the coefficient of determination ( $R^2$ ),  $q_e(\text{exp})$  and the calculated values  $q_e(\text{cal})$  of the pseudo-first-order and pseudo-second-order kinetic model. The experimental sorption capacities  $q_e(\text{exp})$  and the calculated values  $q_e(\text{cal})$  were in good agreement for the pseudo-second-order equation implying that the kinetic data correlates well with pseudo-second-order kinetics. The sorption mechanism is therefore, electrostatic interaction between Pb(II) ions and the negatively charged GO surface containing functional groups as well as abundant oxygen-containing groups on m $\beta$ CD. This is similar to the report by Madarang *et al.* (2012) and Musico *et al.* (2013) which also established that the uptake of Pb<sup>2+</sup> by GO and GO composites of EDTA and poly(*N*-vinylcarbazole), respectively, correlated well with pseudo-second order kinetics.

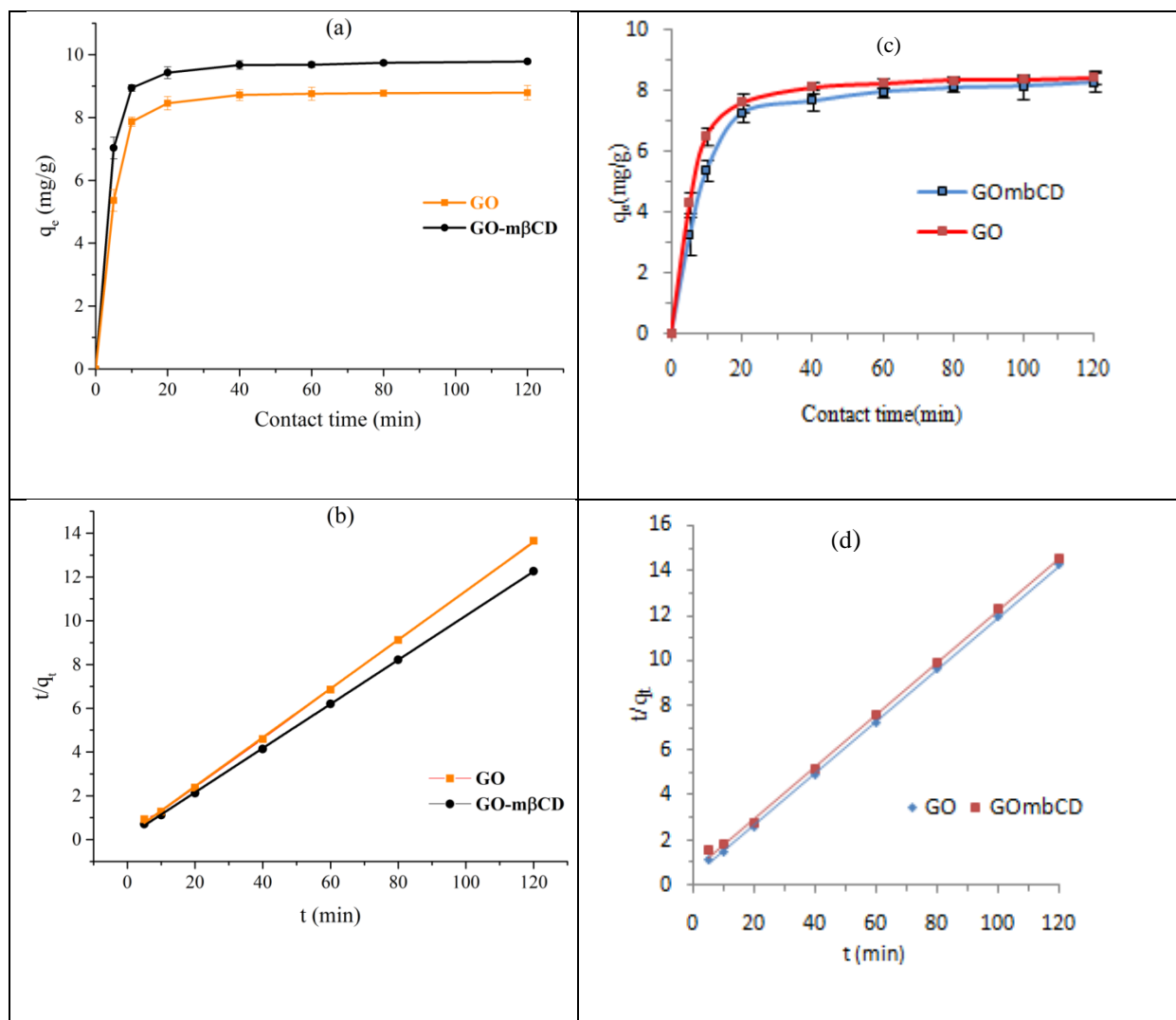


Fig. 17: Effect of contact time on sorption of (a) Pb(II) and (c) Cu(II) on GO and GO-mβCD and pseudo-second-order kinetics of (b) Pb(II) and (d) Cu(II) sorption on GO and GO-mβCD (1mg adsorbent/mL solution, pH: 6, contact time: 120 min, concentration, 10 mg/L)

The kinetic data was applied on both the intra-particle diffusion model (Weber & Morris, 1963) and the liquid film diffusion model (Boyd, Adamson, & Myers, 1947) to determine the diffusion mechanisms of the adsorbents. The intra-particle model (Eq.3) and the liquid film model (Eq.4) are expressed as shown in section 2.7.

The plots of  $q_t$  against  $t$  and  $-\ln(1-F)$  against  $t$  of the experimental data are shown in Fig. 18

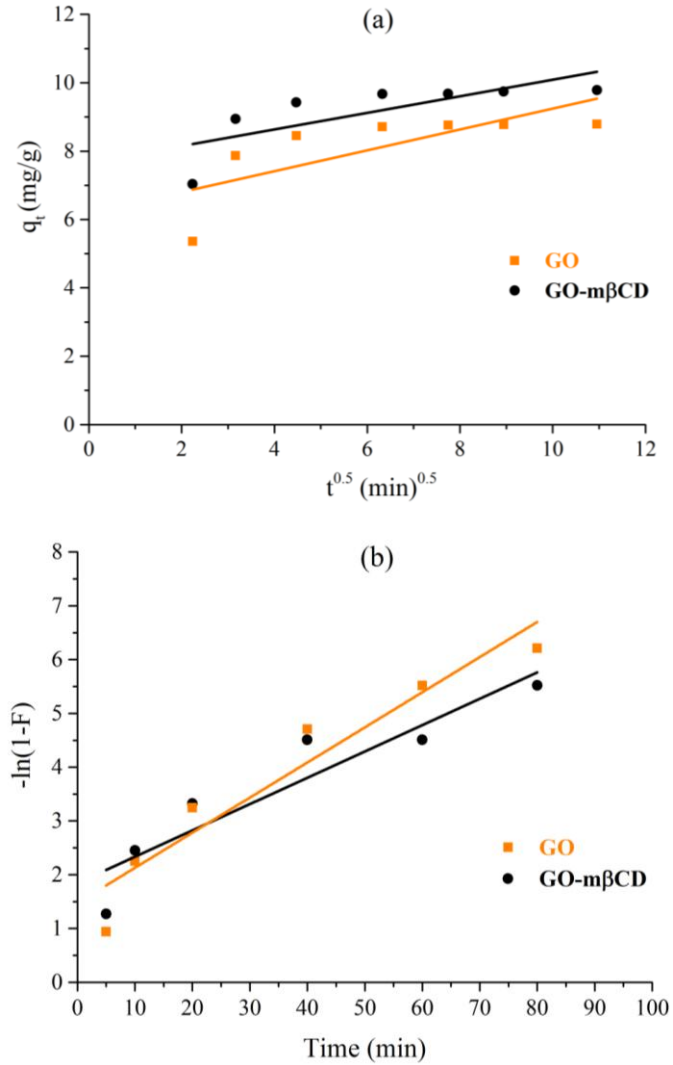


Fig. 18: The plots of intra-particle diffusion (a) and liquid film diffusion (b) for the sorption of Pb(II) on GO and GO-mβCD.

The plots did not give straight lines going through the origin; implying that this sorption was neither controlled by liquid film diffusion nor intra-particle diffusion. In conclusion, the sorption of lead(II) ion by GO and GO-mβCD is governed by pseudo-second-order kinetic model together with liquid film and intra-particle diffusion models.

Table 5: Kinetic parameters of pseudo-first-order and pseudo-second-order equation for Pb(II) and Cu(II) sorption on GO and GO- mβCD at initial concentration of 10 mg/L.

Metal	Adsorbent	Pseudo-first-order				Pseudo-second-order			
		$q_e$ (mg/g) (exp)	$q_e$ (mg/g) (cal)	$k_1$ (g mg <sup>-1</sup> min <sup>-1</sup> )	$R^2$	$q_e$ (mg/g) (exp)	$q_e$ (mg/g) (cal)	$k_2$ (g mg <sup>-1</sup> min <sup>-1</sup> )	$R^2$
Pb	GO	8.792	1.530	0.048	0.913	8.716	9.01	0.066	0.999
	GO-mβCD	9.784	1.974	0.064	0.867	9.675	9.90	0.080	0.999
Cu	GO	9.02	2.223	0.034	0.874	8.43	8.77	0.031	0.999
	GO-mβCD	8.27	3.065	0.048	0.854	8.27	8.70	0.019	0.999

#### 4.1.2.3 Effect of initial concentration

The metal ion uptake by the GO and GO-mβCD adsorbents at different initial metal ion concentration was recorded as shown in Table 6. It was observed that the sorption of Pb(II) ions between the GO and GO-mβCD adsorbents was significantly different ( $p \leq 0.05$ ) whereas the sorption of Cu(II) by the adsorbents was not significantly different. This implies that the attachment of mβCD onto GO did enhance its sorption capacity for Pb(II) ions but not for Cu(II) ions. The sorption of Pb(II) onto the composite is higher than that of Cu(II) despite the fact that Pb(II) is larger (119 pm) than Cu(II) (72 pm). However, their electronegativity follows the order of Pb (II) > Cu(II) that is 2.33 and 1.90, respectively. This could imply that electronegativity is contributing factor to the difference in their sorption.

The experimental values obtained at varying initial metal concentrations in Fig. 19 were fitted onto the Langmuir and Freundlich isotherm models. According to  $q_e$  calculated and  $q_e$  experimental values in Table 7, the Langmuir model better described the experimental data than the Freundlich model. This finding was in agreement with a report by Yusuf *et al.* (2015) on the sorption studies of heavy metals on graphene and its derivatives that shows that most of the experimental data is best fitted to the Langmuir and pseudo-second-order models. Thus, the sorption of Pb(II) and Cu(II) ions onto GO and GO-mβCD can be concluded to be monolayer.

Table 6: The means of metal ions adsorbed at varying initial metal ion concentration.

Metal ions	Initial concentration (mg/L)	10	20	30	40	50	100	150	200
Lead	GO	9.71± 0.048	19.46± 0.018	29.16± 0.03	38.77 ±0.09	48.28 ±0.02	95.30 ±0.04	139.8 ±0.05	181.8 ±0.07
	GO-mβCD	9.88± 0.069	19.64± 0.058	29.42± 0.03	39.38 ±0.06	49.13 ±0.1	97.17 ±0.08	142.5 ±0.04	186.6 ±0.32
	LSD (p≤0.05)	0.06	0.06	0.03	0.05	0.14	0.08	0.62	0.86
Copper	GO	8.92± 0.34	14.62± 0.11	20.02± 0.19	26.16 ±0.14	33.33 ±0.09	58.43 ±0.07	74.24 ±0.16	77.54 ±0.06
	GO-mβCD	8.81± 0.35	14.35± 0.15	19.48± 0.21	25.58 ±0.17	32.18 ±0.21	55.14 ±0.1	69.95 ±0.21	73.24 ±0.32
	LSD (p≤0.05)	0.08	NS	NS	NS	NS	NS	NS	NS

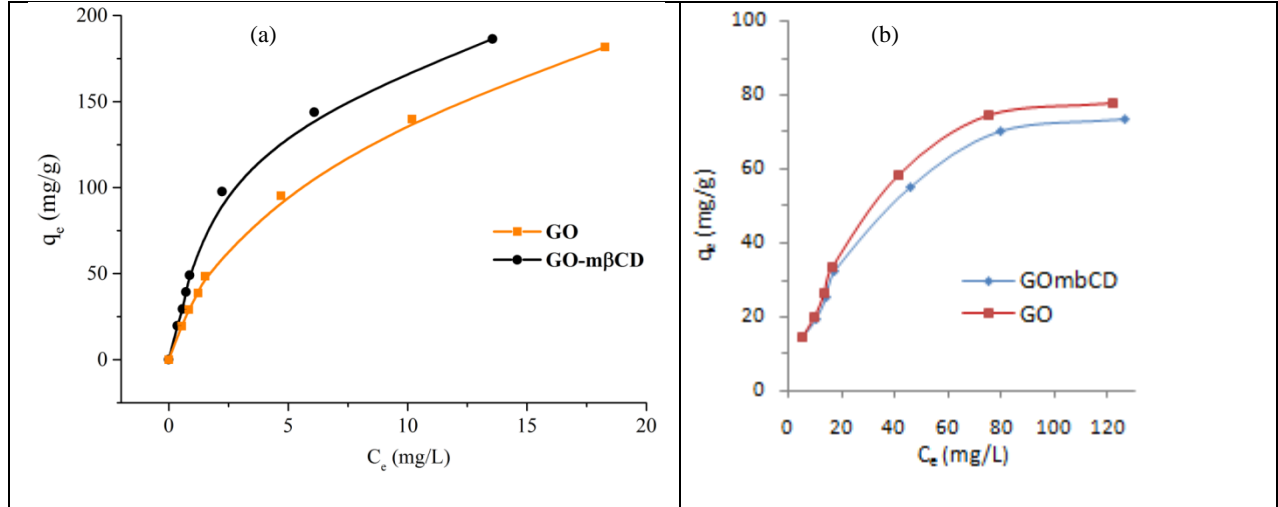


Fig. 19: Sorption isotherm for (a) Pb(II) and (b) Cu(II) by GO and GO-mβCD (pH: 6, 1 mg adsorbent/mL solution, concentration: 10-200 mg/L)

Table 7: Langmuir and Freundlich isotherm constants for Pb(II) sorption on GO and GO-m $\beta$ CD

Adsorbent	Metal	Langmuir constants			Freundlich constants		
		q <sub>max</sub> (mg/g)	b(mg/L)	R <sup>2</sup>	k <sub>f</sub>	N	R <sup>2</sup>
GO	Pb	217.39	0.183	0.999	32.89	1.605	0.986
GO-m $\beta$ CD		312.5	0.188	0.993	41.21	1.626	0.953
GO	Cu	90.09	0.034	0.973	5.90	1.751	0.966
GO-m $\beta$ CD		83.33	0.034	0.973	5.74	1.795	0.972

In addition, the q<sub>max</sub> values also indicate that the Langmuir sorption capacity of GO-m $\beta$ CD (312.5 mg/g) is significantly higher than that of GO (217.39 mg/g) suggesting that the m $\beta$ CD can be used to enhance the lead sorption capacity of GO. Implying, there may have been electrostatic attraction between the abundant hydroxyl groups in the m $\beta$ CD and the Pb(II) ions hence increasing the uptake of the metal ions. In the investigation of the sorption characteristics of  $\beta$ CD modified iron oxide/MWCNT for the sorption of Pb<sup>2+</sup>, Hu *et al.* (2010) also observed that the hydroxyl groups on  $\beta$ CD formed strong complexes with Pb(II) on the surface of iron oxide/MWCNT/CD adsorbent.

On the other hand, the uptake of Pb(II) ions by GO as suggested by Madarang *et al.* (2012) is through ion exchange reaction that takes place between Pb(II) and –COOH or –OH groups of GO as indicated in Eqn 11-14.

However, for Cu(II) the q<sub>max</sub> values indicate that the sorption capacity of GO-m $\beta$ CD (83.33 mg/g) is lower than that of GO (90.09 mg/g) indicating that the m $\beta$ CD did not enhance the sorption capacity of GO for copper ions, this difference is not significant as shown in Table 6. It has been suggested that the removal of Cu(II) by GO is through ion exchange and electrostatic attraction between the Cu(II) and oxygen functional groups (-COOH and -OH) on the GO as shown in Eq. 7-10 (Wu *et al.*, 2013).

In the modification of magnetic nanoparticles with carboxylated  $\beta$ CD (CMCD-MNPs) to study the sorption capacity of the magnetite surface for Cu(II) ions, Badruddoza *et al.* (2011) observed that the multiple hydroxyl and carboxyl functional groups of the adsorbent could have enhanced the sorption capacity of the magnetic nanoparticles. However, in this study, the  $\beta$ CD did not enhance the sorption capacity of the GO.

#### 4.1.2.4 Comparison of the sorption capacities of the adsorbents in this study with those in literature

The  $q_{\max}$  values reported in this study and those reported in literature are varied, this is because there are variations in sorption experimental conditions. For instance, as shown in Table 8, Musico *et al.* (2013) recorded  $q_{\max}= 692.66$  mg/g onto GO at pH 7.0 and 24 h contact time while Sitko *et al.* (2013)] recorded  $q_{\max}= 1119$  mg/g onto GO at pH 5.0 and contact time 2 h. Furthermore, there are variations in the modified Hummer's process used in the synthesis of GO from graphite. Nevertheless, the studies indicate that the modified GO shows higher sorption capacity than GO as reported by Madadrang *et al.* (2012).

Table 8: Comparison of the sorption capacities of the adsorbents in this study with those in literature.

Metal	Adsorbent	Sorption capacity (mg/g)	Conc. (mg/L)	pH	Temp. (K)	Cont. time (h)	Reference
Lead	GO	35.6±1.3		5.6			Lee and Yang (2012)
	GO	1119		5.0	298	2	Sitko <i>et al.</i> (2013)
	GO	367	5-300	6.8	298	24	Madadrang <i>et al.</i> (2012)
	GO	692.66	5-300	7.0	298	24	Musico <i>et al.</i> (2013)
	GO/Poly (N-vinylcarbazole)	887.98	5-300	7.0	298	24	Musico <i>et al.</i> (2013)
	GO-Chitosan	99	50		Room	24	He <i>et al.</i> (2011)
	EDTA/GO	525	5-300	6.8	298	24	Madadrang <i>et al.</i> (2012)
	GO	217.39	10-200	6.0	298	2	This study
Copper	GO-m $\beta$ CD	312.5	10-200	6.0	298	2	This study
	GO	117.5	25-250	5.3		2.5	Wu <i>et al.</i> (2013)
	Carboxyl-m $\beta$ CD-MNPs	47.2	50-200	6.0	298	4	Badruddoza <i>et al.</i> (2011)
	GO	294		5.0	Room	2	Sitko <i>et al.</i> (2013)
	GO	90.09	10-200	6.0	298	2	This study
	GO-m $\beta$ CD	83.33	10-200	6.0	298	2	This study

According to a report by Madadrang *et al.* (2012), the sorption capacity of GO was enhanced by introducing chelating groups of *N*-trimethoxysilylpropyl) ethylenediamine triacetic acid through

silanization reaction to form EDTAGO-silane composite. The study attributed the sorption performance of the composite to the both the presence of –COOH and –OH functional groups of the GO surface and the –COOH groups of the EDTA. The sorption processes responsible the uptake of Pb(II) ions by the composite were as shown in Eqns 11-16.

#### 4.1.3 Competitive sorption studies

The competitive sorption experiments of Cu(II) and Pb(II) by the adsorbents were carried out in Cu(II)/Pb(II) mixture at initial metal ion concentrations of 5 and 10 mg/L. The simultaneous sorption of Pb<sup>2+</sup> and Cu<sup>2+</sup> (binary metal ion system) and single metal (Pb<sup>2+</sup>) ion system onto the GO-mβCD adsorbent is as shown in Fig. 20. The sorption of Pb(II) ions the single and binary metal ion system was not significantly different as indicated in Table 9. This could be attributed to the fact the GO-mβCD could not adsorb Cu(II) ions.

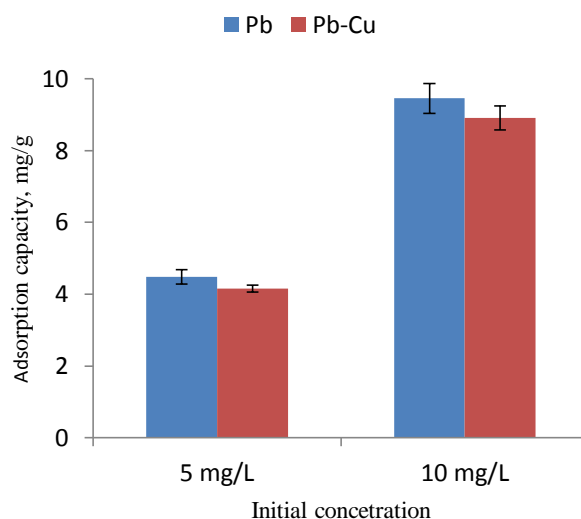


Fig. 20: Sorption of Pb(II) ions onto GO-mβCD in the presence of Cu(II) ions

Table 9: Means of metal ions in a single and binary metal ion system.

Metal ion concentration	5 mg/L	10 mg/L
Single metal ion system (Pb <sup>2+</sup> )	4.48±0.025	9.45±0.421
Binary metal ion system(Pb <sup>2+</sup> and Cu <sup>2+</sup> )	4.16±0.095	8.91±0.335
LSD(p≤0.05)	NS	NS

#### 4.1.4 Regeneration of adsorbent studies

The repeated viability of an adsorbent through sorption-desorption cycles are important because it reduces the overall cost of the adsorbent. This study endeavored in determining the performance of the m $\beta$ CD modified GO, hence the desorption experiments focused only on the GO-m $\beta$ CD adsorbent with the pH adjusted 1.0, 2.0, 3.0, 4.0 and 5.0. Desorption of Pb(II) from GO-m $\beta$ CD increased with decrease in pH with highest desorption obtained at pH 1.0 as shown in Fig. 21. The sorption efficiency of five consecutive cycles at pH 2.0 as also shown in Fig. 22 was above 90%, indicating that GO-m $\beta$ CD can be reused for about five times without significant change in its sorption efficiency. Wu *et al.* (2013) also reported that by adjusting the pH solution the desorption rate for Cu(II) ions using GO adsorbent decreased with increase in pH. The study also indicated that the sorption capacity of GO could maintain above 95% of its initial capability after five cycles and above 90% after ten cycles. In the investigation of desorption of Pb(II) ions from EDTA-GO using HCl solution, Madadrang *et al* (2012) also observed that the desorption rate increased with decrease in the pH value of the washing solution. The study showed that the desorption of Pb(II) ions from EDTA-GO surface was about 9-15% at pH > 6 which increased to about 90% at pH < 2 .

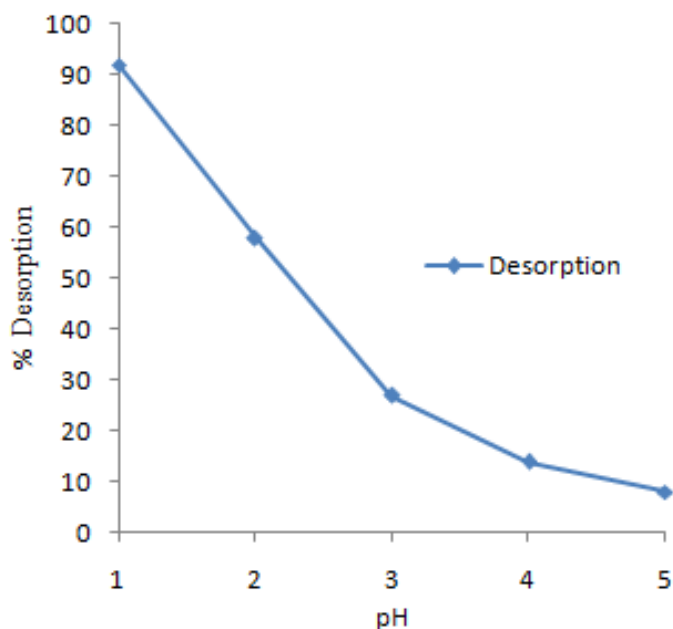


Fig. 21: Desorption of Pb(II) from GO-m $\beta$ CD at different pH values

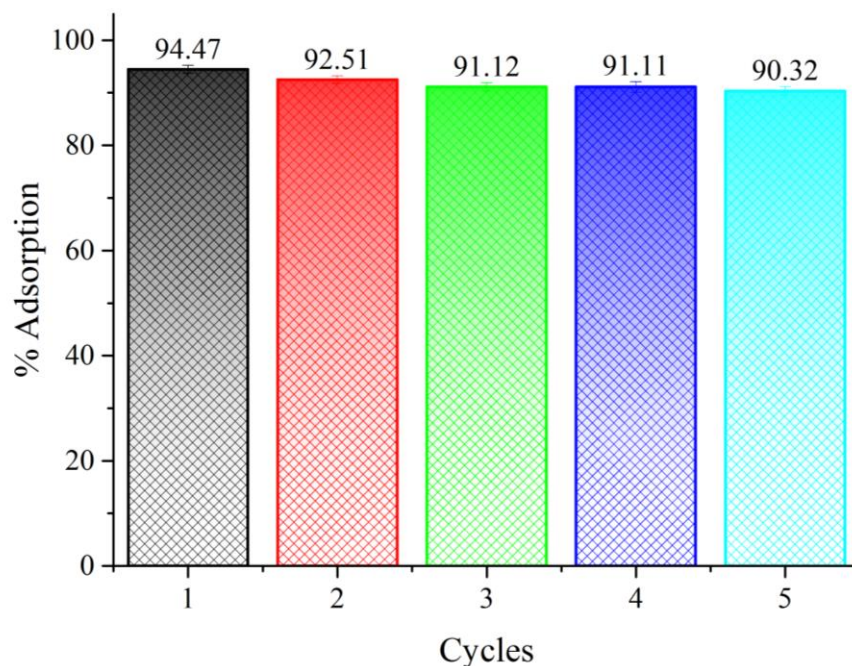


Fig. 22: The reusability of GO-m $\beta$ CD in five consecutive cycles

## 4.2 The oMWCNT-polypyrrole nanocomposite

### 4.2.1 Synthesis and Characterization

Fig. 23 shows the FT-IR spectra of the CNT and the composite, comparison of the FT-IR spectrum of pMWCNT with oMWCNT showed the appearance of new bands at  $1732\text{ cm}^{-1}$  associated with the C=O stretching in the COOH group oxidation of pMWCNT. Similar results were observed after acid treatment by Vukovic *et al.* (2011) and Zhang & Xu (2015). All the three spectra have the bands  $3436\text{ cm}^{-1}$ ,  $2926\text{ cm}^{-1}$  and  $1637\text{ cm}^{-1}$  corresponding to -OH, C-H and C=C stretchings, respectively. However, the  $1637\text{ cm}^{-1}$  band on oMWCNT/Ppy spectrum decreased in intensity because of the  $\pi$ - $\pi$  interaction of CNT with pyrrole. On the other hand, the oMWCNT/Ppy spectrum has the  $1547\text{ cm}^{-1}$  and  $1462\text{ cm}^{-1}$  band for C=C and C-C stretching vibration of pyrrole ring in Ppy, respectively. The characteristic peaks at  $780\text{ cm}^{-1}$  and  $1176\text{ cm}^{-1}$  assigned to pyrrole ring vibrations and  $1317\text{ cm}^{-1}$ ,  $1043\text{ cm}^{-1}$  and  $900\text{ cm}^{-1}$  assigned to C-H in plane bending, C-H in plane deformation and C-H out of plane bending of pyrrole, respectively (Sun *et al.*, 2002).

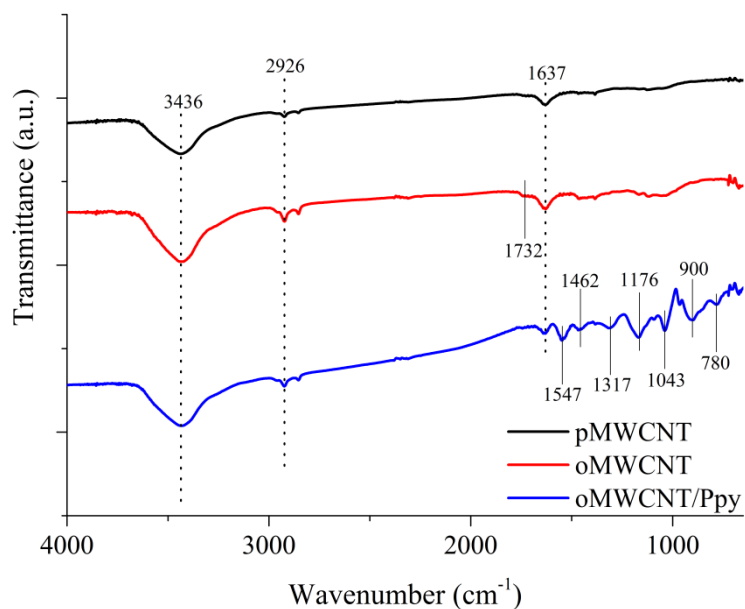


Fig 23: The FT-IR spectra of pMWCNT, oMWCNT and oMWCNT/Ppy

The SEM images of pMWCNT, oMWCNT and the oMWCNT/Ppy are shown in Fig. 24. Due to their nano size and  $\pi$ - $\pi$  interaction, pMWCNT tend to agglomerate (Fig. 24 (a)). However, oMWCNT Fig. 24 (b) is less entangled than pMWCNT. This can be attributed to the oxygen functionalities by acid treatment generating negative charge resulting to repulsion forces between the tubes (Rurlle *et al.*, 2007). On the other hand, the homogenously flower-like particles on the oMWCNT in Fig. 24 (c) reveal the Ppy coating on the oMWCNT. These indicates that the Ppy was incorporated onto the oMWCNT.

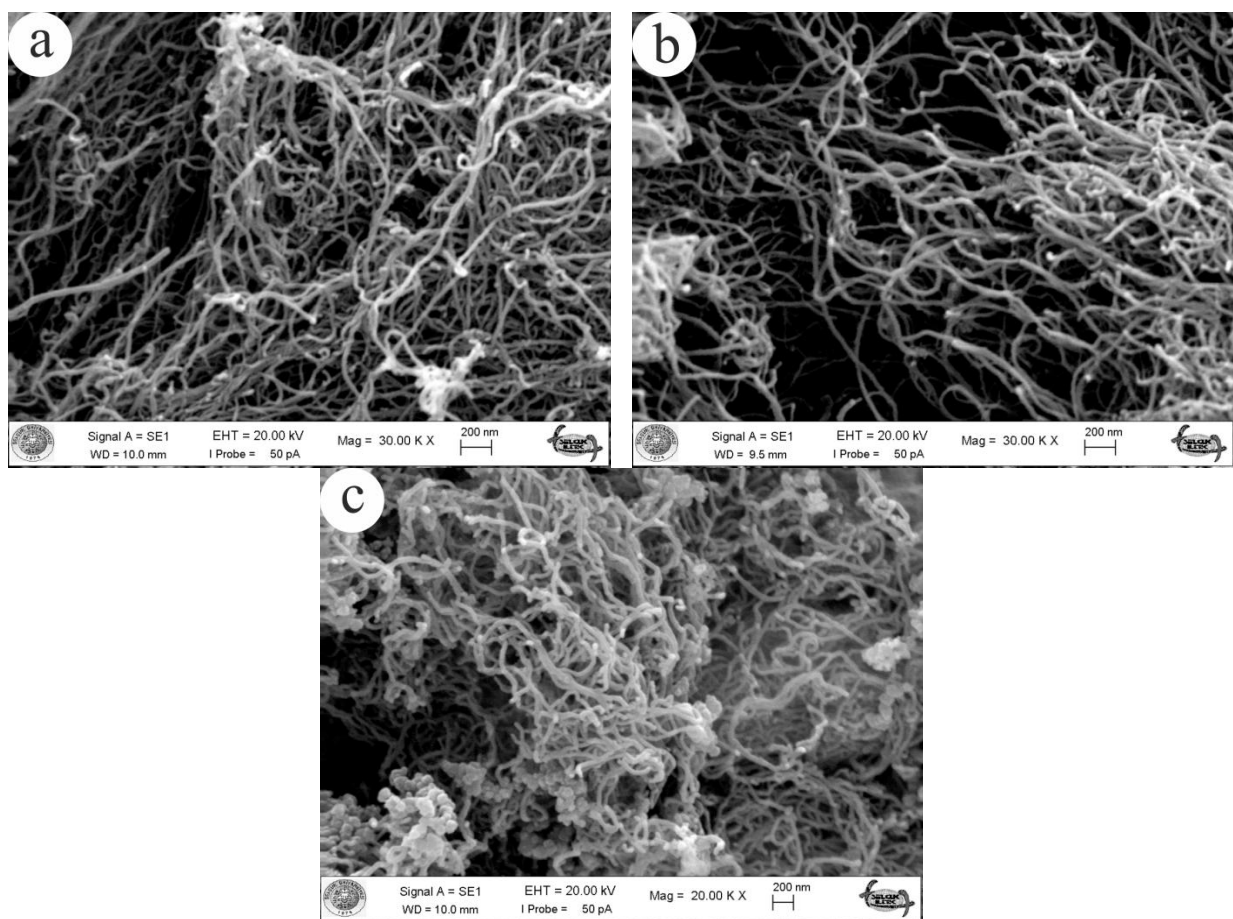


Fig. 24: The SEM micrographs of pMWCNT (a), oMWCNT (b) and the oMWCNT/Ppy (c)

Fig. 25 shows the pore size distribution of the pMWCNT, oMWCNT and oMWCNT/Ppy, which indicates that all the adsorbents are microporous. Their physical properties calculated using NLDFT method and the BET adsorption data is listed in Table 10. Adsorbents porous volume includes principally pores with a diameter less than 2 nm which are considered as microporous. Micropores volume decreased after the acidic treatment of pMWCNT, this evolution could be attributed to the removal of amorphous carbons ( $C_{sp^3}$ ) around pMWCNT as has been noted by Li *et al.* (2006). However, this acid treatment slightly affects the structure of MWCNT, since the pMWCNT and oMWCNT specific surface areas are almost equivalent ( $235.96 \text{ m}^2 \text{ g}^{-1}$  and  $239.91 \text{ m}^2 \text{ g}^{-1}$  respectively). This fact further supports the chemical modification of pMWCNT with acidic treatment. On the other hand, the oMWCNT/Ppy microporous volume, as well as their specific surface area, is lower than those of oMWCNT, this may have resulted by the Ppy occupation of pores.

Table 10: The physical properties of the pMWCNT, oMWCNT and oMWCNT/Ppy

Adsorbent	Pore diameter (Å)	Surface area (m <sup>2</sup> /g)	Pore volume (cm <sup>3</sup> /g)
pMWCNT	14.48	235.96	0.148
oMWCNT	16.57	239.91	0.088
oMWCNT/Ppy	14.48	130.43	0.066

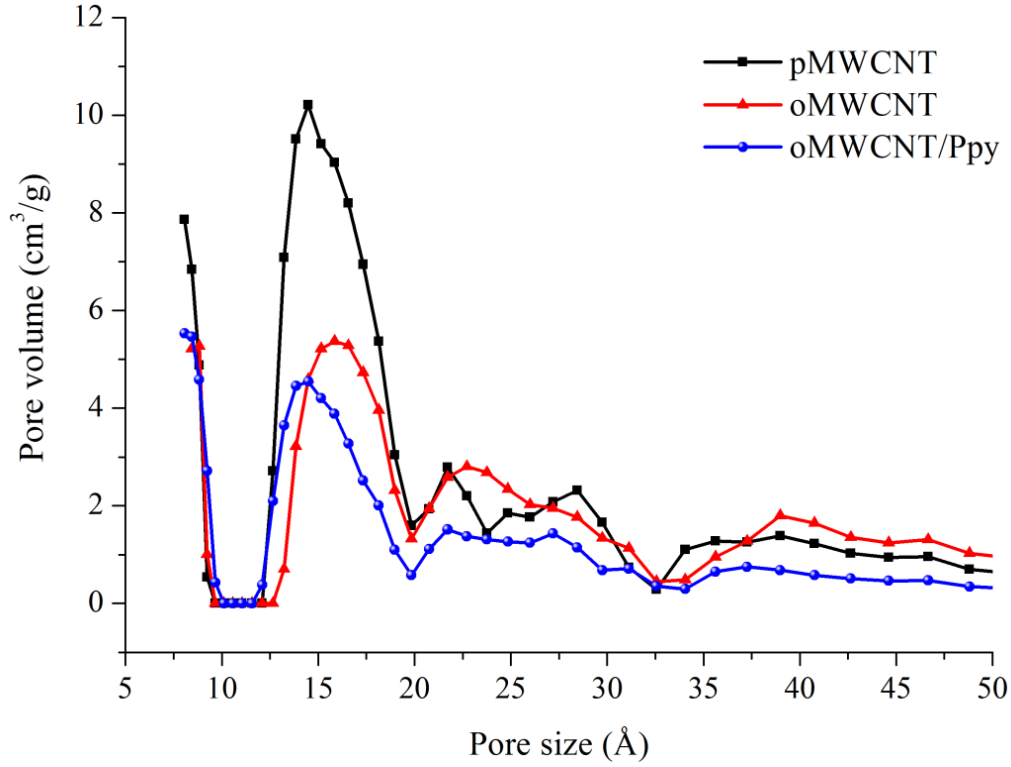


Fig. 25: The particle distribution the pMWCNT, oMWCNT and oMWCNT/Ppy

The Raman spectra of pMWCNT, oMWCNT and oMWCNT/Ppy in Fig. 26 show the changes in graphitic skeleton of CNT. The G-band at  $< 1580 \text{ cm}^{-1}$  is associated with graphitic two dimensional hexagonal lattice associated of  $\text{sp}^2$  carbon stretching modes of carbon while the D-band at  $< 1350 \text{ cm}^{-1}$  represents  $\text{sp}^3$ -hybridized carbon which is associated with disorder in the graphitic skeleton (Costa *et al.*, 2008). The ratio of the intensities of the peaks ( $I_D/I_G$ ) was used to show the alterations on the CNT skeleton. The increase of  $I_D/I_G$  ratio after acid treatment of CNT is an indication of oxidation as was noted by Kitamura *et al.* (2011). The  $I_D/I_G$  ratio of oMWCNT was higher than that of pMWCNT indicating an increase in disorder graphitic CNT resulting

from the etching of the tubes through the acid treatment. Similarly, the  $I_D/I_G$  ratio of oMWCNT/Ppy is higher than that of oMWCNT also showing further changes in the CNT side walls. This could be attributed to the electrostatic interaction between the oMWCNT and Ppy which is further supported by Fig. 24(c).

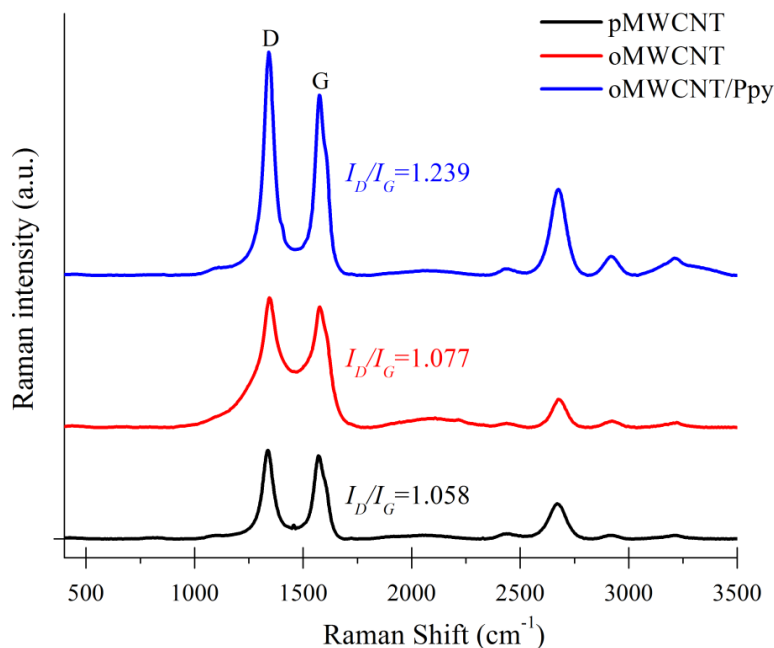


Fig. 26: Raman spectra of pMWCNT, oMWCNT and oMWCNT/Ppy

The thermogravimetric experiments performed on the pMWCNT, oMWCNT and oMWCNT/Ppy samples are shown in Fig. 27. Approximately 1% weight loss at a temperature below 150°C was observed for all the samples which is associated with the evaporation of physisorbed water molecule as has been reported by Datsyuk *et al.* (2008). Above 900°C a further loss of mass estimated at < 2% for both pMWCNT and oMWCNT which corresponds to the degradation of amorphous carbon was observed while a mass loss of about 1.5% between 150-500°C corresponding to degradation of the carboxyl and hydroxyl groups on the oMWCNT walls as noted by Huo *et al.* (2001) and Datsyuk *et al.* (2008). However, while pMWCNT and oMWCNT thermograms show relative thermal stability, oMWCNT/Ppy shows drastic loss in % mass starting from 150 to 1000°C with a residue of 72 wt.%. Thus, the percentage weight content of the Ppy coating on the oMWCNT/Ppy could be calculated by using the oMWCNT residue

which was 95 wt.% at 1000°C as  $95 - 72 = 23$  wt.%. The TGA curves also confirm that the Ppy was successfully attached onto the oMWCNT.

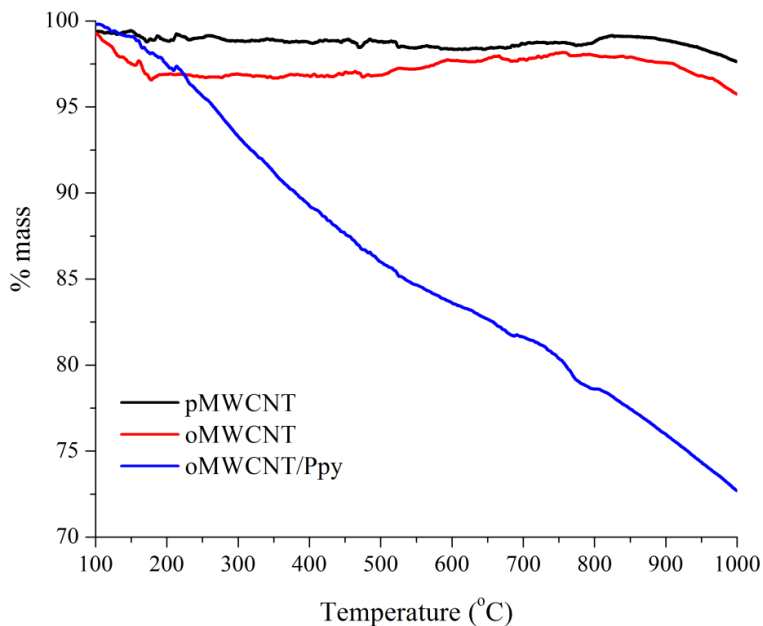


Fig. 27: TGA spectra of pMWCNT, oMWCNT and oMWCNT/Ppy

## 4.2.2 Adsorption studies

### 4.2.2.1 Effect of initial pH

Fig. 28 shows the influence of pH on the adsorption capacity of the pMWCNT, oMWCNT and oMWCNT/Ppy for Pb(II) and Cu(II) ions, respectively. The percentage removal of Pb(II) by pMWCNT, oMWCNT and oMWCNT/Ppy at pH= 6.0 was 13.5%, 46% and 58%, respectively.

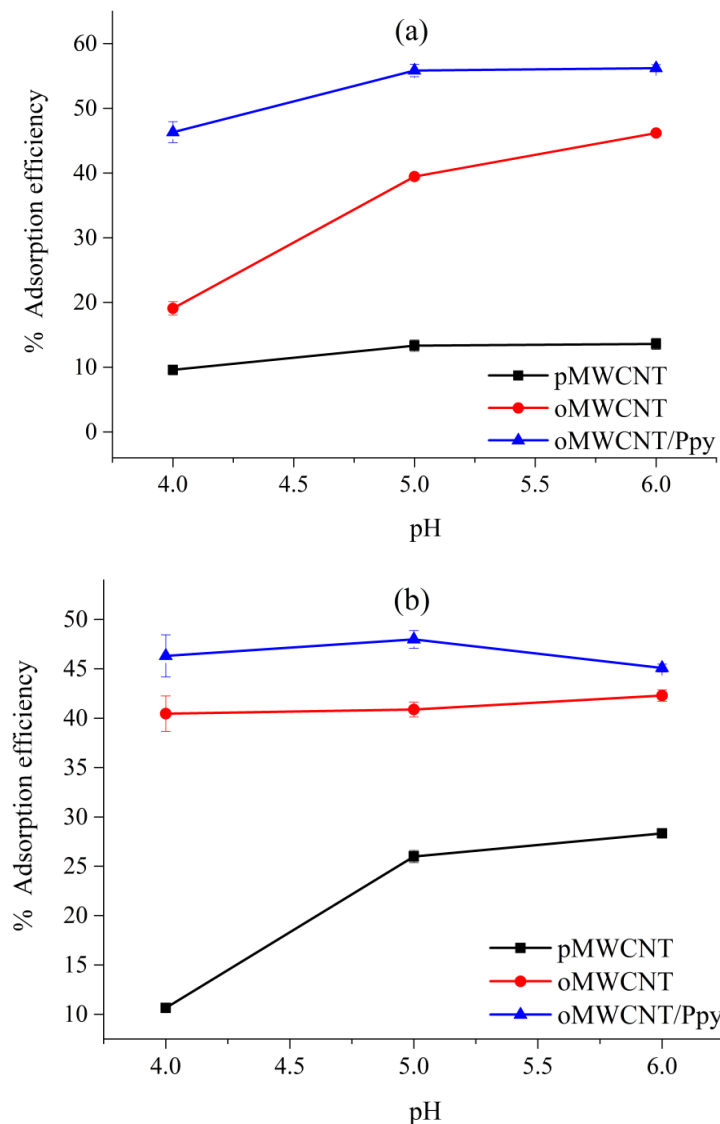


Fig. 28: Effect of pH on sorption of (a) Pb(II) and (b) Cu(II) by pMWCNT, oMWCNT and oMWCNT/Ppy (1 mg/mL dosage, contact time = 1 h, concentration = 10 mg/L)

The sorption efficiency for Pb(II) by oMWCNT increased with increase in pH from 4.0 to 6.0. The lead species in aqueous solutions are known to exist in the forms;  $Pb^{2+}$ ,  $Pb(OH)^+$ ,  $Pb(OH)_2$ , and  $Pb(OH)_3^-$  (Xu *et al.*, 2008). At  $pH < 7$  the dominant Pb(II) species is  $Pb^{2+}$  hence the low  $Pb^{2+}$  sorption at lower pH by all the adsorbents could be attributed to the competition between  $H^+$  and  $Pb^{2+}$  in the solution. However, at higher pH 5.0 and 6.0 there was an increase in uptake of  $Pb^{2+}$  by oMWCNT. This may be attributed to decreased competition for sorption sites between the  $H^+$  and  $Pb^{2+}$ , the negative charges on the oMWCNT walls hence take up the  $Pb^{2+}$  through electrostatic attraction. The sorption of Pb(II) by oMWCNT/Ppy, on the other hand, increased

from pH 4.0 to pH 5.0 and remained almost constant at pH 5.0 and pH 6.0. This is possibly attributed to the fact that the sorption mechanism by oMWCNT/Ppy is different from that of oMWCNT, at low pH the Ppy chain are highly protonated resulting in cationic repulsion of  $\text{Pb}^{2+}$  but as the pH increases there is electrostatic attraction between  $\text{Pb}^{2+}$  and the electron pair of nitrogen atom in the Ppy (Sahmetlioglu *et al.*, 2014). In addition, there was low influence by pH on the sorption of Pb(II) by pMWCNT (Fig. 28a) this is because unlike oMWCNT, pMWCNT have low surface charge that may have an effect on their sorption capacity as pH changes as has been reported by Li *et al.* (2002) and Vukovic *et al.* (2011). At above pH 6 there was precipitation, thus all the experiments involving the sorption of Pb(II) in this study were performed at pH 6.0.

The influence of pH on the sorption capacity of Cu(II) (Fig. 28b) by the oMWCNT/Ppy adsorbent remained almost constant at pH 4.0 and 5.0 with a drop at pH 6.0, while that for pMWCNT and oMWCNT increased with increase in pH. The Cu(II) species are known to exist in aqueous solutions in the forms;  $\text{Cu}^{2+}$ ,  $\text{Cu}(\text{OH})^+$ ,  $\text{Cu}(\text{OH})_2$ ,  $\text{Cu}(\text{OH})_3^-$  and  $\text{Cu}(\text{OH})_4^{2-}$  (Shen *et al.*, 2010). Thus the competition between  $\text{H}^+$  and copper cations for the sorption sites at lower pH and precipitation of  $\text{Cu}(\text{OH})_2$  at  $\text{pH} > 6$  (Wang, Li, & Su, 2009) make it necessary to restrict the study on the effect of pH between 4.0 and 6.0. The maximum sorption of Cu(II) by the oMWCNT/Ppy took place at pH 5.0, indicating that the deprotonation of the amine of the nitrogen in the Ppy by Cu(II) is at lower pH; similar to the observation made by Hosseini *et al.* (2015) and Chaves *et al.* (2015). Similarly, the sorption of Cu(II) by pMWCNT and oMWCNT seemed to be guided by the change in surface charge. Therefore, the subsequent sorption experiments for Cu(II) in this study were performed at pH 5.0.

#### **4.2.2.2 Effect of initial concentration**

The experimental means for the metal ions uptake at varying initial metal ion concentrations were as indicated in Table 11. The results indicate that the sorption of Pb(II) ions by the adsorbents were significantly different as well as the uptake of Cu(II). The sorption isotherms of Pb(II) and Cu(II) with pMWCNT, oMWCNT and oMWCNT/Ppy at initial concentration (10-100 mg/L) are shown in Fig. 29. The Langmuir (Eq.5) and Freundlich (Eq. 6) models – as mentioned in section 2.7 above - were used to describe the isothermic characteristics of the adsorbents.

Table 11: The means of Pb(II) and Cu(II) ions uptake by pMWCNT, oMWCNT and oMWCNT/Ppy at varying initial metal ion concentration

<b>Metal ions</b>	<b>Initial concentration (mg L<sup>-1</sup>)</b>	<b>10</b>	<b>20</b>	<b>30</b>	<b>40</b>	<b>50</b>	<b>100</b>
<b>Lead</b>	<b>pMWCNT</b>	1.23± 0.37	2.46± 0.63	2.52± 1.0	2.84± 0.5	3.10± 0.42	3.90± 0.29
	<b>oMWCNT</b>	5.33± 0.50	10.74 ±0.36	15.38 ±0.36	15.96 ±0.33	16.55 ±0.49	17.40 ±0.08
	<b>oMWCNT/Ppy</b>	7.97± 0.21	14.76 ±0.21	19.56 ±0.47	21.86 ±0.24	21.70 ±0.58	22.10 ±0.41
<b>LSD (p≤0.05)</b>		0.58	1.36	3.28	2.38	3.99	4.55
<b>Copper</b>	<b>pMWCNT</b>	1.11± 0.28	1.76± 0.78	2.36± 0.19	2.74± 0.43	2.95± 0.15	2.90± 0.29
	<b>oMWCNT</b>	2.61± 0.29	5.83± 0.39	7.22± 0.67	8.16± 0.52	8.30± 0.5	8.60± 0.7
	<b>oMWCNT/Ppy</b>	4.32± 0.46	9.66± 0.35	12.60 ±0.30	13.24 ±0.36	13.35 ±0.5	13.10 ±0.6
<b>LSD(p≤0.05)</b>		0.39	1.33	1.32	2.44	3.35	3.32

The constants of Langmuir and Freundlich models are listed in Table 12. The correlation coefficients of Langmuir isotherm are higher than those of Freundlich model, indicating that Langmuir model better described the sorption characteristics of Pb(II) and Cu(II) onto pMWCNT, oMWCNT and oMWCNT/Ppy implying a monolayer sorption mechanism. The  $q_{max}$  and  $k_f$  values also indicate that the best sorption capacity for both Pb(II) and Cu(II) was achieved by the composite oMWCNT/Ppy suggesting that Ppy enhances the sorption capacity of oMWCNT. Despite the fact that the oMWCNT/Ppy shows lower surface area and pore volume than the other adsorbents its sorption capacity increased. This suggests that the deprotonation of the amine of the nitrogen in the Ppy is the possible sorption mechanism taking for Cu(II) and Pb(II) ions (Seid *et al.*, 2014)

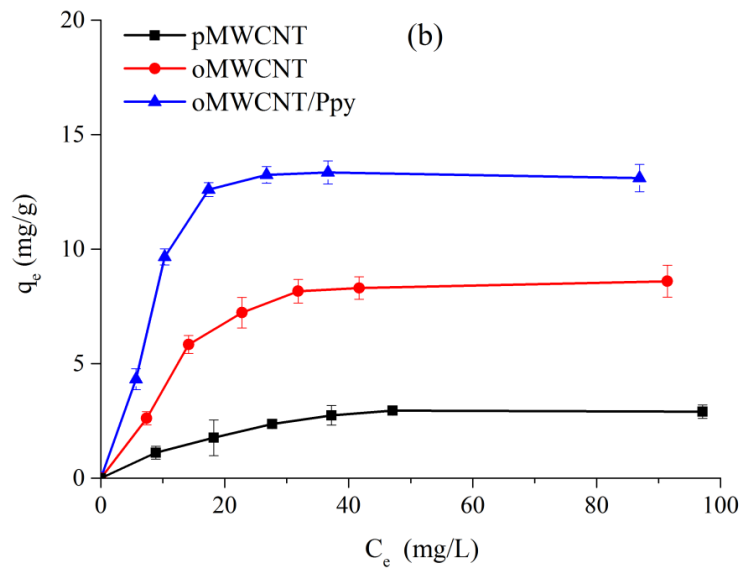
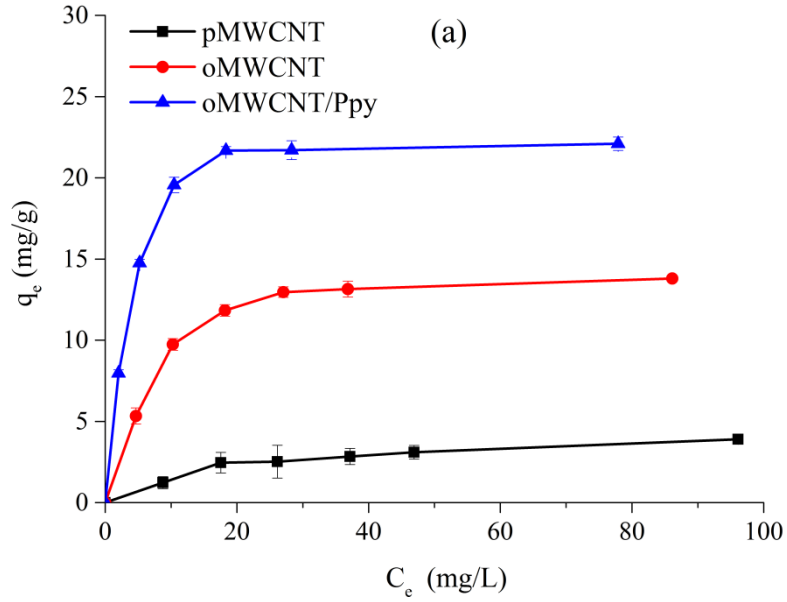


Fig. 29: Sorption isotherm of (a) Pb(II) pH = 6 and (b) Cu(II) pH = 5 on pMWCNT, oMWCNT and oMWCNT/Ppy (pH = 5, m/V = 1 mg/mL, concentration = 10-100 mg/L)

Table 12: Langmuir and Freundlich isothermic constants for Pb(II) and Cu(II) sorption on pMWCNT, oMWCNT and oMWCNT/Ppy

Metal ions	Adsorbent	Langmuir Parameters			Freundlich Parameters		
		$q_{\max}(\text{mg/g})$	$b(\text{mg/L})$	$r$	$K_f(\text{Lg}^{-1})$	$N$	$r$
Pb(II)	pMWCNT	5.15	0.0376	0.957	0.561	2.247	0.887
	oMWCNT	17.54	0.0978	0.973	4.093	3.165	0.793
	oMWCNT/Ppy	26.32	0.220	0.988	8.453	3.676	0.763
Cu(II)	pMWCNT	4.27	0.0399	0.981	0.507	2.336	0.843
	oMWCNT	16.95	0.0267	0.925	0.824	1.515	0.886
	oMWCNT/Ppy	24.39	0.0427	0.879	3.396	2.747	0.624

#### 4.2.2.3 Effect of contact time

The kinetic data collected in this study was fitted to the pseudo-first order as per Lagergren & Svenska (1898) and pseudo-second order as stated by Ho and McKay (2000) rate of sorption kinetic models and the results are listed in Table 13.

The  $q_e$  (cal) values (Table 13) are in agreement with the  $q_e$  experimental value in (Fig. 30) for pseudo-second order. The high  $R^2$  values and the close agreement between the experimental sorption capacities  $q_{e(\text{exp})}$  and the calculated values  $q_{e(\text{cal})}$  implies that the sorption of Pb(II) and Cu(II) follow pseudo-second order kinetics suggesting that the uptake process of these ions is through chemisorptions which are, similar to the observation made by Rao *et al.* (2007) in the review of the sorption of divalent metals from aqueous solutions by CNT.

Table 13 also shows that Pb(II) was more favorably adsorbed onto the adsorbents in this study than Cu(II). The competitive sorption of metals onto oxidized CNT has been studied and different orders of affinity of metals have been reported. Li *et al.* (2003a) found the order Pb(II) > Cu(II) > Cd(II), Stafiej & Pyrznska (2007) reported the order as Cu(II) > Pb(II) > Co(II) > Zn(II) > Mn(II) while the study by Tofighy & Mohammadi (2011) was in the metal order of Pb(II) > Cd(II) > Co(II) > Zn(II) > Cu(II). Similarly, the competitive sorption of metal ions onto pristinene CNTs by Salam (2013) reported metal affinity in the order Cu(II) > Pb(II) > Zn(II) > Cd(II) and that of CNTs modified by 8-hydroxyquinoline by Kosa *et al.* (2012) was in the order Cu(II) > Pb(II)  $\approx$  Zn(II) > Cd(II). Researchers have attributed this phenomenon to different factors;

which include the mode of preparation of the CNTs and the properties of the ions in the aqueous solutions. The difference could also be attributed to their respective electronegativities that allow leads ions to take up more bonding electrons than copper.

Table 13: Kinetic parameters of pseudo-first order and pseudo-second order equation for Pb(II) and Cu(II) sorption on pMWCNT, oMWCNT and oMWCNT/Ppy at concentration = 10 mg/L

Metal ions	Adsorbent	Pseudo-first order				Pseudo-second order			
		$q_e$ (mg/g)-exp	$q_e$ (mg/g)-cal	$k_1$ (g mg <sup>-1</sup> min <sup>-1</sup> )	$R^2$	$q_e$ (mg/g)-exp	$q_e$ (mg/g)-cal	$k_2$ (g mg <sup>-1</sup> min <sup>-1</sup> )	$R^2$
Pb(II)	pMWCNT	1.433	0.925	0.024	0.590	1.458	1.567	0.0616	0.995
	oMWCNT	4.151	4.70	0.044	0.835	4.171	4.950	0.0104	0.995
	oMWCNT/Ppy	5.720	1.511	0.024	0.453	5.720	5.882	0.0358	0.998
Cu(II)	pMWCNT	1.431	0.055	0.027	0.976	1.431	1.569	0.0467	0.998
	oMWCNT	3.175	3.663	0.039	0.941	3.175	3.663	0.0171	0.992
	oMWCNT/Ppy	4.268	2.506	0.040	0.924	4.268	4.566	0.0293	0.999

The removal of Pb(II) from aqueous solution by the adsorbents as a function of time showed that 40 min was sufficient for oMWCNT/Ppy, while pMWCNT, oMWCNT required 60 min (Fig. 30a). The removal of Pb<sup>2+</sup> by pMWCNT, eMWCNT and dMWCNT was reported to take an equilibrium time of 90 min (Vukovic *et al.*, 2011). This indicates that the sorption in this study was a fast process. The removal of Cu(II) ions for all the adsorbents the equilibrium time was 60 min (Fig. 30b). The different equilibrium time in the sorption of Pb(II) in the different sorbents could be attributed to the difference in the mean pore diameter of the adsorbents.

The experimental data was also fitted onto the intra-particle diffusion model according to Weber & Morris (1963) and the liquid film diffusion model according to Boyd, Adamson, & Myers (1947) in order to determine the diffusion mechanisms.

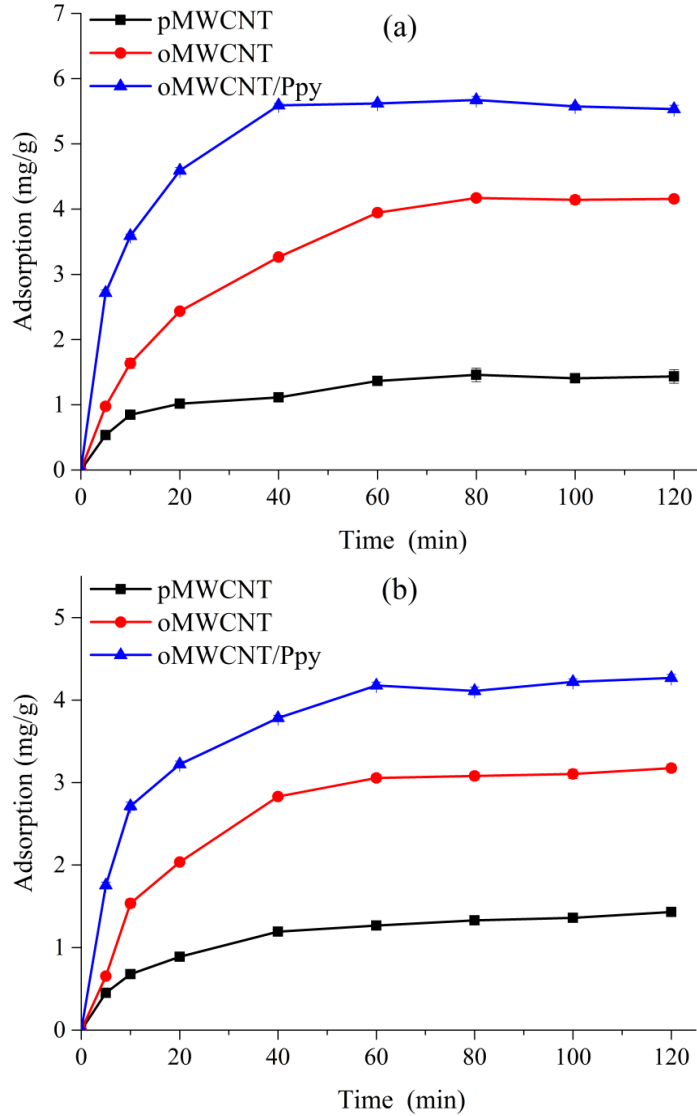


Fig. 30: Effect of contact time on sorption of (a) Pb(II) pH = 6 and (b) Cu(II) pH = 5 on pMWCNT, oMWCNT and oMWCNT/Ppy (m/V = 1 mg/mL, concentration = 10 mg/L)

Application of the intra-particle diffusion model to the experimental data for the metal diffusion in this study is shown in Fig. 31. The model indicates that intra-particle diffusion was not the rate determining step in the sorption process in this study. In addition, the liquid film diffusion model also assumes that the flow of the adsorbate particles through a liquid film is the rate determining step in a sorption process.

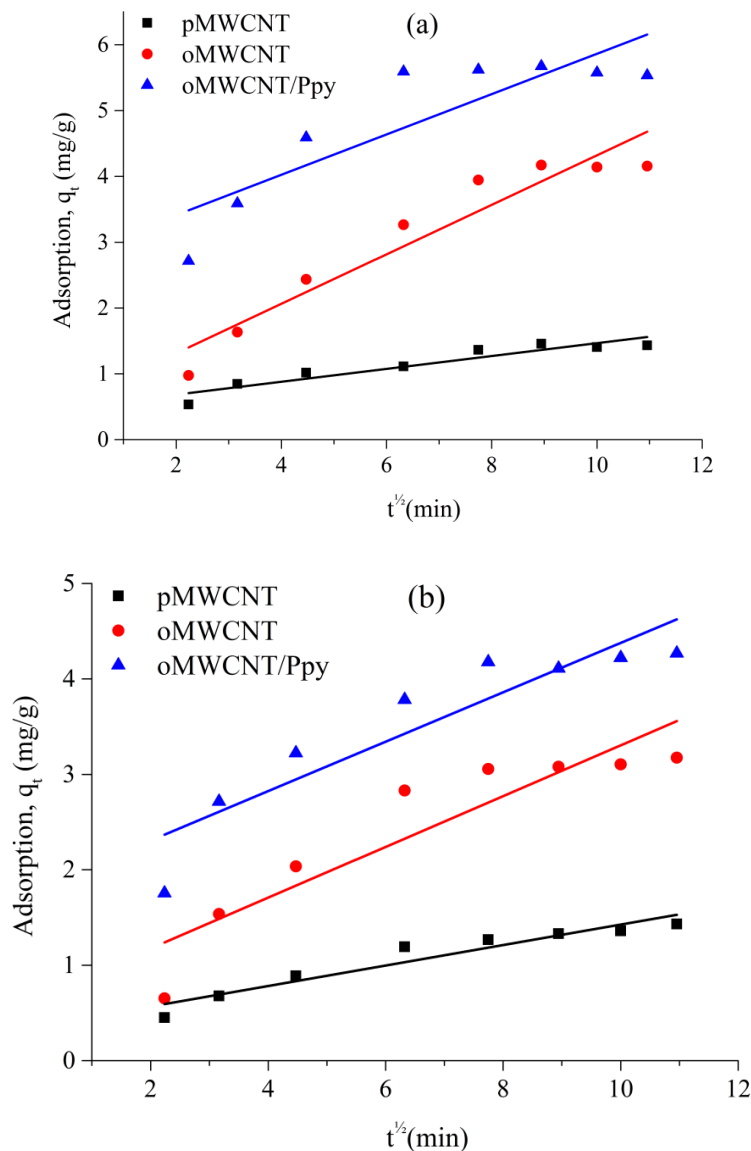


Fig. 31: Plots of intra-particle diffusion for the sorption of (a) Pb(II) and (b) Cu(II) on pMWCNT, oMWCNT and oMWCNT/Ppy ( $m/V = 1\text{mg/mL}$ , concentration =  $10\text{ mg/L}$ )

#### 4.2.2.4 Comparison of the sorption capacities of the adsorbents in this study with those in literature

The maximum sorption capacity ( $q_{\text{max}}$ ) values of the oMWCNT/Ppy were compared to the metal sorption capacities (Langmuir isotherm model) reported in other studies using different types of CNT as shown in Table 14. The  $q_{\text{max}}$  is seen to differ widely, and this could be attributed to the fact that these experiments were performed under different conditions such as pH and initial concentration and the CNT preparation in these studies are diverse.

Table 14: Comparison of the sorption capacities of the adsorbents in this study with those in literature

<b>Metal</b>	<b>Adsorbent</b>	<b>Sorption capacity, <math>q_{max}</math> (mg/g)</b>	<b>Conditions</b>	<b>References</b>
<b>Pb(II)</b>	Acidified MWCNT	17.44	pH 5, $C_o = 10\text{mg/L}$	Li <i>et al.</i> (2002)
	CNT	102.04	pH 5, Contact time = 80min	Kabbashi <i>et al.</i> (2009)
	MWCNT	15.9	pH 6	Ren <i>et al.</i> (2011)
	MWCNT modified with 2-vinylpyridine	22.04	pH 6	Ren <i>et al.</i> (2011)
	Raw CNT	2.94	pH 6.2, $C_o = 5-100\text{mg/L}$ , $T = 25^\circ\text{C}$	Vukovic <i>et al.</i> (2011)
	Oxidized MWCNT	37.36	pH 6.2, $C_o = 5-100\text{mg/L}$ , $T = 25^\circ\text{C}$	Vukovic <i>et al.</i> (2011)
	Oxidized MWCNT/ ethylenediamine	44.19	pH 6.2, $C_o = 5-100\text{mg/L}$ , $T = 25^\circ\text{C}$	Vukovic <i>et al.</i> (2011)
	Oxidized MWCNT	117.64	pH 7, $C_o = 1200\text{mg/L}$ ,	Tofighy & Mohammadi (2011)
	oMWCNT/Ppy	26.32	pH 6 $C_o = 10-100\text{mg/L}$	<b>This study</b>
<b>Cu(II)</b>	HNO <sub>3</sub> - modified CNT	28.49	pH 5, $C_o = 10\text{mg/L}$	Li <i>et al.</i> (2003a)
	CNT	26.41	pH 5, $C_o = 5\text{mg/L}$	Li <i>et al.</i> (2010)
	CNT/calcium alginate	84.88	pH 5, $C_o = 5\text{mg/L}$	Li <i>et al.</i> (2010)
	As grown CNT	14.4	pH 5.4, $C_o = 20\text{mg/L}$	Li <i>et al.</i> (2003d)
	Oxidized CNT	27.6	pH 5.2, $C_o = 20\text{mg/L}$	Li <i>et al.</i> (2003d)
	As produced CNT	8.25	pH 6, $T = 300\text{K}$	Wu (2007)
	HNO <sub>3</sub> - modified CNT	13.87	pH 6, $T = 300\text{K}$	Wu (2007)
	NaOCl –modified CNT	47.39	pH 6, $T = 300\text{K}$	Wu (2007)
	Oxidized MWCNT	64.93	pH 7, $C_o = 1200\text{mg/L}$ , $T = 298$	Tofighy & Mohammadi (2011)
	oMWCNT/Ppy	24.39	pH 5 $C_o = 10-100\text{mg/L}$ , $T = 298$	<b>This study</b>

For instance, as shown in Table 14, the CNT oxidized by NaOCl have higher sorption capacity than the CNT that was oxidized by HNO<sub>3</sub> as shown by Wu (2007). However, in almost all the studies, the sorption capacity of the modified CNT is higher compared to that of raw CNT which is in concurrence with that observed in this study. Therefore, oMWCNT/Ppy has shown considerable removal efficiency for Pb(II) and Cu(II) from aqueous solutions compared to individual oMWCNT adsorbent.

#### 4.2.3 Competitive sorption studies

The uptake of Pb(II) and Cu(II) by oMWCNT/Ppy in binary system was performed using the synthesized composite of oMWCNT/Ppy and the result is as shown in Fig. 32.

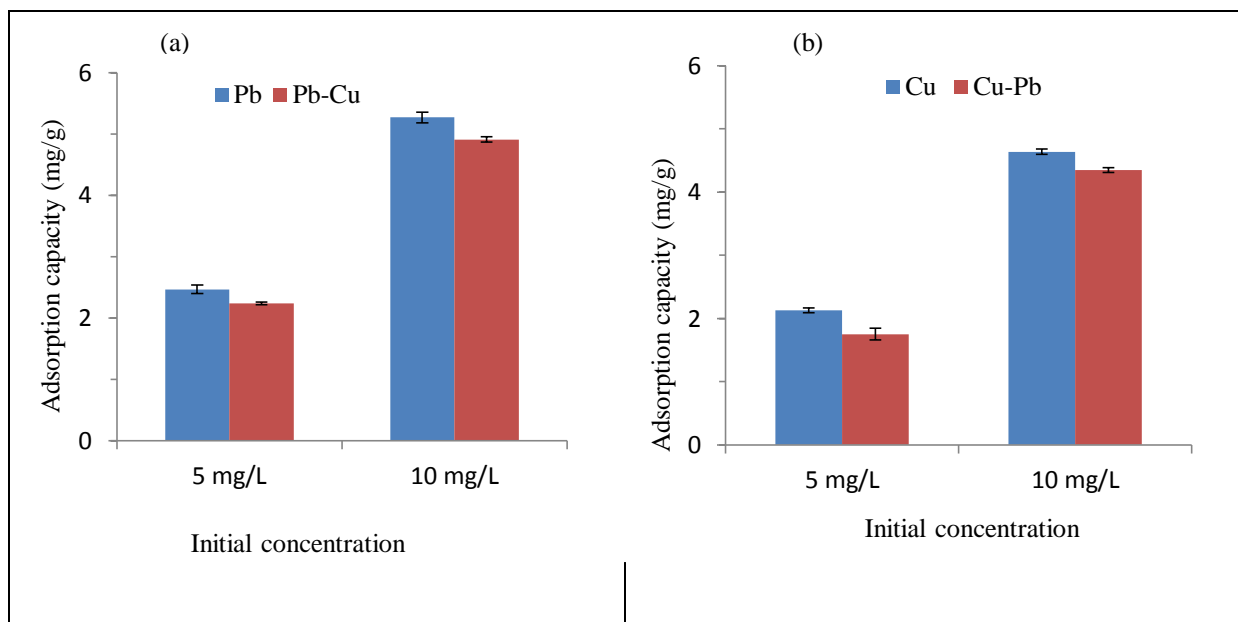


Fig. 32: Sorption of (a) Pb(II) ions and (b) Cu(II) ions onto oMWCNT/Ppy in a single and binary metal ion system

The sorption of both Pb(II) and Cu(II) onto the composite when in the binary metal ion system was found to be significantly lower than the sorption in a single metal ion system. Stafiej & Pyrznska (2007) also found that the sorption of Cu<sup>2+</sup> by CNT decreased when it is in a binary metal system with other metal ions. In another study carried out on both single and competitive sorption of Pb<sup>2+</sup>, Cu<sup>2+</sup> and Cd<sup>2+</sup> onto CNT, Li *et al.* (2003a) established that the sorption of these

metal ions decreased from 97.08, 28.49 and 10.86 mg L<sup>-1</sup> to 27.6, 17.6 and 2.4 mg L<sup>-1</sup>, respectively, in a tertiary metal ion system.

#### 4.2.4 Studies on the regeneration of the adsorbents

The sorption-desorption process was pH dependent, with desorption increasing with increase in the pH value of the washing solution. The reusability of oMWCNT/Ppy for the removal of Pb(II) was maintained above 95% while that for Cu(II) was above 90% of its initial capability, after five successive sorption/desorption cycles at pH 2. The percentage reusability for Pb(II) and Cu(II) for the first consecutive five cycles were as follows; 97, 97, 97, 96, 96 and 95, 93, 93, 92, 91, respectively as shown in Fig 33. This indicates that the oMWCNT/Ppy adsorbent can be reused or regenerated up to five times with a loss of about 10% of its initial sorption capacity. In a related study, on the repeated availability of MWCNTs/iron oxide/ $\beta$ CDs for Pb(II) ions sorption-desorption cycles, the composite was found to have lost about 5% of its sorption efficiency after five cycles Hu *et al.* (2010). Similarly, Vukovic *et al.* (2011) reported that desorption of Pb<sup>2+</sup> from MWCNT and composites after using five times was above 90%. The adsorbents; pristine, ethylenediamine and diethylenetriamine modified multi-walled carbon nanotubes (raw-MWCNT, e-MWCNT and d-MWCNT) exhibited 98.5%, 96.7% and 97.4% desorption deficiency at pH 1.5

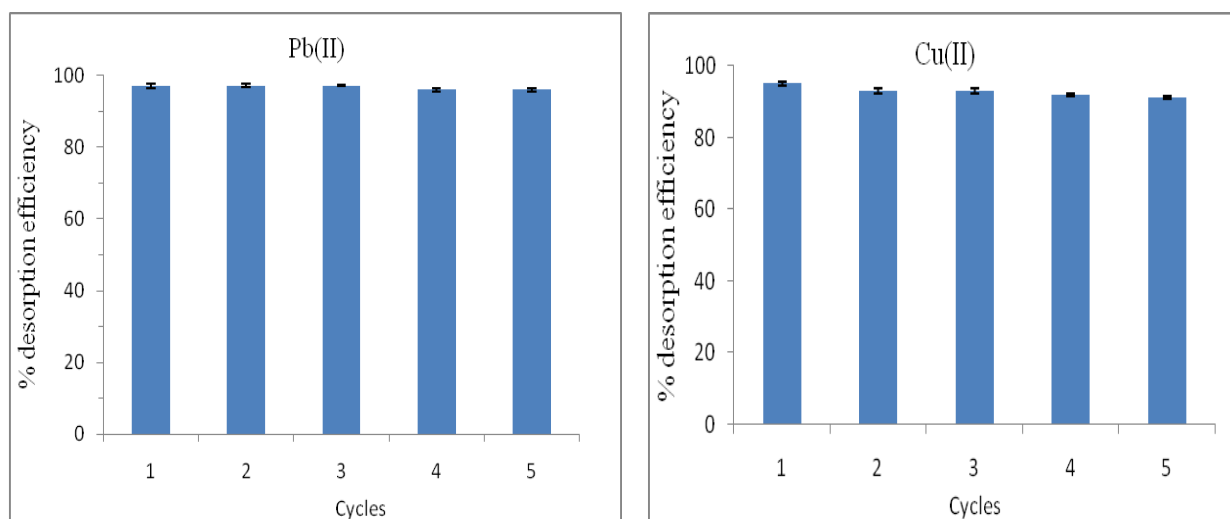


Fig 33: The reusability of oMWCNT/Ppy in five cycles

## CHAPTER 5

### SUMMARY, CONCLUSIONS AND RECOMMENDATIONS

#### 5.1 Summary

GO-m $\beta$ CD has been prepared and the characterization using FTIR, Raman spectroscopy, XRD and SEM showed that m $\beta$ CD was successfully attached to GO. The sorption equilibrium and kinetics of the adsorbents were well described by Langmuir isotherm and pseudo second order models, respectively. The maximum Pb(II) sorption capacity of GO-m $\beta$ CD (at pH=6 and room temperature) was 312.5 mg/g and GO (217.39 mg/g) but maximum Cu(II) sorption capacity for GO (90.9 mg/g) and GO-m $\beta$ CD (83.33 mg/g). This indicates that the m $\beta$ CD significantly ( $p \leq 0.05$ ) enhanced the sorption capacity of GO for Pb(II) ions but not for Cu (II) ions. The results show that sorption of both Pb(II) decreased slightly when the sorption took place in the presence of the other metal ion. The desorption studies show that the adsorbent GO-m $\beta$ CD can be used for five time with non-significant loss of its initial sorption capacity for Pb(II) ions.

The oMWCNT/Ppy has been synthesized and characterized by SEM, FTIR, Raman spectroscopy and TGA showed that oMWCNT/Ppy. The sorption tests considering the influence of pH, contact time and initial metal ion concentration reveals that removing Pb(II) and Cu(II) is mainly pH and time dependent. The sorption processes conformed to the Langmuir isotherm and pseudo-second order kinetic models. The maximum sorption capacity oMWCNT/Ppy was determined as 26.32 mg/g and 24.39 mg/g for Pb(II) and Cu(II), respectively. The Ppy, therefore, significantly ( $p \leq 0.05$ ) improved the sorption capacity of MWCNT for both Pb(II) and Cu(II) ions. The optimum pH of solution for sorption of Pb(II) and Cu(II) was 6 and 5 for respectively, with the order of metal affinity on the adsorbents being Pb(II) > Cu(II). The competitive studies show that the sorption efficiency of the oMWCNT/Ppy composite for both Pb(II) and Cu(II) significantly decreases ( $p \leq 0.05$ ) in a binary metal ion system compared to a single metal ion system. The desorption studies indicate that the composite adsorbent oMWCNT/Ppy can be used up to five cycles with minimum loss of its initial sorption capacity.

#### 5.2 Conclusions

- This study shows that GO-m $\beta$ CD nanocomposites can significantly remove Pb(II) ions (312.5 mg/g) from aqueous solutions compared to GO (217.39 mg/g) hence it can be applied as an adsorbent in wastewater treatment for the removal of Pb(II) ions.

- Optimum sorption would be achieved when the solution is at pH 6 and the adsorbent can be reused in five sorption/desorption cycles
- The oMWCNT/Ppy nanocomposites, on the other hand, can be applied in the removal of Pb(II) and Cu(II) ions with maximum sorption of 26.32 mg/g and 24.39 mg/g compared to oMWCNT with sorption capacity of 17.54 mg/g and 16.95 mg/g, respectively.
- This can be attained when the solution pH for Pb(II) and Cu(II) ions is 6 and 5, respectively.
- The adsorbent can be reused in five cycles with minimum loss of its efficiency.

### **5.3 Recommendations**

The GO-m $\beta$ CD composite can be used to sorb Pb(II) ions from wastewater with the maximum adsorption capacity achieved at pH 6 at 298 K.

The oMWCNT/Ppy suitable for adsorption of both Pb(II) and Cu(II) and full potential can be achieved at pH 6 and 5 at 298 K, respectively.

The presence of Cu(II)/Pb(II) in the solution does affect the sorption of the other ion when using oMWCNT/Ppy

Both adsorbents can be reused for up to five consecutive cycles and retain about 90% of their initial sorption capacities.

### **5.4 Suggestions for future studies**

More of other heavy metal species and these derivatives need to be investigated to come up with a wider conclusion on the sorption capacity of these derivatives on various toxicological heavy metal species that raise lots of concern in water destined for and after use.

Further derivatization could be carried out to incorporate magnetic particles to enhance the separation of the adsorbents from water after sorption has taken place.

## REFERENCES

- Abbas, A., Al-Amer, A. M., Laoui, T., Al-Marri, M. J., Nasser, M. S., Khraisheh, M., & Atieh, M. A. (2016). Heavy metal removal from aqueous solution by advanced carbon nanotubes: critical review of adsorption applications. *Separation and Purification Technology*, 157, 141-161.
- Abdolmaleki, A., Mallakpour, S., & Borandeh, S. (2015). Efficient heavy metal ion removal by triazinyl- $\beta$ -cyclodextrin functionalized iron nanoparticles. *RSC Advances*, 5(110), 90602-90608.
- Alawa, B., Srivastava, J., Srivastava, A., & Palsania, J. (2015). Adsorption of heavy metal Pb (II) from synthetic waste water by polypyrrole composites. *International Journal of Chemical Studies*, 3, 04-08.
- Al-Rashdi, B., Somerfield, C., & Hilal, N. (2011). Heavy metals removal using adsorption and nanofiltration techniques. *Separation & Purification Reviews*, 40(3), 209-259.
- Alsewaleem, F. D., & Aljlil, S. A. (2013). Recycled polymer/clay composites for heavy-metals adsorption. *Materials Technology*, 47, 525-529.
- Amer, M. W., Khalili, F. I., & Awwad, A. M. (2010). Adsorption of lead, zinc and cadmium ions on polyphosphate-modified kaolinite clay. *Journal of Environmental Chemistry and Ecotoxicology*, 2(1), 001-008.
- Annadurai, G., Juang, R. S., & Lee, D. J. (2003). Adsorption of heavy metals from water using banana and orange peels. *Water Science and Technology*, 47(1), 185-190.
- An, H. K., Park, B. Y., & Kim, D. S. (2001). Crab shell for the removal of heavy metals from aqueous solution. *Water Research*, 35(15), 3551-3556.
- An, K. H., Kim, W. S., Park, Y. S., Choi, Y. C., Lee, S. M., Chung, D. C., ... & Lee, Y. H. (2001). Supercapacitors using single-walled carbon nanotube electrodes. *Advanced Materials*, 13(7), 497-500.
- An, X., Jimmy, C. Y., Wang, Y., Hu, Y., Yu, X., & Zhang, G. (2012). WO<sub>3</sub> nanorods/graphene nanocomposites for high-efficiency visible-light-driven photocatalysis and NO<sub>2</sub> gas sensing. *Journal of Materials Chemistry*, 22(17), 8525-8531.

- Andrade, N. F., Martinez, D. S. T., Paula, A. J., Silveira, J. V., Alves, O. L., & Souza Filho, A. G. (2013). Temperature effects on the nitric acid oxidation of industrial grade multiwalled carbon nanotubes. *Journal of Nanoparticle Research*, *15*(7), 1761.
- de Andrés, J. M., Orjales, L., Narros, A., de la Fuente, M. D. M., & Rodríguez, M. E. (2013). Carbon dioxide adsorption in chemically activated carbon from sewage sludge. *Journal of the Air & Waste Management Association*, *63*(5), 557-564.
- Babel, S., & Kurniawan, T. A. (2003). Low-cost adsorbents for heavy metals uptake from contaminated water: a review. *Journal of Hazardous Materials*, *97*(1-3), 219-243.
- Badruddoza, A. Z. M., Tay, A. S. H., Tan, P. Y., Hidajat, K., & Uddin, M. S. (2011). Carboxymethyl- $\beta$ -cyclodextrin conjugated magnetic nanoparticles as nano-adsorbents for removal of copper ions: synthesis and adsorption studies. *Journal of Hazardous Materials*, *185*(2-3), 1177-1186
- Balandin, A. A., Ghosh, S., Bao, W., Calizo, I., Teweldebrhan, D., Miao, F., & Lau, C. N. (2008). Superior thermal conductivity of single-layer graphene. *Nano Letters*, *8*, 902-907.
- Barakat, M. A. (2011). New trends in removing heavy metals from industrial wastewater. *Arabian Journal of Chemistry*, *4*(4), 361-377.
- Bertinato, J., & L'Abbé, M. R. (2004). Maintaining copper homeostasis: regulation of copper-trafficking proteins in response to copper deficiency or overload. *The Journal of Nutritional Biochemistry*, *15*(6), 316-322.
- Bhaumik, M., Setshedi, K., Maity, A., & Onyango, M. S. (2013). Chromium (VI) removal from water using fixed bed column of polypyrrole/Fe<sub>3</sub>O<sub>4</sub> nanocomposite. *Separation and Purification Technology*, *110*, 11-19.
- Biesaga, M., & Pyrzynska, K. (2006). The evaluation of carbon nanotubes as a sorbent for dicamba herbicide. *Journal of Separation Science*, *29*(14), 2241-2244.
- Biškup, B., & Subotić, B. (2005). Removal of heavy metal ions from solutions using zeolites. III. Influence of sodium ion concentration in the liquid phase on the kinetics of exchange processes between cadmium ions from solution and sodium ions from zeolite A. *Separation Science and Technology*, *39*(4), 925-940.
- Boyd, G. E., Adamson, A. W., & Myers Jr, L. S. (1947). The exchange adsorption of ions from aqueous solutions by organic zeolites. II. Kinetics<sup>1</sup>. *Journal of the American Chemical Society*, *69*(11), 2836-2848.

- Brodie, B. C. (1859). XIII. On the atomic weight of graphite. *Philosophical Transactions of the Royal Society of London*, 149, 249-259
- Buglione, L., Bonanni, A., Ambrosi, A., & Pumera, M. (2012). Gold Nanospacers greatly enhance the capacitance of electrochemically reduced graphene. *ChemPlusChem*, 77(1), 71-73.
- Chang, Q., & Wang, G. (2007). Study on the macromolecular coagulant PEX which traps heavy metals. *Chemical Engineering Science*, 62(17), 4636-4643.
- Chang, Y. H., Wu, M. S., & Lin, K. F. (2014). Grafting polyimide to MWCNT for enhancing dispersion and properties of MWCNT/polyetherimide nanocomposites. *Journal of Polymer Research*, 21(4), 419.
- Chávez-Guajardo, A. E., Medina-Llamas, J. C., Maqueira, L., Andrade, C. A., Alves, K. G., & de Melo, C. P. (2015). Efficient removal of Cr (VI) and Cu (II) ions from aqueous media by use of polypyrrole/maghemite and polyaniline/maghemite magnetic nanocomposites. *Chemical Engineering Journal*, 281, 826-836.
- Che, G., Lakshmi, B. B., Martin, C. R., Fisher, E. R., & Ruoff, R. S. (1998). Chemical vapor deposition based synthesis of carbon nanotubes and nanofibers using a template method. *Chemistry of Materials*, 10(1), 260-267.
- Cohen-Tanugi, D., & Grossman, J. C. (2012). Water desalination across nanoporous graphene. *Nano Letters*, 12(7), 3602-3608.
- Costa, S., Borowiak-Palen, E., Kruszynska, M., Bachmatiuk, A., & Kalenczuk, R. J. (2008). Characterization of carbon nanotubes by Raman spectroscopy. *Materials Science-Poland*, 26(2), 433-441.
- Dai, L., He, P., & Li, S. (2003). Functionalized surfaces based on polymers and carbon nanotubes for some biomedical and optoelectronic applications. *Nanotechnology*, 14(10), 1081.
- Dameron, C., & Howe, P. D. (1998). Copper Environmental Health criterion 200. *Geneva: World Health Organization*.
- Datsyuk, V., Kalyva, M., Papagelis, K., Parthenios, J., Tasis, D., Siokou, A., ... & Galiotis, C. (2008). Chemical oxidation of multiwalled carbon nanotubes. *Carbon*, 46(6), 833-840.
- Ding, H. & Ram, M. K (2005). Applications of ordered ultrathin conducting polymeric films of polypyrrole. *Supramolecular Engineering of Conducting Materials*, 199231

- Diniz, C. V., Doyle, F. M., & Ciminelli, V. S. (2002). Effect of pH on the adsorption of selected heavy metal ions from concentrated chloride solutions by the chelating resin Dowex M-4195. *Separation Science and Technology*, 37(14), 3169-3185.
- Droste, R. L., & Gehr, R. L. (1997). *Theory and practice of water and wastewater treatment* (pp. 622-629). New York etc: Wiley.
- Elmorsi, T. M. (2011). Equilibrium isotherms and kinetic studies of removal of methylene blue by adsorption onto *miswak* leaves as a natural adsorbent. *Journal of Environmental Protection*, 2(6), 817-827
- Fan, L., Zhang, Y., Luo, C., Lu, F., Qiu, H., & Sun, M. (2012). Synthesis and characterization of magnetic  $\beta$ -cyclodextrin–chitosan nanoparticles as nano-adsorbents for removal of methyl blue. *International Journal of Biological Macromolecules*, 50(2), 444-450.
- Febrianto, J., Kosasih, A.N., Sunarso, J., Ju, Y. H., & Ismadji, S (2009). Equilibrium and kinetics in adsorption of heavy metals using biosorbents: a summary of recent studies. *Journal of Hazardous Materials*, 162, 616-645
- Feng, Y. S., Ma, J. J., Lin, X. Y., Zhang, J. S., Lv, P., Xu, H. J., & Luo, L. B. (2012). Covalent functionalization of graphene oxide by 9-(4-aminophenyl) acridine and its derivatives. *Chinese Chemical Letters*, 23(12), 1411-1414.
- Fu, F., & Wang, Q. (2011). Removal of heavy metal ions from wastewaters: a review. *Journal of Environmental Management*, 92(3), 407-418.
- Gao, B., Kleinhammes, A., Tang, X. P., Bower, C., Fleming, L., Wu, Y., & Zhou, O. (1999). Electrochemical intercalation of single-walled carbon nanotubes with lithium. *Chemical Physics Letters*, 307(3-4), 153-157.
- Gao, Z., Bandosz, T. J., Zhao, Z., Han, M., Liang, C., & Qiu, J. (2008). Investigation of the role of surface chemistry and accessibility of cadmium adsorption sites on open-surface carbonaceous materials. *Langmuir*, 24(20), 11701-11710.
- Gardiner, D. J. (1989). *Practical Raman Spectroscopy*; Springer-Verlag: Berlin
- Geim, A. K., & Novoselov, K. S. (2007). The rise of graphene. In *Nanoscience and Technology: A Collection of Reviews from Nature Journals* (pp. 11-19).
- Goyer, R. A., & Clarkson, T. W. (1996). Toxic effects of metals. *Casarett & Doull's Toxicology. The Basic Science of Poisons, Fifth Edition, Klaassen, CD [Ed]. McGraw-Hill Health Professions Division, ISBN, 71054766.*

- Guo, Y., Guo, S., Ren, J., Zhai, Y., Dong, S., & Wang, E. (2010). Cyclodextrin functionalized graphene nanosheets with high supramolecular recognition capability: synthesis and host-guest inclusion for enhanced electrochemical performance. *ACS Nano*, 4(7), 4001-4010.
- Gupta, V. K., Moradi, O., Tyagi, I., Agarwal, S., Sadegh, H., Shahryari-Ghoshekandi, R., ... & Garshasbi, A. (2016). Study on the removal of heavy metal ions from industry waste by carbon nanotubes: effect of the surface modification: a review. *Critical Reviews in Environmental Science and Technology*, 46(2), 93-118.
- Hao, L., Song, H., Zhang, L., Wan, X., Tang, Y., & Lv, Y. (2012). SiO<sub>2</sub>/graphene composite for highly selective adsorption of Pb (II) ion. *Journal of Colloid and Interface Science*, 369(1), 381-387.
- Hasar, H. (2003). Adsorption of nickel (II) from aqueous solution onto activated carbon prepared from almond husk. *Journal of Hazardous Materials*, 97(1-3), 49-57.
- He, T., Qi, X., Chen, R., Wei, J., Zhang, H., & Sun, H. (2012). Enhanced optical nonlinearity in noncovalently functionalized amphiphilic graphene composites. *ChemPlusChem*, 77(8), 688-693.
- Ho, Y. S., & McKay, G. (2000). The kinetics of sorption of divalent metal ions onto sphagnum moss peat. *Water research*, 34(3), 735-742.
- Horne, M. T., & Dunson, W. A. (1995). Effects of low pH, metals, and water hardness on larval amphibians. *Archives of Environmental Contamination and Toxicology*, 29(4), 500-505.
- Hosseini, S., Mahmud, N. E., Yahya, R. B., Ibrahim, F., & Djordjevic, I. (2015). Polypyrrole conducting polymer and its application in removal of copper ions from aqueous solution. *Materials Letters*, 149, 77-80.
- Hu, H., Xin, J. H., Hu, H., Wang, X., & Lu, X. (2014). Organic liquids-responsive  $\beta$ -cyclodextrin-functionalized graphene-based fluorescence probe: label-free selective detection of tetrahydrofuran. *Molecules*, 19(6), 7459-7479.
- Hu, J., Shao, D., Chen, C., Sheng, G., Li, J., Wang, X., & Nagatsu, M. (2010). Plasma-induced grafting of cyclodextrin onto multiwall carbon nanotube/iron oxides for adsorbent application. *The Journal of Physical Chemistry B*, 114(20), 6779-6785.
- Huang, Z., Liu, S., Zhang, B., Xu, L., & Hu, X. (2012). Equilibrium and kinetics studies on the absorption of Cu (II) from the aqueous phase using a  $\beta$ -cyclodextrin-based adsorbent. *Carbohydrate Polymers*, 88(2), 609-617.

- Huang, Z. H., Zheng, X., Lv, W., Wang, M., Yang, Q. H., & Kang, F. (2011). Adsorption of lead (II) ions from aqueous solution on low-temperature exfoliated graphene nanosheets. *Langmuir*, 27(12), 7558-7562.
- Hou, P., Liu, C., Tong, Y., Xu, S., Liu, M., & Cheng, H. (2001). Purification of single-walled carbon nanotubes synthesized by the hydrogen arc-discharge method. *Journal of Materials Research*, 16(9), 2526-2529.
- Iijima, S. (1991). Helical microtubules of graphitic carbon. *Nature*, 354(6348), 56.
- Joachim, W. H., & Felistas, P. P. (2000). Handbook on ingredients for aquaculture feeds. p, 478.
- Kabbashi, N. A., Atieh, M. A., Mamun, A. A., Mirghami, M. E. S., Alam, M. D. S., & Yahya, N. (2009). Kinetic adsorption of application of carbon nanotubes for Pb(II) removal from aqueous solution. *Journal of Environmental Science*, 21, 539-544
- Karnitz Jr, O., Gurgel, L. V. A., De Melo, J. C. P., Botaro, V. R., Melo, T. M. S., de Freitas Gil, R. P., & Gil, L. F. (2007). Adsorption of heavy metal ion from aqueous single metal solution by chemically modified sugarcane bagasse. *Bioresource Technology*, 98(6), 1291-1297.
- Khan, Z., Chetia, T. R., Vardhaman, A. K., Barpuzary, D., Sastri, C. V., & Qureshi, M. (2012). Visible light assisted photocatalytic hydrogen generation and organic dye degradation by CdS–metal oxide hybrids in presence of graphene oxide. *RSC Advances*, 2(32), 12122-12128.
- Kimani, N. (2007) Blood lead levels in Kenya: A case study for children and adolescents in selected areas of Nairobi and Olkalou, Nyandarua District.
- Kim, J. H., Nam, K. W., Ma, S. B., & Kim, K. B. (2006). Fabrication and electrochemical properties of carbon nanotube film electrodes. *Carbon*, 44(10), 1963-1968.
- Kitamura, H., Sekido, M., Takeuchi, H., & Ohno, M. (2011). The method for surface functionalization of single-walled carbon nanotubes with fuming nitric acid. *Carbon*, 49(12), 3851-3856.
- Konios, D., Stylianakis, M. M., Stratakis, E., & Kymakis, E. (2014). Dispersion behaviour of graphene oxide and reduced graphene oxide. *Journal of Colloid and Interface Science*, 430, 108-112.
- Konkena, B., & Vasudevan, S. (2012). Covalently linked, water-dispersible, cyclodextrin: reduced-graphene oxide sheets. *Langmuir*, 28(34), 12432-12437.

- Kosa, S. A., Al-Zhrani, G., & Salam, M. A. (2012). Removal of heavy metals from aqueous solutions by multi-walled carbon nanotubes modified with 8-hydroxyquinoline. *Chemical Engineering Journal*, *181*, 159-168.
- Kuila, T., Bose, S., Mishra, A. K., Khanra, P., Kim, N. H., & Lee, J. H. (2012). Chemical functionalization of graphene and its applications. *Progress in Materials Science*, *57*(7), 1061-1105.
- Kurniawan, T. A., Chan, G. Y., Lo, W. H., & Babel, S. (2006a). Physico-chemical treatment techniques for wastewater laden with heavy metals. *Chemical Engineering Journal*, *118*(1-2), 83-98
- Kurniawan, T. A., Chan, G. Y., Lo, W. H., & Babel, S. (2006b). Comparisons of low-cost adsorbents for treating wastewaters laden with heavy metals. *Science of the Total Environment*, *366*(2-3), 409-426.
- Lagergren, S. & Svenska, B. K. (1898). Zur Theorie der sogenannten adsorptiogeloester stoffe, *Veteskapsakad, Handle*, *24*, 1-39
- Lawrence, R. C., & Brian, W. S. (2002). Heavy metals in fertilizers: Considering for setting regulations in Oregon, Oregon Department of Agriculture Salem Oregon. Department of Environmental and Molecular Toxicology Oregon State University, Corvallis Oregon.
- Lee, C., Wei, X., Kysar, J. W., & Hone, J. (2008). Measurement of the elastic properties and intrinsic strength of monolayer graphene. *Science*, *321*(5887), 385-388
- Lee, Y. C., & Yang, J. W. (2012). Self-assembled flower-like TiO<sub>2</sub> on exfoliated graphite oxide for heavy metal removal. *Journal of Industrial and Engineering Chemistry*, *18*(3), 1178-1185.
- Leng, Y., Guo, W., Su, S., Yi, C., & Xing, L. (2012). Removal of antimony (III) from aqueous solution by graphene as an adsorbent. *Chemical Engineering Journal*, *211*, 406-411.
- Li, L., Fan, L., Sun, M., Qiu, H., Li, X., Duan, H., & Luo, C. (2013). Adsorbent for chromium removal based on graphene oxide functionalized with magnetic cyclodextrin-chitosan. *Colloids and Surfaces B: Biointerfaces*, *107*, 76-83.
- Li, Y. H., Di, Z., Ding, J., Wu, D., Luan, Z., & Zhu, Y. (2005). Adsorption thermodynamic, kinetic and desorption studies of Pb<sup>2+</sup> on carbon nanotubes. *Water Research*, *39*(4), 605-609.

- Li, Y. H., Ding, J., Luan, Z., Di, Z., Zhu, Y., Xu, C., ... & Wei, B. (2003a). Competitive adsorption of  $Pb^{2+}$ ,  $Cu^{2+}$  and  $Cd^{2+}$  ions from aqueous solutions by multiwalled carbon nanotubes. *Carbon*, *41*(14), 2787-2792
- Li, Y. H., Wang, S., Zhang, X., Wei, J., Xu, C., Luan, Z., & Wu, D. (2003b). Adsorption of fluoride from water by aligned carbon nanotubes. *Materials Research Bulletin*, *38*(3), 469-476.
- Li, Y. H., Wang, S., Luan, Z., Ding, J., Xu, C., & Wu, D. (2003c). Adsorption of cadmium (II) from aqueous solution by surface oxidized carbon nanotubes. *Carbon*, *41*(5), 1057-1062.
- Li, Y. H., Luan, Z., Xiao, X., Zhou, X., Xu, C., Wu, D., & Wei, B. (2003d). Removal of  $Cu^{2+}$  ions from aqueous solutions by carbon nanotubes. *Adsorption Science & Technology*, *21*(5), 475-485.
- Li, Y. H., Wang, S., Wei, J., Zhang, X., Xu, C., Luan, Z., ... & Wei, B. (2002). Lead adsorption on carbon nanotubes. *Chemical Physics Letters*, *357*(3-4), 263-266.
- Li, Y. H., Zhu, Y., Zhao, Y., Wu, D., & Luan, Z. (2006). Different morphologies of carbon nanotubes effect on the lead removal from aqueous solution. *Diamond and Related Materials*, *15*(1), 90-94.
- Li, Y., Liu, F., Xia, B., Du, Q., Zhang, P., Wang, D., ... & Xia, Y. (2010). Removal of copper from aqueous solution by carbon nanotube/calcium alginate composites. *Journal of Hazardous Materials*, *177*(1-3), 876-880.
- Liu, C., Bai, R., & San Ly, Q. (2008). Selective removal of copper and lead ions by diethylenetriamine-functionalized adsorbent: behaviors and mechanisms. *Water Research*, *42*(6-7), 1511-1522.
- Liu, M., Chen, C., Hu, J., Wu, X., & Wang, X. (2011). Synthesis of magnetite/graphene oxide composite and application for cobalt (II) removal. *The Journal of Physical Chemistry C*, *115*(51), 25234-25240.
- Liu, X., Pan, L., Lv, T., Lu, T., Zhu, G., Sun, Z., & Sun, C. (2011). Microwave-assisted synthesis of ZnO-graphene composite for photocatalytic reduction of Cr (VI). *Catalysis Science & Technology*, *1*(7), 1189-1193.
- Long, R. Q., & Yang, R. T. (2001). Carbon nanotubes as superior sorbent for dioxin removal. *Journal of the American Chemical Society*, *123*(9), 2058-2059.

- Loska, K., & Wiechuła, D. (2003). Application of principal component analysis for the estimation of source of heavy metal contamination in surface sediments from the Rybnik Reservoir. *Chemosphere*, *51*(8), 723-733.
- Lu, C., & Chiu, H. (2006). Adsorption of zinc (II) from water with purified carbon nanotubes. *Chemical Engineering Science*, *61*(4), 1138-1145.
- Lu, C., & Liu, C. (2006). Removal of nickel (II) from aqueous solution by carbon nanotubes. *Journal of Chemical Technology & Biotechnology: International Research in Process, Environmental & Clean Technology*, *81*(12), 1932-1940.
- Ma, P. C., Siddiqui, N. A., Marom, G., & Kim, J. K. (2010). Dispersion and functionalization of carbon nanotubes for polymer-based nanocomposites: a review. *Composites Part A: Applied Science and Manufacturing*, *41*(10), 1345-1367.
- Macht, F., Eusterhues, K., Pronk, G. J., & Totsche, K. U. (2011). Specific surface area of clay minerals: Comparison between atomic force microscopy measurements and bulk-gas (N<sub>2</sub>) and-liquid (EGME) adsorption methods. *Applied Clay Science*, *53*(1), 20-26.
- Madadrang, C. J., Kim, H. Y., Gao, G., Wang, N., Zhu, J., Feng, H., ... & Hou, S. (2012). Adsorption behavior of EDTA-graphene oxide for Pb (II) removal. *ACS Applied Materials & Interfaces*, *4*(3), 1186-1193.
- Mahmud, H. N. M. E., Hosseini, S., & Binti Yahya, R. (2014). Polymer adsorbent for removal of lead ions from aqueous solution. *International Journal of Technical Research and Application*, *11*, 04-08
- Malhotra, B. D., Srivastava, S., & Augustine, S. (2015). Biosensors for food toxin detection: Carbon nanotubes and graphene. *MRS Online Proceedings Library Archive*, 1725.
- Marcano, D. C., Kosynkin, D. V., Berlin, J. M., Sinitskii, A., Sun, Z., Slesarev, A., ... & Tour, J. M. (2010). Improved synthesis of graphene oxide. *ACS nano*, *4*(8), 4806-4814.
- Marques, P. A. S. S., Rosa, M. F., & Pinheiro, H. M. (2000). pH effects on the removal of Cu<sup>2+</sup>, Cd<sup>2+</sup> and Pb<sup>2+</sup> from aqueous solution by waste brewery biomass. *Bioprocess Engineering*, *23*(2), 135-141.
- Massoumi, B., Jaymand, M., Samadi, R., & Entezami, A. A. (2014). *In situ* chemical oxidative graft polymerization of thiophene derivatives from multi-walled carbon nanotubes. *Journal of Polymer Research*, *21*(5), 442.

- Mohanty, K., Das, D., & Biswas, M. N. (2008). Treatment of phenolic wastewater in a novel multistage external loop airlift reactor using activated carbon. *Separation and Purification Technology*, 58(3), 311-319
- Montes-Navajas, P., Asenjo, N. G., Santamaría, R., Menendez, R., Corma, A., & García, H. (2013). Surface area measurement of graphene oxide in aqueous solutions. *Langmuir*, 29(44), 13443-13448.
- Mortvedt, J. J. (1995). Heavy metal contaminants in inorganic and organic fertilizers: *Nutrient Cycling in Agroecosystems*, 10, 55-61
- Mousa, M. A., & Khattab, Y. A. (2003). The counteracting effect of vitamin – C (L – ascorbic acid) on the physiological perturbations induced by ochratoxin intoxication in the African catfish (*Clarias gariepinus*). *Journal of Egypt Academic Environmental Development*, 4(1), 117 – 128
- Needleman H. (2004). Lead poisoning. *Annual Review of Medicine*, 55, 209
- Musico, Y. L. F., Santos, C. M., Dalida, M. L. P., & Rodrigues, D. F. (2013). Improved removal of lead (II) from water using a polymer-based graphene oxide nanocomposite. *Journal of Materials Chemistry A*, 1(11), 3789-3796.
- Ndeda, L. A., & Manohar, S. (2014). Determination of heavy metals in Nairobi Dam, Kenya. *IOSR Journal of Environmental Science, toxicology and Food Technology*, 8(5), 68-73
- Nordberg, G.F., Flower, B., Nordberg, M., & Friberg, L. (2007). Handbook on the toxicology of metals, third ed., Academic Press.
- Novoselov, K. S., Geim, A. K., Morozov, S. V., Jiang, D. A., Zhang, Y., Dubonos, S. V., ... & Firsov, A. A. (2004). Electric field effect in atomically thin carbon films. *Science*, 306(5696), 666-669
- Ochieng, E. Z., Lalah, J.O., & Wandiga, S. O. (2007). Analysis of heavy metals in water and surface sediments in five Rift Valley lakes in Kenya for assessment of recent increase in anthropogenic activities. *Bulletin of Environmental Toxicology*, 79, 570-576
- Odiere, W.O. (1999). *Environmental Physiology of Animals and Pollution*. Diversified Resources Ltd, Lagos. 261
- Okeyo, B. & Wangila, A. (2012). Lead poisoning in Owino Uhuru slums in Mombasa-Kenya eco-ethics international- Kenya chapter

- Omastova, M., Trchova, M., Kovarova, J., & Stejskal, J.(2003). Synthesis and structural study of polypyrroles prepared in the presence of surfactants. *Synthetic metals*, 138, 447-455
- Opeyemi, O., Adebola, O., Gururaj, M. N., & Aderemi, O. (2014). Adsorption of lead over graphite oxide. *Molecular and Biomolecular Spectroscopy*, 118, 857-860
- Osswald, S., Havel, M., & Gogosti, Y. (2007). Monitoring oxidation of multi walled carbon nanotubes by Raman spectroscopy. *Journal of Raman Spectroscopy*, 38, 728-736
- Pan, S.C., Lin, C.C., & Hwa, D. (2003). Reusing sewage sludge ash as adsorbent for copper removal from wastewater. *Resource Conservation and Recycling*. 39, 79-90
- Park, S., & Rouff, R.S. (2009). Chemical methods for the production of graphenes. *Nature Nanotechnology*, 4, 217-224
- Peigney, A., Laurent, C., Flahaut, E., Bacsá, R.R., & Rousset, A. (2001). Specific surface area of carbon nanotubes and bundles of carbon nanotubes. *Carbon*, 39(4), 507-514.
- Peng, X., Li Y, Luan, Z., Di, Z., Wang, H., Tian, B., & Jia, Z. (2003). Adsorption of 1, 2-dichlorobenzene from water to carbon nanotubes, *Chemical Physics Letters*, 376(1-2), 154-158.
- Prasad, A. S., & Oberleas, D. (1976). *Trace elements in human health and disease*, vol I &II. Academic press, India, 201-205.
- Pruneanu, S., Resel, R., Leising, G., Brie, M., & Graupner, W. (1997). Structural investigations on polypyrrole and poly (vinyl chloride)-polypyrrole composite films. *Materials Chemistry and Physics*, 48, 240–245
- Qui H, Lu LV, Pan B, Zhang Q, Zhang W, Zhang Q.(2009). Critical review of the adsorption kinetic models. *Journal of Zhejiang University Science A*, 10, 716-24
- Rao, G.P., Lu C., & Su F. (2007). Sorption of divalent metal ions from aqueous solution by carbon nanotubes. A review. *Separation and Purification Technology*, 58, 224-231
- Rao, M., Parwate, A.V., & Bhole A.G. (2002). Removal of Cr<sup>6+</sup>, and Ni<sup>2+</sup> from aqueous solution using bagasse and fly ash. *Waste Management*, 22, 821-830
- Rao, M.M., Ramesh, A., Rao, G.P.C. & Seshaiyah, K, (2006). Removal of copper and cadmium from aqueous solutions by activated carbon derived from ceiba pentandra hulls. *Journal of Hazardous Materials B*, 129, 123-129

- Raymundo-Pinero, E., Azais, P., Cacciaguera, T., & Beguin, F.(2005). KOH and NaOH activation mechanism of multiwalled carbon nanotubes with different structural organization. *Carbon*, 43(4), 786-795
- Ren, Y., Yan, N., Wen, Q., Fan, Z., Wei, T., Zhang, M., & Ma, J. (2011). Graphene/ $\delta$ -MnO<sub>2</sub> composite as adsorbent for the removal of nickel ions from wastewater. *Chemical Engineering Journal*, 175, 1–7
- Ren, X. M., Shao, D. D., Zhao, G. X., Sheng, G. D., Hu, J., Yang, S. T., & Wang, X. K. (2011). Plasma induced multi-walled carbon nanotube grafted with 2-vinylpyridine for preconcentration of Pb(II) from aqueous solutions. *Plasma Process and Polymers*, 8, 589-598
- Reza, R. & Singh, G. (2010). Heavy metal contamination and its indexing approach for river water. *International Journal of Environmental Science and Technology*, 7, 785-792
- Rizzarelli, E., & Vecchio, G. (1999). Metal complexes of functionalized cyclodextrins as enzyme models and chiral receptors. *Co-ordination Chemistry Reviewers*, 188(1), 343-364
- Roberts, M.W., Clemons, C.B., Wilber, J.P., Young, G.W., Buldum, A., & Quinn, D.D. (2010). Continuum plate theory and atomistic modeling to find the flexural rigidity of graphene sheet interacting with substrate. *Journal of Nanotechnology*, (2010), article id 868492, 8
- Rurle, B., Peeterbroeck, S., Gouttebaron, R., Godfroid, T., Monteverde, F., Dauchot, J., Alexandre, M., Hecq, M., Dubois, P. (2007). Functionalization of carbon nanotubes by atomic nitrogen formed in microwave plasma Ar+N<sub>2</sub> and subsequent poly grafting. *Journal of Materials Chemistry*, 17, 157-159
- Ryan, E. M., Tartakovsky, A. M., & Amon C. (2011). Pore-scale modeling of competitive adsorption in porous media. *Journal of Contaminant Hydrology*, 120, 56-78.
- Sahmetlioglu, E., Wilma, E., Acts, E., & Skylark, M. (2014). Polypyrrole/multi-walled carbon nanotubes for the solid phase extraction of lead (II) in water samples. *Atlanta*, 119, 447-451.
- Salam, M.A. (2013). Removal of heavy metal ions from aqueous solutions with multi-walled carbon nanotubes: Kinetics and thermodynamic studies. *International Journal of Environmental Science and Technology*, 10, 677-688
- Saito, R., Hoffman, M., Dresselhaus, G., Jairo, A., & Dresselhaus, M. S. (2011). Raman spectroscopy of graphene and carbon nanotubes. *Advance in Physics*, 30, 413-550

- Seid, L., Chouder, D., Maouche, N., Bakas, I., & Barka, N. (2014). Removal of Cd (II) and Co (II) ions from aqueous solutions by polypyrrole particles: Kinetics, equilibrium and thermodynamics. *Journal of the Taiwan Institute of Chemical Engineers*, 45, 2969-2974
- Sekar, M., Sarthe, V., & Rengaraj, S. (2004). Kinetics and equilibrium adsorption study of lead (II) onto activated carbon prepared from coconut shell. *Journal of Colloid and Interface Science*, 279, 307-313.
- Shanshan, W., Yang, L., Xiaobin, F., Fengbao, Z., & Guoliang, Z. (2014). B-cyclodextrin functionalization graphene oxide; an efficient and recyclable adsorbent for the removal dye pollutants. *Frontiers of Chemical Science and Engineering*. 9(1), 77-83
- Shen, G., Li, J., Shao, D., Hu, J., Chen, C., Chen, Y., & Wang, X. (2010). Adsorption of copper (II) on multi-walled carbon nanotubes in the absence and presence of humic and fluvic acids. *Journal of Hazardous Materials*, 178, 333-340
- Shim, J. W., Park, S. J., & Ryu Swae, K. (2001). Effect of modification with HNO<sub>3</sub> and NaOH on metal adsorption by pitch-based activated carbon fibers. *Carbon*, 39, 1635–1642.
- Singh Chauhan, S. M., & Mishra, S. (2011). Use of graphite oxide and graphene oxide as catalysts in the synthesis of dipyrromethane and calix [4] pyrrole. *Molecules*, 16(9), 7256-7266.
- Sitko, R., Turek, E., Zawisza, B., Malicka, E., Talik E, Heimann J, Gagor A, Feist, B., & Wrzali, R. (2013). Adsorption of divalent metal ions from aqueous solutions using graphene oxide. *Dalton Transactions*, 42, 5682-5689
- Sobhy & Reyad, N.A.S.A, (2015). Using polypyrrole nano-composites coated on rice husks ash for the removal of anions, heavy metals, COD from textile wastewater. *HBRC journal*.
- Song, W., Hu, J., Zhao, Y., Shao, D., & Li, J. (2013). Efficient removal of cobalt from aqueous solution using β-cyclodextrin modified graphene oxide. *RSC Advances*, 3, 9514
- Spain, E., Keyes, T. E., & Forster, R. J. (2013). Polypyrrole–gold nanoparticle composites for highly sensitive DNA detection. *Electrochimica Acta*, 109, 102–109.
- Stafiej, A. & Pyrznska K. (2007). Adsorption of heavy metal ions with carbon nanotubes. *Separation and Purification Technology*, 58, 49-52
- Stokinger, H. E. (1981). The metals. In: *Pathy's industrial hygiene and toxicology*: (3<sup>rd</sup> edition vol.2 Clayton G.D, Clayton F.E. Eds) New York. A *Wiley-Interscience publication*, John Wiley and Sons, pp. 1493-2060

- Stoller, M. D., Park, S., & Zhu, Y. W. (2008). Graphene-based ultracapacitors. *Nano Letters*, 8, 3498–3502
- Sudaryanto, Y., Hartoro, S. B., Irawaty, W., Hindarso, H., & Ismadji, S. (2006). High surface area activated carbon prepared from cassava peel by chemical activation. *Bioresource Technology*, 97, 734-739
- Sui, Z., Meng, Q., Zhang, X., Ma, R., & Cao, B. (2012). Green synthesis of carbon nanotubes–graphene hybrid aerogels and their use as versatile agents for water purification. *Journal of Materials Chemistry*, 22, 8767-8771
- Sun, X., Xu, Y., Wang, J., & Mao, S. (2002). The composite film of polypyrrole and functionalized multi-walled carbon nanotubes as an electrical material for supercapacitors, *International Journal of Electrochemical Science*, 7, 3205-3214.
- Sun, Y., Zhang, J.P., Yang, G. & Li, Z.H. (2007). Preparation of activated carbon with large specific surface area from reed black liquor. *Environmental Technology*, 28(5), 491-497
- Suraj, G., Lyer, C. S., & Lalithambika, C. S. P (1998). Adsorption of cadmium and copper by modified kaolinites. *Applied Clay Science*, 13, 293-306.
- Tofiqhy, M. A. & Mohammadi, T. (2011). Adsorption of divalent heavy metal ions from water using carbon nanotube sheets. *Journal of Hazardous Materials*, 185, 140-147
- Unuabonah, I. E., Olu-Owolabi, B. I., Adebowale, K. O., & Ofomaja, A. E. (2007). Adsorption of lead and cadmium ions from aqueous solutions by tripolyphosphate-impregnated kaolinite clay. *Colloids and Surfaces A: Physicochemical Engineering Aspects*, 282, 202-211.
- US EPA (1980). U.S Environmental Protection Agency. Ambient water quality criteria for copper and lead. Springfield, VA: *National Technical Information Service*, 81,117-681
- U.S. Environmental Agency, Drinking Water Contaminants (2016).  
<http://www.epa.gov/safewater/contaminants/index.html>, July 20, 2016
- Vosylienė, M. Z., & Kazlauskienė, N. (2004). Evaluation of the Svede pond water effect on fish (after accidental discharge of the Kairiai dump filtrate into the environment). Protection and management of water bodies. Proceedings of International Science Conference Kaunas, 219–223.

- Vukovic, G. D., Marinkovic, A. D., Skapin, S.D., Ristic, M. D., Aleksic, R., Peric-Grujic, A. A., Uskokovic, P. S.(2011). Removal of lead from water by amino modified multi-walled carbon nanotubes, *Chemical Engineering Journal*, 173, 855-865
- Vyas, R. K. & Kumar, S. (2006). Determination of micropore volume and surface area of zeolite molecular sieves by D-R and D-A equations. A comparative study. *Indian Journal of Chemical Technology*, 11, 704-709
- Wan Ngah, W.S. & Hanafiah, M.A.K.M. (2008). Removal of heavy metal ions from wastewater by chemically modified plant wastes as adsorbents: A review. *Bioresource Technology*, 99, 3935-3948
- Wang, C., Zhan, L., Qiao, W., & Ling, L. (2011). Preparation of graphene nanosheets through detonation. *New Carbon Materials*, 26(01), 16-20
- Wang, H., Liu, Y., Zeng, G., Hu, X., Hu, X., Li, T., Li, H., Wang, Y., & Jiang, L. (2014). Grafting of  $\beta$ -cyclodextrin to magnetic graphene oxide via ethylenediamine and application for Cr (VI) removal. *Carbohydrate Polymers* 113: 166–173
- Wang, X. S., Li, Z. Z., & Su, C. (2009). A comparative study of removal of Cu(II) from aqueous solutions by locally low-cost materials: marine microalgae and agricultural by-products, *Desalination*, 235, 146-159
- Wang, Z.F., Liu, J.J., Wang, W.X., Chen, H.R., Liu, Z.H., Yu, Q.K., Zeng, H.D., & Sun, L.Y. (2013). Aqueous phase preparation of graphene with low defect density and adjustable layer. *Chemical Communications*, 49, 10835–10837.
- Weber, W. J. & Morris, J. C. (1963). Kinetics of adsorption on carbon from solutions. *Journal of Sanitation and Engineering ASC*, 89, 31-59.
- Wepasnick K.A., Smith B. A., Schrote K. E., Wilso H. K., Diegemann S. R., & Fairbrothe D. H. (2011). Surface and structural characterization of multi-walled carbon nanotubes following different oxidative treatments. *Carbon*. 49, 24-36
- Wong, K.K., Lee, C.K., Low, K.S., Haron, M.J. (2003). Removal of Cu and Pb by tartaric acid modified rice husks from aqueous solution. *Chemosphere*, 50, 23-28
- Wu, C. H. (2007). Studies of the equilibrium and thermodynamics of the adsorption of  $\text{Cu}^{2+}$  onto as-produced and modified carbon nanotubes. *Journal of Colloid and Interface Science*. 311, 338-346

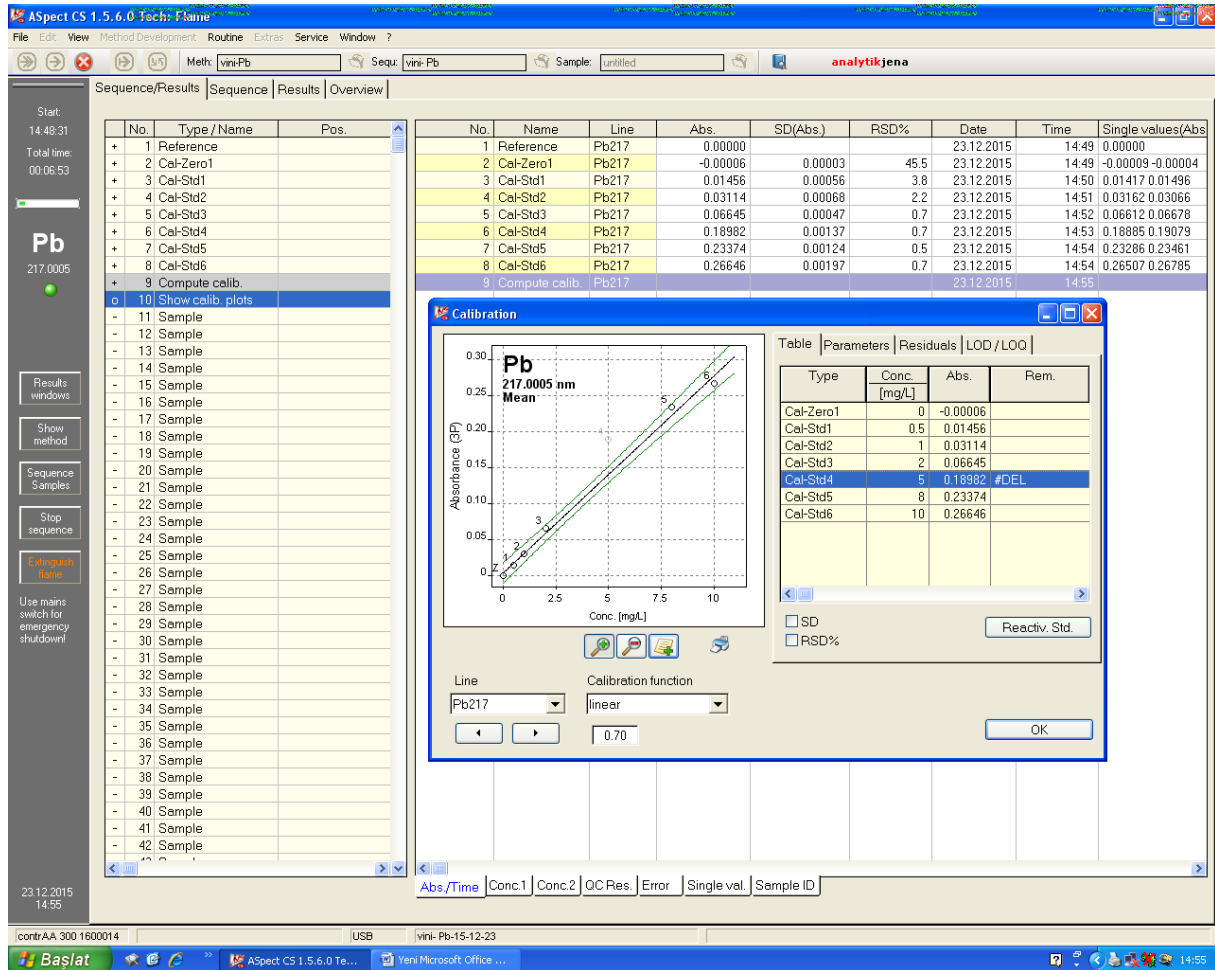
- Wu, T. -W & Lin, S. -H. (2006). Characterization and electrical properties of polypyrrole/multi-walled carbon nanotubes composites synthesized by *in situ* chemical oxidation polymerization. *Journal of Polymer Science Part B: Polymer Physics*, 44(10), 1413-1418
- Wu, W., Yang, Y., Zhuo, H., Ye, T., Huang, Z., Liu, R. & Kuang, Y. (2013). Highly efficient removal of Cu(II) from aqueous solution by using graphene oxide. *Water, Air and Soil Pollution*, 224, 1372
- Xing, Y., Li, L., Chusuei C. C., & Hull, R. V. (2005). Sonochemical oxidation of multi-walled carbon nanotubes. *Langmuir*, 21, 4185-4190.
- Xu, C., Wang, J., Wan, L., Lin, J., & Wang, X. (2011). Microwave-assisted covalent modification of graphene nanosheets with hydroxypropyl- $\beta$ -cyclodextrin and its electrochemical detection of phenolic organic pollutants. *Journal of Materials Chemistry*, 21(28), 10463-10471.
- Xu, D., Tan, X., Chen, C., & Wang, X. (2008). Removal of Pb(II) from aqueous solutions by oxidized multi-walled carbon nanotubes, *Journal of Hazardous Materials*, 154, 407- 416
- Yang, S. T., Chang, Y. L., Wang, H. F., Liu, G. B., Chen, S., Wang, Y. W., ... (2010). Folding/aggregation of graphene oxide and its application in Cu(II) removal. *Journal of Colloid and Interface Science*, 351, 122–127.
- Yusuf, M., Elfghi, F. M., Zaidi, S. A., Abdullah, E. C., & Khan, M. A. (2015). Application of graphene and its derivatives as an adsorbent for heavy metals and dye removal: a systematic and comprehensive overview. *RSC Advances*, 5, 50392
- Zadeh, E. M., Yu, A., Fu, L., Dehghan, M., Sbarski, I., & Harding, I. (2014). Physical and thermal characterization of graphene oxide modified gelatin based thin films. *Polymer composites*. Doi.org/10.1002/pc.22865
- Zhang, W. J., Shi, X. H., & Zhang, Y. X. (2013). Synthesis of water-soluble magnetic graphene nanocomposites for recyclable removal of heavy metal ions. *Journal of Materials Chemistry A*: 1, 1745–1753
- Zhang, S. -P., Liu, B., Li, C. -Y., Chen, W., Yao, Z. -J., Yan, D. -T., Yu, R. -B., & Song, H. -O. (2014). Enhanced dispersibility and thermal stability of  $\beta$ -cyclodextrin functionalized graphene. *Chinese Chemical Letters*, 25, 355-358.

- Zhang, Z. & Xu, X. (2015). Nondestructive covalent functionalization of carbon nanotubes by selective oxidation of the original defects with  $K_2FeO_4$ . *Applied Surface Science*, 346, 520-527
- Zhao, G., Li, J., Re, X., Chen, C., & Wang, X. (2011). Few layered graphene oxide nanosheets as superior sorbents for heavy metal ion pollution management. *Environmental Science and Technology*, 45(24), 10454-10462
- Zhu, W.Z., Miser, D.E., Chan, W.G., & Hajaligol, M.R. (2003). Characterization of multiwalled carbon nanotubes prepared by carbon arc cathode deposit. *Materials Chemistry and Physics*, 82(3), 638-647
- Zhuo, W., Li, W., Xie, Y., Wang, L., Pan, K., Tian, G., Li, M., Wang, G., Qu, Y., & Fu, Y. (2014). Fabrication of non-covalently functionalized brick like  $\beta$ -cyclodextrins graphene composite dispersions with favourable stability. *RSC Advances*, 4, 2813-2819

# APPENDICES

## Appendix 1

Calibration of AAS instrument for analysis of levels of lead and copper ions.



Copper

Aspect CS 1.5.6.0 Tech: Flame

File Edit View Method Development Routine Extras Service Window 2

Meth: vini-Cu Sequ: vini-Cu Sample: untitled analytikjena

Sequence/Results Sequence Results Overview

Start: 14:12:46  
Total time: 00:14:10

**Cu**  
324.7540

Results windows  
Show method  
Sequence Samples  
Stop sequence  
Single point file  
Use mains switch for emergency shutdown!

No.	Type/Name	Pos.
+ 1	Reference	
+ 2	Cal-Zero1	
+ 3	Cal-Std1	
+ 4	Cal-Std2	
+ 5	Cal-Std3	
+ 6	Cal-Std4	
+ 7	Cal-Std5	
+ 8	Cal-Std6	
+ 9	Compute calib.	
o 10	Show calib. plots	
- 11	Sample	
- 12	Sample	
- 13	Sample	
- 14	Sample	
- 15	Sample	
- 16	Sample	
- 17	Sample	
- 18	Sample	
- 19	Sample	
- 20	Sample	
- 21	Sample	
- 22	Sample	
- 23	Sample	
- 24	Sample	
- 25	Sample	
- 26	Sample	
- 27	Sample	
- 28	Sample	
- 29	Sample	
- 30	Sample	
- 31	Sample	
- 32	Sample	
- 33	Sample	
- 34	Sample	
- 35	Sample	
- 36	Sample	
- 37	Sample	
- 38	Sample	
- 39	Sample	
- 40	Sample	
- 41	Sample	
- 42	Sample	

No.	Name	Line	Abs.	SD(Abs.)	RSD%	Date	Time	Single value
1	Reference	Cu324	0.00000			23.12.2015	14:14	0.00000
2	Cal-Zero1	Cu324	0.00004	0.00005	137.6	23.12.2015	14:15	0.00008 0.00
3	Cal-Std1	Cu324	0.05931	0.00464	7.8	23.12.2015	14:16	0.05603 0.06
4	Cal-Std2	Cu324	0.13477	0.00243	1.8	23.12.2015	14:18	0.13305 0.13
5	Cal-Std3	Cu324	0.25690	0.00108	0.4	23.12.2015	14:19	0.25767 0.25
6	Cal-Std4	Cu324	0.57721	0.00985	1.7	23.12.2015	14:21	0.57024 0.58
7	Cal-Std5	Cu324	0.84681	0.00073	0.1	23.12.2015	14:22	0.84733 0.84
8	Cal-Std6	Cu324	0.94429	0.01539	1.6	23.12.2015	14:23	0.93340 0.95
9	Compute calib.	Cu324				23.12.2015	14:23	

**Calibration**

Table Parameters Residuals LOD / LOQ

Type	Conc. [mg/L]	Abs.	Rem.
Cal-Zero1	0	0.00004	
Cal-Std1	0.5	0.05931	
Cal-Std2	1	0.13477	
Cal-Std3	2	0.25690	
Cal-Std4	5	0.57721	#DEL
Cal-Std5	8	0.84681	
Cal-Std6	10	0.94429	

Line: Cu324 Calibration function: linear

0.70

SD  RSD%

Abs/Time Conc.1 Conc.2 QC-Res Error Single val. Sample ID

23.12.2015 14:26

contrAA 300 1600014 USB vini-Cu-15-12-23

Başlat Aspect CS 1.5.6.0 Te... 14:26